

**OPTICAL REMOTE SENSING OF SURFACE ROUGHNESS  
THROUGH THE TURBULENT ATMOSPHERE**

**John S. Peacock  
B.S. in Physics and Mathematics  
Elmhurst College, 1984**

**A thesis submitted to the faculty  
of the Oregon Graduate Center  
in partial fulfillment of the  
requirements for the degree  
Master of Science  
in  
Applied Physics**

**May 1989**

The thesis "Optical Remote Sensing of Surface Roughness Through the Turbulent Atmosphere" by John S. Peacock has been examined and approved by the following Examination Committee:

---

J. Fred Holmes, Advisor  
Professor

---

Richard A. Elliott  
Professor

---

V. S. Rao Gudimetla  
Assistant Professor

## ACKNOWLEDGMENT

I would like to dedicate this work to three groups of individuals without whom this thesis would have never been a reality. First and foremost, to my Father and God, who has been my source of constant encouragement, joy and reason for living. May all men come to realize the great pleasure that comes from knowing You. Secondly, to my close friends, Ted, Kris and Bret, who are some of the reasons God has given me for living. I will always judge my friendships by the depth we have shared and will always consider life special because of the time we have spent together. Finally to my parents for giving me life, teaching me of God's love and showing me the value of honest work.

I would also like to express my sincere gratitude to the people who pragmatically guided me along in my pursuit and completion of this thesis. I particularly want to thank: Dr. J. Fred Holmes for the conception of this thesis problem and his persistence in helping me to complete it; Dr. V. S. Rao Gudimetla for his consistent and patient help in defining the problem and soon to be Dr. Doug Draper for his unflinching efforts in helping me to solve the problem.

Finally a special thank you to Bev Kyler for her unflinching efforts in preparing and completing this manuscript.

## Table Of Contents

1.	Introduction	1
	1.1 A Historical Perspective of Laser Speckle Applications	1
	1.2 A Brief Overview of the Thesis Problem	5
2.	Theory	9
	2.1 The Requirements For a Diffuse Target	9
	2.2 Statistical Properties of Speckle Phase Measurements In The Diffraction Regime	11
3.	Target Analysis	16
	3.1 Experimental Set Up For Measuring Surface Profiles	16
	3.2 Target Types	21
	3.3 Average Surface Height (R.M.S.)	22
	3.4 Surface Height Distribution	24
	3.5 Autocorrelation Function and Correlation Length for Surface Profiles	33
	3.6 Power Spectrum of the Surface Profile	40
	3.7 Summary of Results	42
4.	Speckle Phase Analysis	44
	4.1 The Experimental Set Up For Measuring The Phase Of The Fields Present In The Speckle Pattern	44
	4.1.1 Transmitter/Receiver System	44
	4.1.2 Amplifiers and Phase Detectors	48
	4.1.3 A/D and Computer	55
	4.2 Phase Data Analysis Tools	56
	4.2.1 Unraveling The Phase Difference Data	57
	4.2.2 Filtering and Creating the Phase Difference Density Function	67
	4.2.3 Fitting a Gaussian Curve to the Phase Density Functions	73
5.	Conclusions	77
	5.1 Summary of the Experimental Results	77
	5.2 Discussion of Results	87
	References	89
	Appendix 1	92

Appendix 2

98

Vita

118

## LIST OF FIGURES

1.1	Transmitter/receiver configuration	2
1.2	Typical example of laser speckle pattern	3
2.1	Probability density function for the phase of the fields measured in the speckle pattern in the Fresnel diffraction regime, ignoring atmospheric interaction. $\sigma$ is the standard deviation of the phase of the fields measured at the target. $\theta$ is the standard deviation of the phase of the fields measured at the receiver. Both $\sigma$ and $\theta$ are in units of radians.	15
3.1	Experimental set up for measuring the surface characteristics using a profilometer.	17
3.2	Stylus tip of profilometer and typical example of a surface profile.	19
3.3	Typical example of the digitized surface profile signal.	20
3.4	Average normalized histogram for 8 grit sandblasted aluminum target. The erratic line represents the measured histogram. The smooth line is a Gaussian curve with a variance equal to the variance of the measured histogram.	27
3.5	Normalized histogram for 30 grit sandblasted aluminum and a Gaussian curve of equal variance.	28
3.6	Normalized histogram for 24 grit sandblasted aluminum and a Gaussian curve of equal variance.	29
3.7	Normalized histogram for 16 grit sandblasted aluminum and a Gaussian curve of equal variance.	30
3.8	Normalized histogram for 8 grit sandblasted aluminum and a Gaussian curve of equal variance.	31

3.9	Normalized histogram for 600 grit silicon carbide sandpaper and a Gaussian curve of equal variance.	32
3.10	The average of the 12 autocorrelation function for the 30 grit sandblasted aluminum target.	36
3.11	The average of the 12 autocorrelation function for the 16 grit sandblasted aluminum target.	37
3.12	The average of the 12 autocorrelation function for the 8 grit sandblasted aluminum target.	38
3.13	The average of the 12 autocorrelation function for the 600 grit sandpaper. The autocorrelation function for the sandpaper shows periodicity.	39
3.14	The average power spectrum for each diffuse target type.	41
4.1	The transmitter/receiver optical system used to measure the phase of the fields present in the speckle pattern. The pattern is generated in the far field.	45
4.2	Electronic instrumentation used to measure the phase difference data.	49
4.3	Example of the functionality of the phase detector. Phase difference values greater than $\pi$ or less than 0 (radians) are mapped into the primary zone in the phase detector output.	53
4.4	Typical example of the two channels of phase difference data, outputted by the phase detector.	54
4.5	A simulation of a constantly increasing optical phase difference and the corresponding two channels of phase detector output (or PD data).	60
4.6	An example illustrating the necessity of having two channels of output for the phase detector in order to resolve phase changes greater than $\pi$ .	62

4.7	Phase difference (PD) data unfolded into the 0 to $2\pi$ interval. The optical phase difference is linearly increasing in time in this example.	64
4.8	An example of the two channels of 0 to $2\pi$ phase difference data being unfolded into the actual optical phase changes (which are greater than $2\pi$ ). In this example the optical phase difference (not shown) is increasing at a constant linear rate.	65
4.9	A typical example of the two channels of phase difference (PD) data and the corresponding unfolded data (optical phase difference data). (a) and (b) are the two channels of PD data varying between 0 and $\pi$ and $\pi/2$ out of phase. (c) and (d) are the PD data unfolded into the 0 to $2\pi$ interval. Both these channels are $\pi$ out of phase. (e) represents the totally unfolded PD data (optical phase difference data).	66
4.10	A typical example of optical phase difference data (OPD) for a 70 millisecond sampling period.	69
4.11	A 10 point running average (low pass filtering) of the OPD data (=AOPD).	70
4.12	An example of the method by which the optical phase difference (OPD) data is high pass filtered (HPFOPD) to remove the fluctuations caused by macrovariations in the surface characteristics of the diffuse target.	71
4.13	A probability density function for the HPFOPD data of Figure 4.12.	72
4.14	A typical example of the probability density function corresponding to the HPFOPD data (3.5 seconds worth of data). (a) The original density function before the truncation of the tails of the curve. (b) A blow-up of the same curve with the truncated region indicated.	74



4.15	A typical HPFOPD probability density function along with the corresponding best fit Gaussian curve.	76
5.1	The best fit Gaussian curves corresponding to the first set of HPFOPD data taken on each target type is shown above. From this data it is apparent that as the target roughness ( $\sigma_h$ ) increases so does the width of the HPFOPD density function.	79
5.2	The best fit Gaussian curves corresponding to the second set of HPFOPD data taken on each target type is shown above. From this data it can be seen that as the target roughness ( $\sigma_h$ ) increases so does the width of the HPFOPD density function.	80
5.3	The best fit Gaussian curves corresponding to the third set of HPFOPD data taken on each target type is shown above. From this data it can be seen that as the target roughness ( $\sigma_h$ ) increases so does the width of the HPFOPD density function.	81
5.4	The standard deviations of the best fit Gaussian curves ( $\sigma_\phi$ ) for Figures 5.1-5.3 is plotted against the standard deviations of the standard deviations of the phase of the fields measured at the target ( $\sigma_\theta$ ).	82
5.5	The best fit Gaussian curves corresponding to the first set of HPFOPD data is shown for several different target types. From this data it can be seen that as the target roughness ( $\sigma_h$ ) increases so does the width of the HPFOPD density function.	84
5.6	The best fit Gaussian curves corresponding to the second set of HPFOPD data is shown for several different target types.	85
5.7	The standard deviations of the best fit Gaussian curves ( $\sigma_\phi$ ) for Figures 5.1-5.3 and Figures 5.4-5.5 are plotted against the standard deviations of the phase of the fields measured at the target ( $\sigma_\theta$ ).	86

ABSTRACT

OPTICAL REMOTE SENSING OF SURFACE ROUGHNESS  
THROUGH THE TURBULENT ATMOSPHERE

John S. Peacock

Oregon Graduate Center, 1989

Supervising Professor: J. Fred Holmes

The purpose of this work was to determine the feasibility of remotely distinguishing between optically diffuse targets by statistically analyzing the phase of the light scattered from the target. The work was performed using a CO<sub>2</sub> cw coherent LIDAR system with the targets located at a range of 1000 meters.

In the first part of this work, the surface height data for each diffuse target type was measured using a surface profilometer (contact technique). The types of targets tested were sandblasted aluminum, silicon carbide sandpaper and flame sprayed aluminum.

In the second part of this work, the characteristics of the returned speckle pattern were analyzed. The speckle pattern was mixed with an optical local oscillator in the receiver plane to create a heterodyned signal

at 100 kHz. Since the phase of the optical wave is preserved in the heterodyne process, it can be recovered from the signal. The difference between the phase of the fields at two points in the receiver plane was measured. Phase difference (PD) data rather than single point data was used to reduce phase fluctuations (errors) due to the laser transmitter and mechanically induced phase changes. The phase data was "unwrapped" to provide true phase rather than just the zero to  $\pi$  principal values provided by the phase detector.

The unwrapped phase difference data was then used to create a probability density function (PDF) for the phase difference. From the measured PDFs it is possible to remotely distinguish at fairly long ranges (kilometers) between diffuse targets with different surface roughness and to measure the surface height variance.

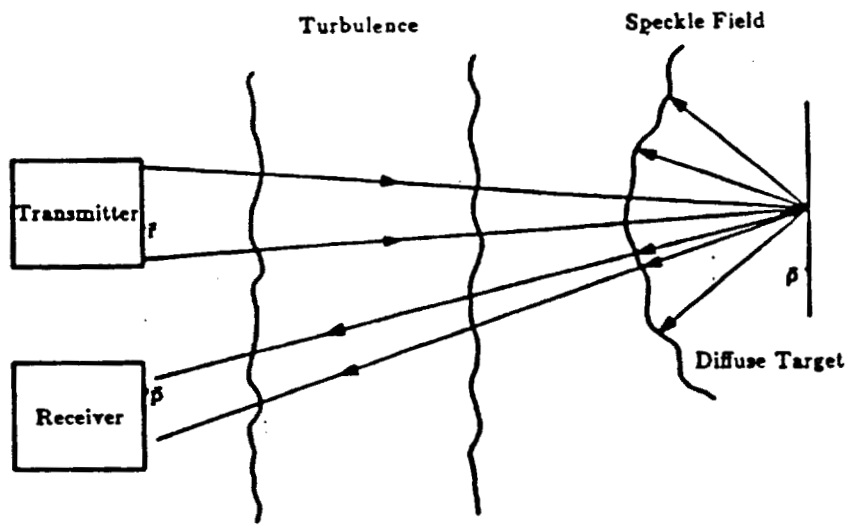
## CHAPTER 1

### INTRODUCTION

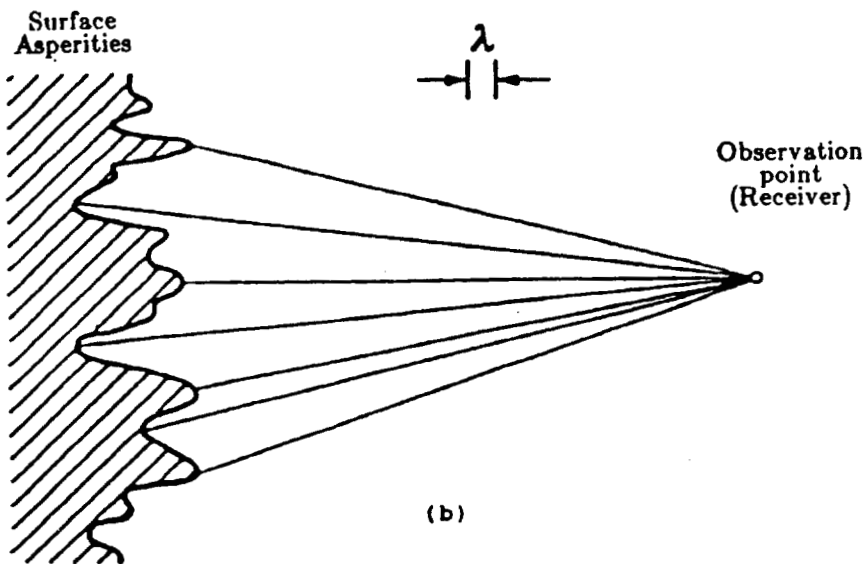
Since shortly after the invention of the laser, researchers have been using lasers to determine the surface characteristics of materials. Speckle is, in itself, a product of a materials surface characteristic. Laser speckle is produced when coherent light (usually a laser) strikes a rough surface (see Fig 1.1a). The light is backscattered with different phases due to the individual surface asperities (see Fig 1.1b). At the transmitter plane the coherent components of light scattered from the rough surface (diffuse target) combine to form an interference pattern. The interference pattern formed (see Fig 1.2) is made up of a random assortment of bright and dark blotches and is known as laser speckle (or a speckle pattern).

#### 1.1 A Historical Perspective of Laser Speckle Applications

Some of the earliest work done in determining the surface characteristics of a material using a laser beam, did not capitalize on the speckle pattern produced [1]. Instead the researcher suppressed the speckle compo-



(a)



(b)

Figure 1.1 Transmitter/Receiver Configuration.

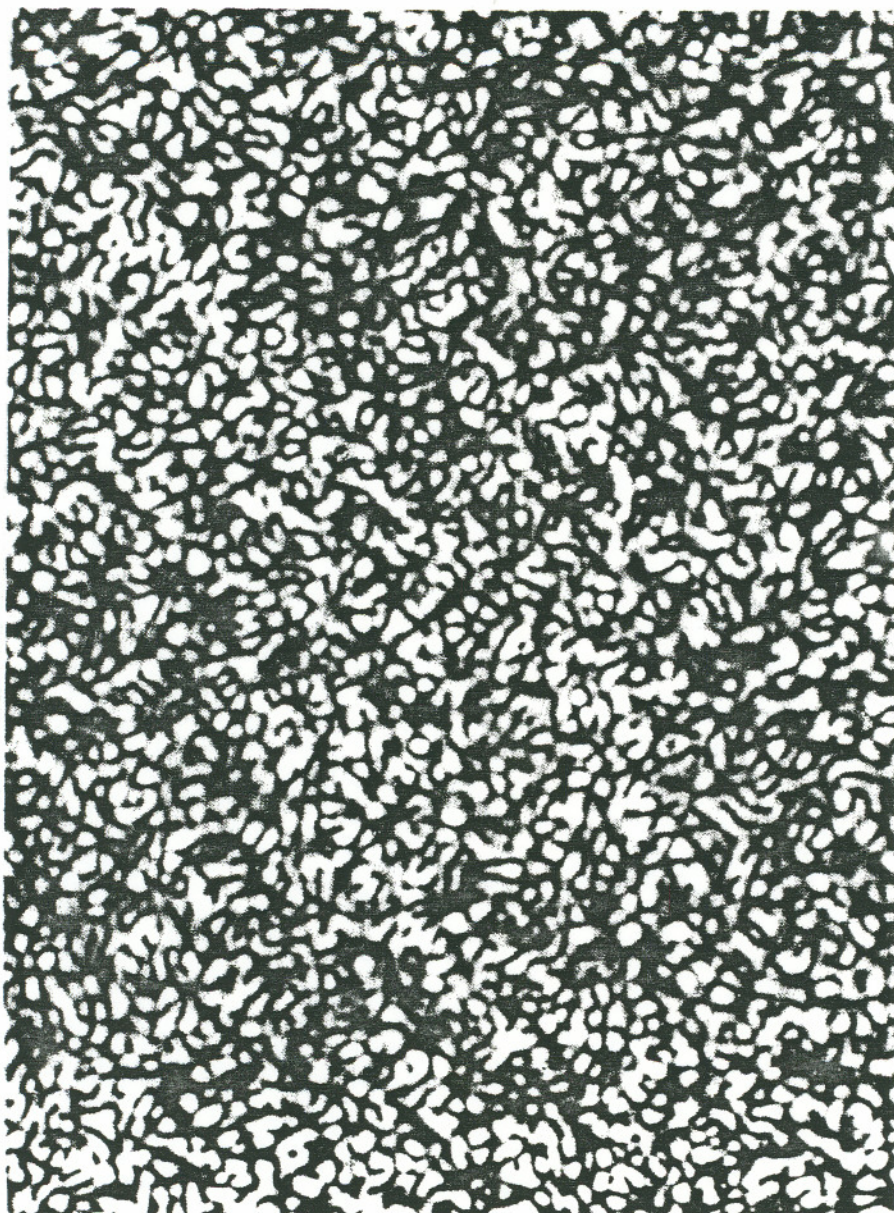


Figure 1.2 Typical example of laser speckle pattern.

component of the return radiation and concentrated on using the specular component (mirror like return) of the return radiation to access the surface attributes.

In the 70's researchers began to make use of the speckle component (pattern) of light scattered from the diffuse target. These efforts focused primarily on using the statistical attributes of the intensity of the fields present in the speckle pattern. It was found that the surface roughness could be directly linked to the contrast of the speckle pattern produced [2,3]. Further efforts showed that by using dichromatic or polychromatic light to produce speckle patterns, a relationship between speckle contrast and surface roughness could be derived [4,5].

In the late 70's and early 80's the advent of optical heterodyne techniques, made it experimentally more attractive to use the phase instead of the intensity of the speckle pattern in measuring the surface characteristics of a material [6]. However the experimental success of such techniques has been very limited. One exception, was the work done by Kadono, Takai and Asakura [7]. Their work showed that it is possible to correlate the phase statistics of the speckle pattern with the r.m.s. roughness of a diffuse target. However their measurements were taken with an optical imaging system in a laboratory setting and could not be compared quantitatively to the work performed in this thesis.

In this project the phase of the fields present in the speckle pattern were measured in the Fresnel diffraction region and not subject to the graces of a laboratory setting. This work parallels Kadono's work by measuring experimentally the phase statistics of laser speckle in the diffraction plane, while Kadono's work was done in the image plane. The present work also goes one step further, in that the experiment was performed out of the laboratory setting and subject to atmospheric effects on the light propagating to and from the target. The targets were also remotely located (1000 meters away) and a reflecting rather than a transmitting (Kadono) diffuse target was used to generate the speckle pattern. Yet qualitatively the present work also indicates a definite relationship between the statistics of the phase of the fields present in the speckle pattern and the r.m.s. roughness of the diffuse targets.

## **1.2 A Brief Overview of the Thesis Problem**

In this work the feasibility of remotely distinguishing between optically diffuse targets is investigated. The work was performed using a CO<sub>2</sub> cw coherent LIDAR system. The transmitted laser beam propagates about 1000 meters, through a turbulent atmosphere, to illuminate a diffuse target. The target scatters the beam back and the returned radiation creates a speckle pattern in the transmitter/receiver plane. The refractive



turbulence and wind in the atmosphere randomly moves the transmitted beam about the target and consequently creates a random motion in the speckle pattern in the transmitter/receiver plane. The phase of the speckle pattern was measured at two points in the receiver plane using a heterodyne process. The random movement of the speckle pattern in the receiver plane allows the sampled data set to contain a complete statistical representation of the phase of the fields present in the speckle pattern.

In the first part of this work, the surface attributes of each diffuse target type were measured using a surface profilometer (contact technique). The types of targets tested were sandblasted aluminum, silicon carbide sandpaper and flame sprayed aluminum. The attributes measured on each of the diffuse targets include: the r.m.s. surface height variance, the surface height distribution, the autocorrelation function and the associated correlation length, and the power spectrum of the spatial frequencies. These measurements were used as a reference for the second part of this work (non-contact technique).

In the second part of this work, the characteristics of the returned speckle pattern were analyzed. The speckle pattern was mixed with an optical local oscillator in the receiver plane to create a heterodyned signal at 100 kHz. Since the phase of the optical wave is preserved in the heterodyne process, it can be recovered from the signal. The difference

between the phase of the fields at two points in the receiver plane was measured. Phase difference (PD) data rather than single point data was used to reduce phase fluctuations (errors) due to the laser transmitter and mechanically induced phase changes.

A phase detector was used to extract the PD data from the heterodyned signal. The phase difference (PD) data was restricted to values between 0 and  $\pi$  by the dynamic range of the phase detector. However the phase of the received optical signal can change by many times  $2\pi$ . Therefore the output of the phase detector needs to be unfolded. This can be accomplished in principle by keeping track of the points in time where the PD data crosses the 0 or  $\pi$  boundary. In this way the PD data can be unfolded in time into phase changes much greater than the 0 to  $\pi$  range of the phase detector. Although unfolding is simple in concept, in practice it can be quite difficult to implement.

The diffuse targets that create the laser speckle pattern consist of two different attributes that affect the phase statistics of the speckle pattern. The first attribute is the microvariations in the surface; this attribute is generally uniform throughout the target and is responsible for such target characteristics as r.m.s. surface roughness, or correlation length. Macrovariations constitute the second attribute and represent large changes in the surface characteristics, such as a warped target, or nonuniformity in target

thickness. Consequently the unfolded phase difference data needs to be high pass filtered to eliminate slow phase changes caused by macrovariations in the target's surface characteristics.

The high pass filtered, totally unfolded phase difference data was then used to create a probability density function (PDF) of the phase difference values. From the PDF's, of the PD data, the targets can clearly be distinguished. As the r.m.s. roughness of the target increases, the corresponding width of the PDF also increases. It is concluded that the phase statistics of the speckle pattern created by a diffuse target are a means by which the target's r.m.s. roughness can be determined. This makes it possible to distinguish, remotely through the atmosphere, between diffuse targets based purely upon the signature of the light scattered by the target.

## CHAPTER 2

### THEORY

The theory corresponding to the two areas of experimental research performed in this thesis have only been partially developed. First, the theoretical description of a diffuse target is somewhat vague. Although much work has been done on characterizing the return radiation from diffuse targets, little effort has been expended in describing the physical make up of the surface of a diffuse target. Secondly, to the knowledge of the author, there exists no theoretical prediction of the statistical nature of the phase of the fields present in the speckle pattern for this system (which includes atmospheric turbulence). However, the theory for systems without turbulence show similiar qualitative results.

#### 2.1 The Requirements For A Diffuse Target

The most comprehensive source of requirements for the structure of a good diffuse target is Goodman's paper, in Dainty's book LASER SPECKLE AND RELATED PHENOMENA [10]. In Goodman's analysis he states several assumptions about the diffuse target on which he develops his work. These assumption have come to be regarded as the quantitative

requirements for the physical surface characteristics of a diffuse target. Goodman makes five assumptions about diffuse surfaces in the development of the statistical nature of laser speckle. They are:

1. The r.m.s. target roughness is many times greater than the wavelength of the light illuminating the surface (Rayleigh's Criteria).
2. The fluctuations in the surface heights of the diffuse surface (target) follow a Gaussian distribution.
3. The target correlation length has no effect on the correlation length of the fields (speckle size) measured in the speckle pattern.
4. The normalized correlation coefficient of the surface heights follows a Gaussian distribution.
5. The amplitude and phase produced by any scattering center on the surface of the target are completely independent.

The applicability of the first three assumptions to this thesis will be discussed in Chapter 3. The last two assumptions were not tested in this or any other work known to this author.

The lack of experimental data on the surface characteristics of diffuse targets has prompted the work done in Chapter 3. Although little work

has been previously done on measuring the surface characteristics of a diffuse target, much work has been done in measuring and developing standards for the amount of energy returned from a diffuse target. Several researchers have already addressed the topic of target reflectance measurements for the diffuse targets used in this thesis [8,9].

## **2.2 Statistical Properties Of Speckle Phase Measurements In The Diffraction Regime.**

The most general results for the statistical attributes of the phase of the fields present in a speckle pattern were developed by Goodman [10]. He concluded that the phase of the fields present in the speckle pattern would obey a uniform distribution (phase density function) in the primary interval. In other words, the phase of the fields present in the speckle pattern are equally likely to take on any value between  $-\pi$  and  $\pi$ . However, this conclusion was based upon the assumption that the diffuse target r.m.s. roughness was many times the wavelength of the light illuminating the target. Goodman's conclusion is no longer valid when the target roughness is on the order of the wavelength of the light [11].

When the target r.m.s. roughness is much less than the wavelength of the light the target assumes a mirror-like nature. A laser illuminating

such a target would produce a specular return; this in turn causes the phase of the fields present in the receiver plane to all have approximately the same value. This produces a delta function in the probability density function (PDF) for the phase of the fields present in the speckle pattern at the receiver plane.

Thus at the two extremes of target roughness are two entirely different PDFs. Targets that are optically rough (r.m.s. roughness  $\gg \lambda$ ) produce a uniform PDF. While at the other extreme, targets that are optically smooth (r.m.s. roughness  $\ll \lambda$ ) produce a delta function PDF. When a diffuse targets r.m.s. roughness is on the order of the wavelength of the illuminating light the corresponding PDF falls somewhere between being uniform and being a delta function.

The region in which the r.m.s. roughness of the target is on the order of wavelength of the light, is known as the resonance domain [12]. A target satisfying this criteria is called an optically weak diffuser. The phase statistics expected when the targets r.m.s. roughness is in this domain have not been fully developed. The speckle phase statistics in the resonance domain depend in part on the r.m.s. roughness of the target [11] (shown in laboratory tests neglecting atmospheric influences). The diffuse targets tested in this thesis all had r.m.s. surface roughnesses in the resonance domain. Thus in theory it may be possible to discriminate between

diffuse targets of different r.m.s. roughness depending on the distribution of the phase of the fields measured in the speckle pattern.

The development of the speckle phase statistics in the resonance domain is not completely void of information. Much of the work was completed by Uozumi and Asakura in 1980 [11]. In their work Uozumi and Asakura developed the probability density function for the speckle phase in the image and diffraction region (Fresnel). Unfortunately their probability density function for the speckle phase in the Fresnel diffraction region was developed without considering the effects of atmospheric interaction on the laser beam. Given the remote nature of the work done in this thesis (2000 meters of atmospheric interaction) their theoretical results cannot be compared quantitatively with the experimental results measured in this thesis.

The lack of theory on the PDF for the speckle phase in the Fresnel diffraction regime under the influence of atmospheric conditions has made it impossible to analytically check the experimental results of this thesis. However, the theoretical results given by Uozumi and Asakura have been very beneficial in predicting qualitatively what type of PDF to expect. In the Uozumi and Asakura work they showed, that for a target whose surface height fluctuations obey a Gaussian distribution, the resulting PDF for the phase of the fields present in the speckle pattern was also Gaussian, when the target's r.m.s. roughness was in the resonance domain. They also



concluded that as the r.m.s. surface roughness of a target progressed from a mirror-like finish, to a surface whose r.m.s. roughness was many times the wavelength of the light, the PDF corresponding to the phase of the fields present in the speckle pattern went from a delta function to a uniform distribution (see Fig 2.1). Thus, although no theoretical work exists to predict the PDF for the phase of the speckle pattern in the Fresnel regime, under the influence of atmospheric interaction, the work of Uozumi and Asakura suggests on a qualitative level the expected PDF will be Gaussian distributed when the target's r.m.s. roughness is in the resonance domain.

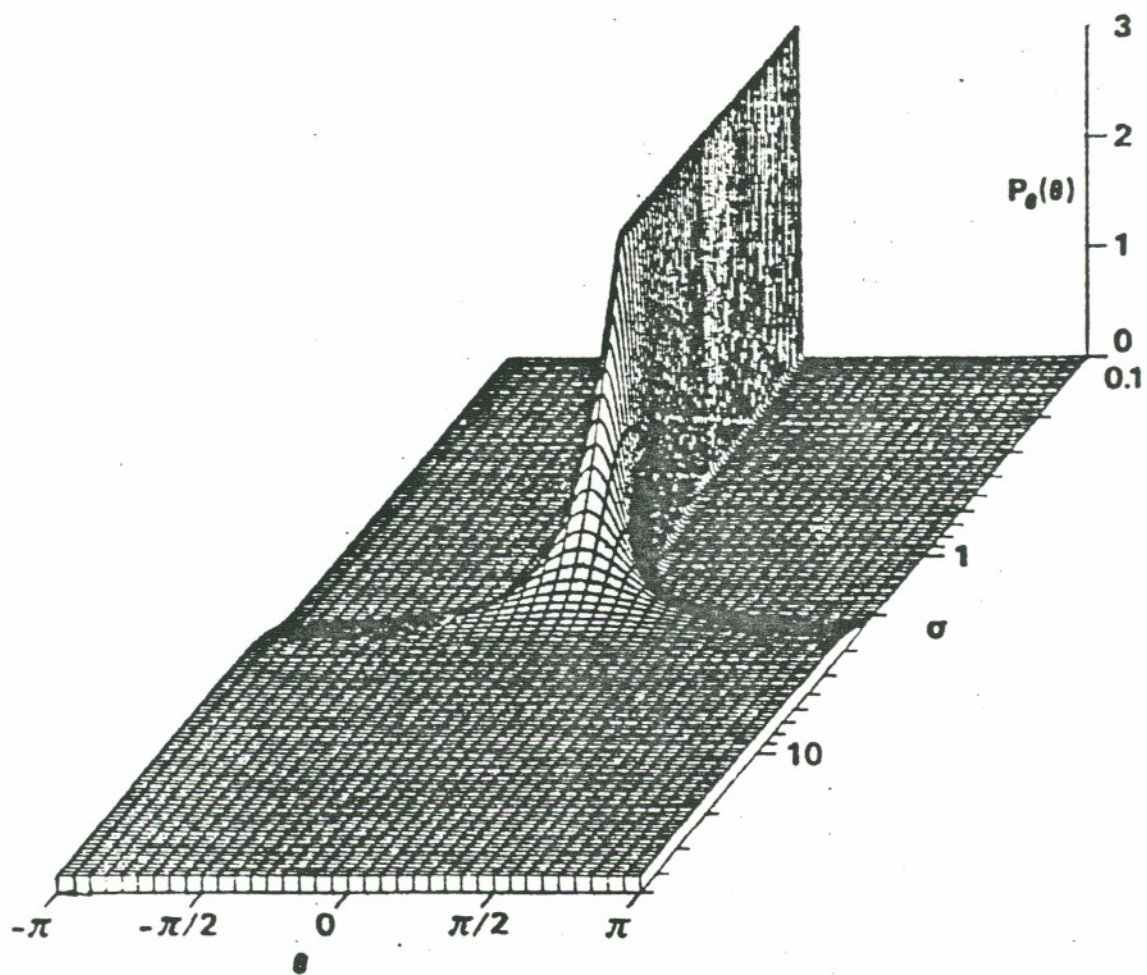


Figure 2.1 Probability density function for the phase of the fields measured in the speckle pattern in the Fresnel diffraction regime, ignoring atmospheric interaction.  $\sigma$  is the standard deviation of the phase of the fields measured at the target.  $\theta$  is the standard deviation of the phase of the fields measured at the receiver. Both  $\sigma$  and  $\theta$  are in units of radians.

## CHAPTER 3

### TARGET ANALYSIS

The first step in the investigation of this thesis problem was to analyze several types of diffuse targets. The types of diffuse targets investigated included sandblasted aluminum, silicon carbide sandpaper and flame sprayed aluminum. Four different surface characteristics were measured on each of the diffuse targets. First the surface height variance (surface height fluctuations) was measured for each target type. Secondly Goodman's assumption [10] that the surface height fluctuations follow a Gaussian distribution was tested. The third attribute measured was the diffuse surface autocorrelation function and its associated correlation length. Finally a power spectrum of the spatial frequencies for each diffuse target type was produced.

#### 3.1 Experimental Set Up For Measuring Surface Profiles.

A Mitutoyo profilometer was used to capture the raw surface profile data (Fig. 3.1). The profilometer consists of a sharp stylus that travels along the surface of the diffuse target at a fixed rate. As the stylus travels along the surface of the material it produces an output voltage

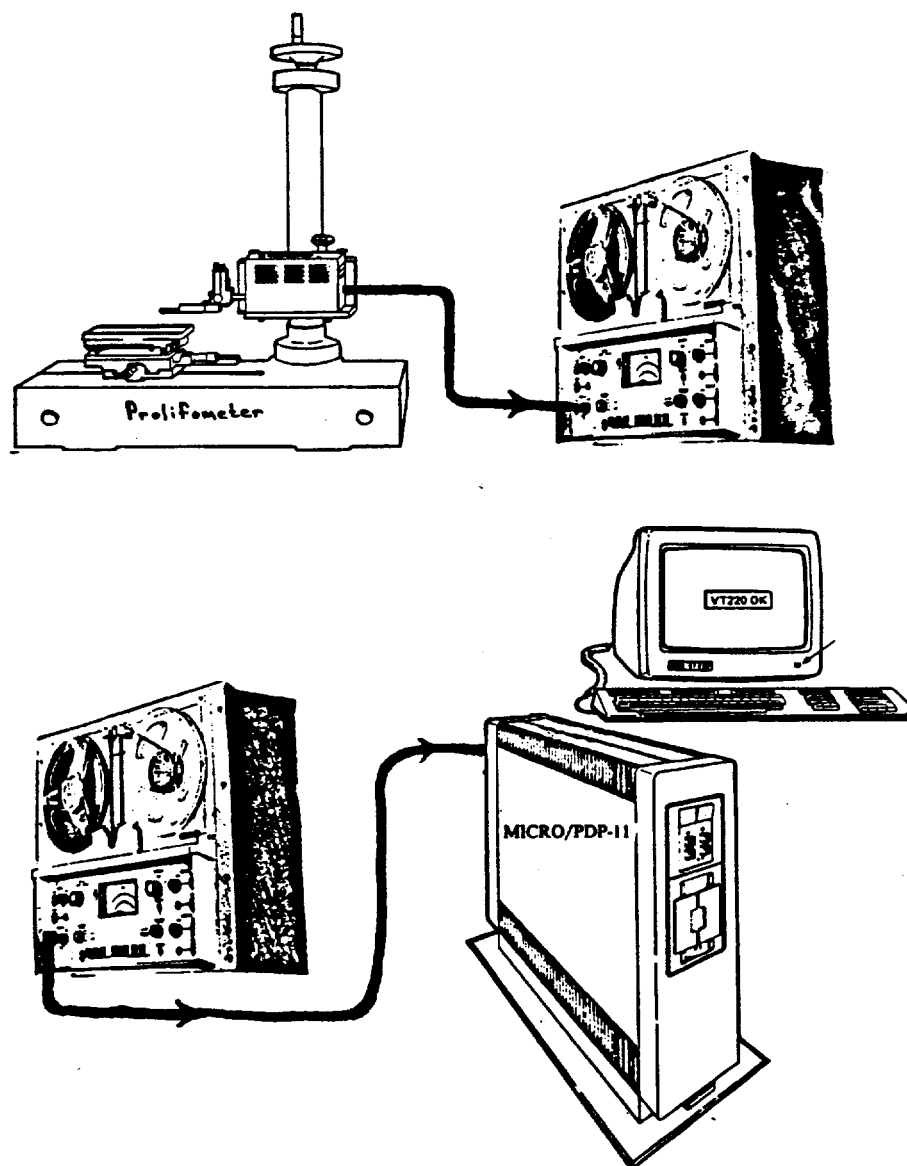


Figure 3.1 Experimental set up for measuring the surface characteristics using a profilometer.

proportional to its vertical displacement. This output voltage is, in essence, a trace of the surface profile in time (Fig. 3.2). The profilometer has a built-in analyzer that converts the output signal into surface characteristics such as, the height of the largest peak, root mean square (r.m.s.) surface height, and arithmetic mean height. Unfortunately the analyzer on the profilometer has only limited analysis abilities, so it was used only to acquire the surface height variance (r.m.s.<sup>2</sup>) of each diffuse target.

To acquire the rest of the statistical characteristics of the surface profile, the profilometer was modified to allow direct access to the analog voltage signal that represented the surface profile. The analog signal was a  $\pm 2$  volt signal that was high pass filtered to eliminate any gradual changes in the target surface height. These gradual changes are often caused by a warped target or nonuniformity in the thickness of the diffuse target. Using this analog signal the raw surface height data was recorded on an analog tape using an instrumentation tape recorder.

At a later time the tape was played back and fed into a micro PDP-11 computer via an A/D (analog to digital converter), for digitization. Using the PDP-11 the analog data was digitized at a sample rate of 250 Hz ( $\Delta t = 4$  msec) and stored on a magnetic tape cartridge. The digitized signal ranged between 1638 to 2458 with a mean value of 2048. A typical example of the digitized data is shown in Figure 3.3. The digitized surface

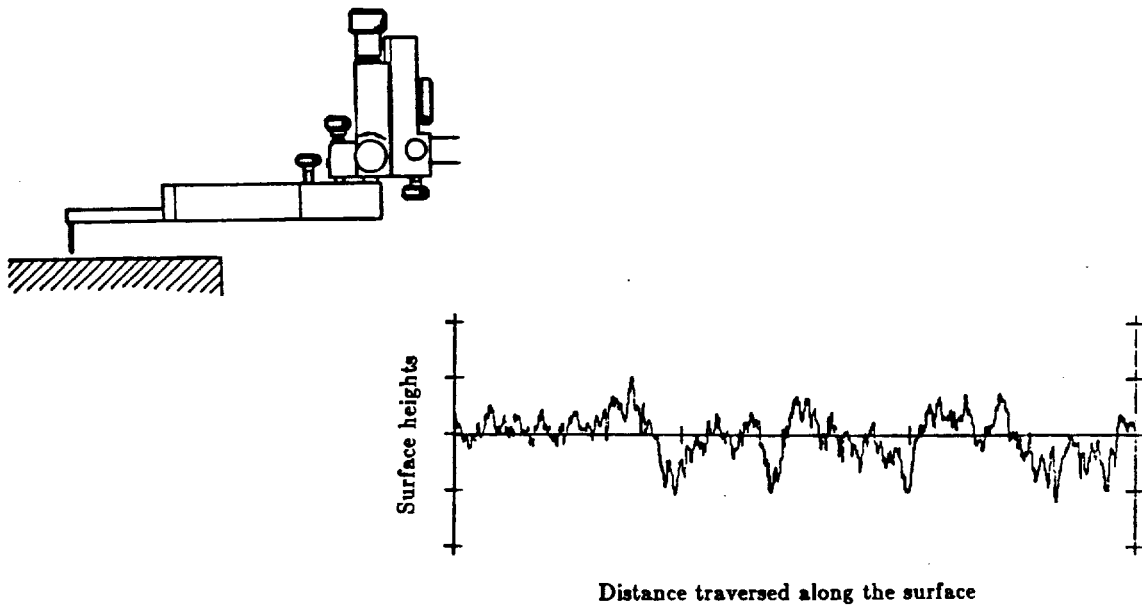


Figure 3.2 Stylus tip of profilometer and typical example of a surface profile.

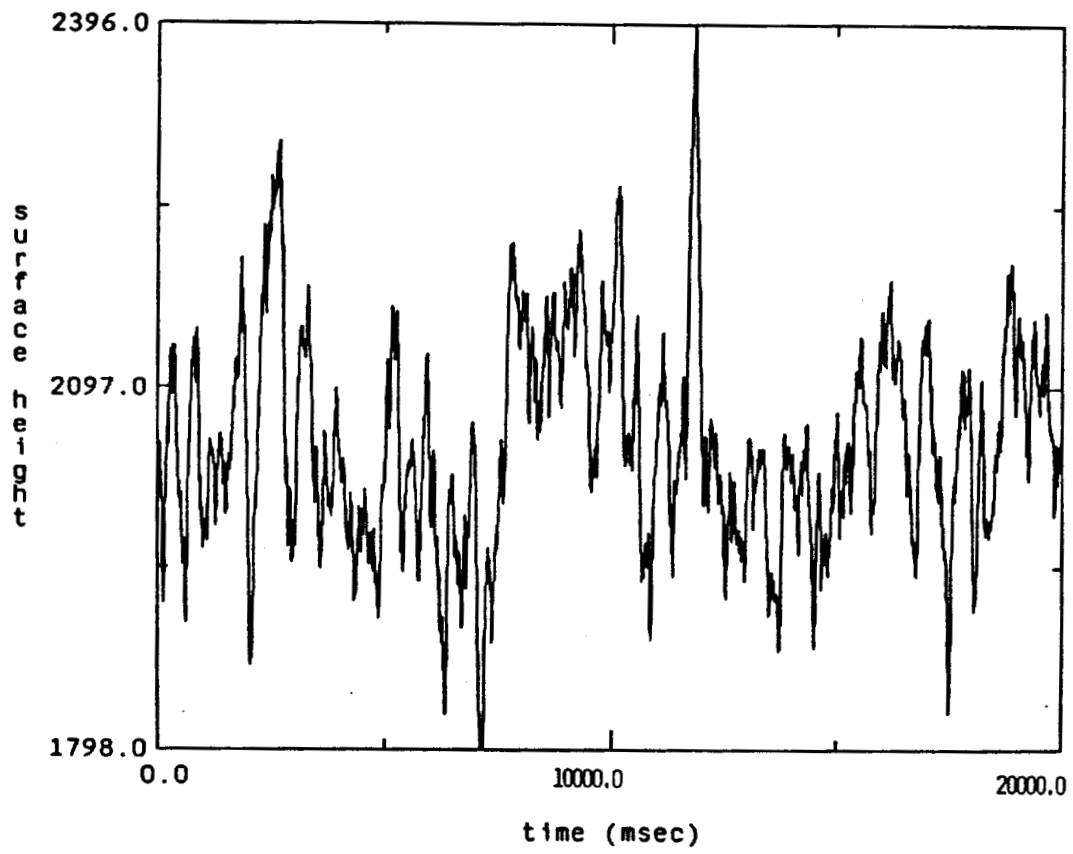


Figure 3.3 Typical example of the digitized surface profile signal.

profile data recorded on the magnetic tape was then transferred to a Microvax II for processing. This process was not performed on the flame sprayed aluminum target (however the r.m.s. surface roughness of the target was measured using the profilometer).

As stated earlier the profilometer traversed the rough surface at a fixed rate. The traversing of the surface lasted for a period of 20 seconds. The average distance traversed by the profilometer, over the rough surface, in one trace (20 sec.) was 8.93 millimeters. From here on, the phrase tracing of the diffuse target (surface), refers to the 20 second stretch of digitized surface profile data that was recorded on magnetic tape. Since the analog signal was sampled at a rate of 250 Hz there will be 5000 points in each file created by tracing the surface.

Each diffuse target type was probed 12 times. The target was probed six times in each of two perpendicular directions. The probings of the target were done along the edge and in the middle of the target. All this was done to insure an accurate statistical representation of the target's surface characteristics.

### **3.2 Target Types**

Six different diffuse targets were created for use in this experiment. A



4 x 4 foot piece of 4046 aluminum was attached by screws and glue to a plywood backing, and then sandblasted. The four grit sizes used in the creation of these targets were 8, 16, 24 and 30. From here on, in this paper, the sandblasted aluminum target created using 8 grit sand will be referred to as 8 grit sandblasted aluminum target, etc. The fifth target was a 600 grit silicon carbide sandpaper and the sixth a sandblasted aluminum target flame sprayed with tungsten nickle.

### 3.3 Average Surface Height (R.M.S.)

The root mean square (r.m.s.) deviation of the surface heights of the targets from the mean were calculated using the intrinsic function of the profilometer. The governing equation is shown in (3.1).

$$\text{r.m.s.} = \left[ \frac{1}{L} \int_0^L F(x)^2 dx \right]^{1/2} \quad (3.1)$$

where  $F(x)$  represents the surface profile and  $L$  is the length of the sample. The  $F(x)$  signal already has the mean surface height subtracted out, so equation (3.1) represents the analog (or continuous) standard deviation of the surface height profile. This data will be useful for comparison at a later time to the sample standard deviation of the digitized surface profile data.

The r.m.s surface height was measured 12 times on each target type. The average of the 12 measurements for each diffuse target is shown in Table 3.1. The average of the 12 r.m.s. measurements is referred to in this thesis as the average surface height of the target.

**TABLE 3.1**

**R.M.S. Surface Heights for Diffuse Targets**

Probing Number	Sandblasted Aluminum ( $\mu\text{m}$ )				Sand Paper ( $\mu\text{m}$ ) 600 Grit	Flame Sprayed Aluminum ( $\mu\text{m}$ )
	30 Grit	24 Grit	16 Grit	8 Grit		
1	5.2	7.0	8.3	12.0	6.6	30.7
2	4.2	9.2	7.3	11.2	7.0	45.7
3	5.2	7.4	8.0	14.0	7.6	39.0
4	5.1	7.4	8.8	14.1	7.3	37.2
5	4.5	7.4	8.7	15.2	5.9	40.2
6	5.0	7.1	8.6	13.2	5.8	50.0
7	4.7	7.3	8.0	9.5	6.3	50.0
8	4.9	7.5	7.8	11.1	5.6	37.5
9	4.4	7.0	7.9	14.5	6.8	33.5
10	5.0	6.8	7.5	11.0	7.7	40.7
11	4.7	6.6	8.0	10.6	8.2	36.5
12	4.9	7.1	8.7	9.5	9.1	33.0
Average R.M.S. Surface Height	4.8	7.3	8.1	12.2	7.0	39.5

### 3.4 Surface Height Distribution

In Goodman's paper [10] he assumes that the distribution of surface height fluctuations (deviation of the surface profile from the mean height) is a Gaussian random process. From the digitized surface profile data (the trace) the accuracy of this assumption was tested. This assumption was not tested for the flame sprayed aluminum target.

The digitized surface profile data consisted of a digital signal varying between 1638 and 2458 that corresponds to the  $\pm 2$  volts analog signal (surface profile). The amplitude of the signal represents the height of the surface profile above or below the midpoint value (2048). From the data taken on each trace of the diffuse target, a histogram was formed of the digital values. The histogram represents the number of times a surface height value was measured above or below the average (mean) surface height. Since each diffuse target was traced 12 times (files formed), there were 12 histograms formed for each diffuse target type. The 12 histograms were averaged together to form an average histogram for each target. The average histogram for each target was then normalized so that the sum of the amplitudes on the curve is one. The average normalized histogram, of the surface height distribution, for one diffuse target type is shown in Figure 3.4.

The sample variance was measured for the average histograms on each diffuse target. The square root of these variance values were calculated and Table 3.2 is a list of the sample standard deviation for each of the averaged histograms. These values were used to generate a Gaussian curve of equal variance. These curves were also normalized to a total amplitude sum of one and overlaid on their respective averaged histogram (also shown in Figure 3.4).

The sample standard deviations listed in Table 3.2 represent the standard deviation of the digitized surface heights from the mean height. These values can be compared directly to the analog values of the surface profiles standard deviation in Table 3.1. By doing this a conversion factor between the digital heights (in integers) and the analog heights (in microns) can be obtained. The best approximation suggests 1 micron equals approximately 7.56 digital increments. This is used to convert the digital numbering basis in Figure 3.4 to a metric numbering basis in Figures 3.5-3.9. Figures 3.5-3.9 represent the averaged histogram for each diffuse target type overlaid with a Gaussian curve of equal variance. From Figures 3.5 - 3.9 it can be concluded that the surface height fluctuations, for all five targets, follow a Gaussian distribution reasonably closely.

**Table 3.2****Sample Standard Deviation for the Digitized Surface Profiles**

(in digital increments)	Sandblasted		Aluminum		Sandpaper
	30 Grit	24 Grit	16 Grit	8 Grit	600 Grit
Digital Standard Deviation	36.5	55.0	60.4	93.5	55.7

Thus Goodman's assumption that a diffuse target's surface height fluctuations obey a Gaussian distribution, is accurate for sandblasted aluminum and 600 grit silicon carbide sandpaper targets.

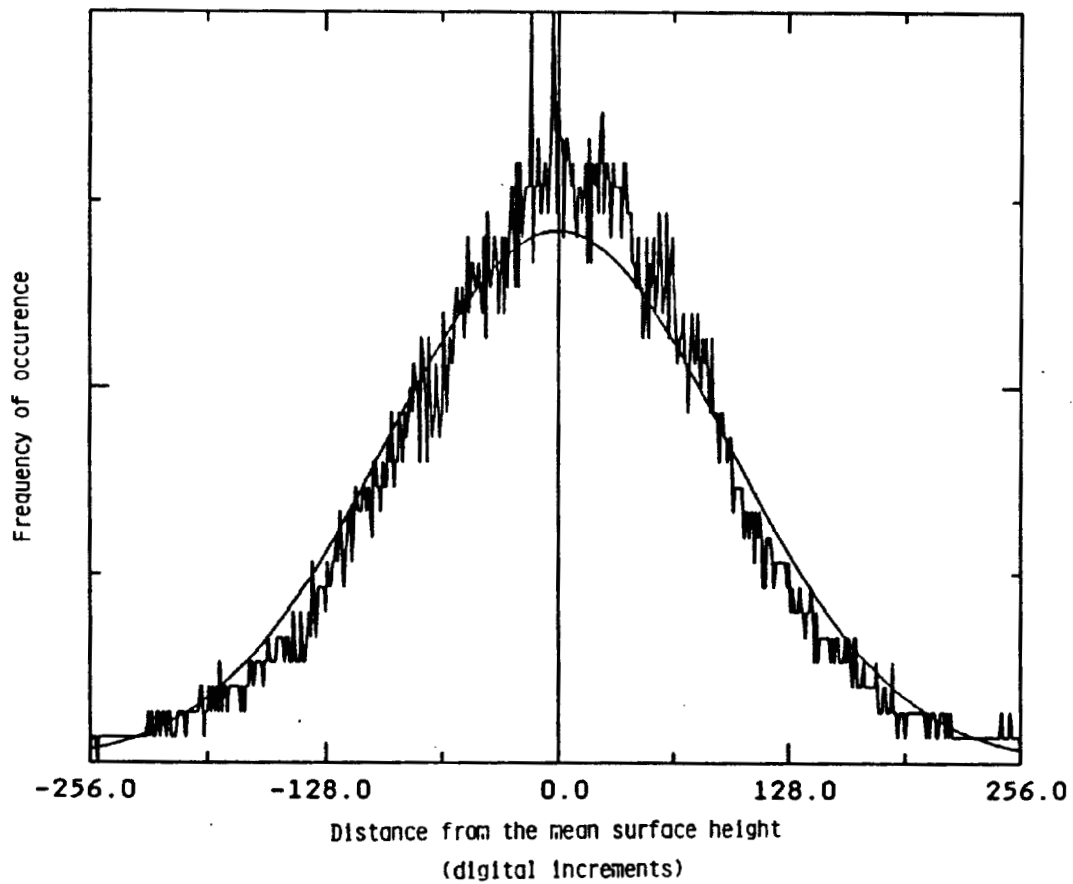


Figure 3.4 Average normalized histogram for 8 grit sandblasted aluminum target. The erratic line represents the measured histogram. The smooth line is a Gaussian curve with a variance equal to the variance of the measured histogram.

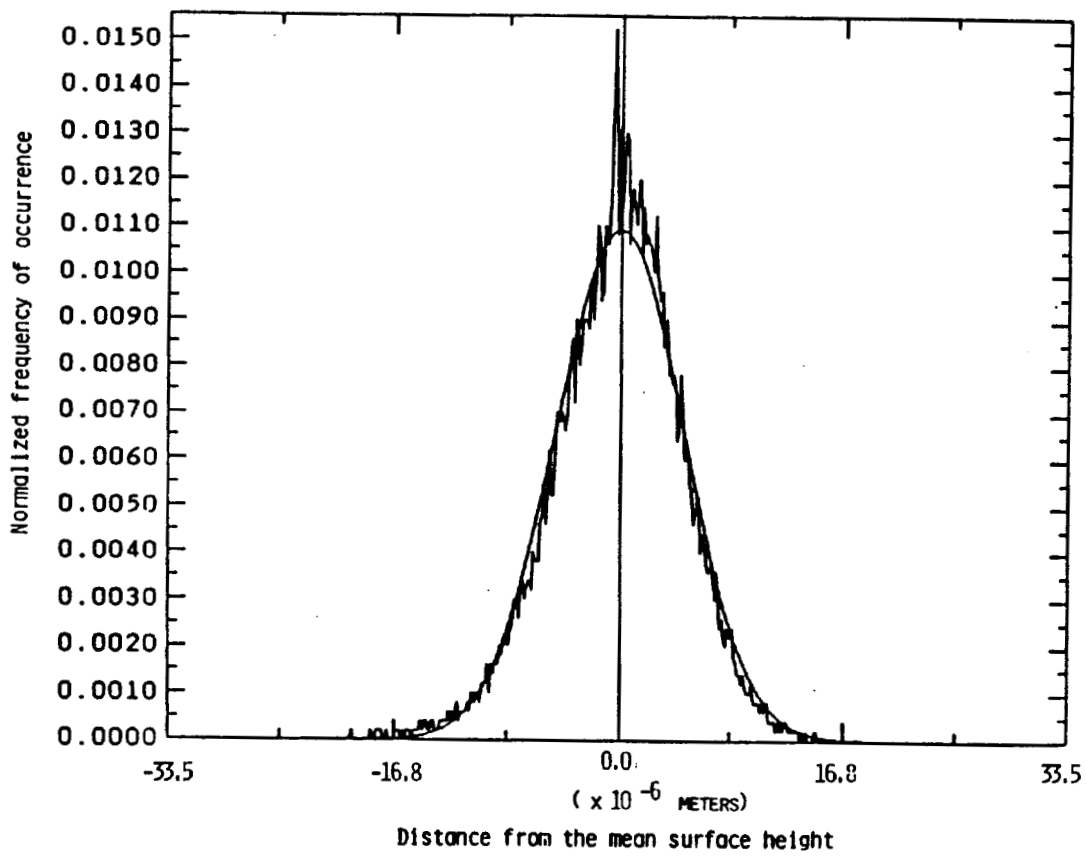


Figure 3.5 Normalized histogram for 30 grit sandblasted aluminum and a Gaussian curve of equal variance.

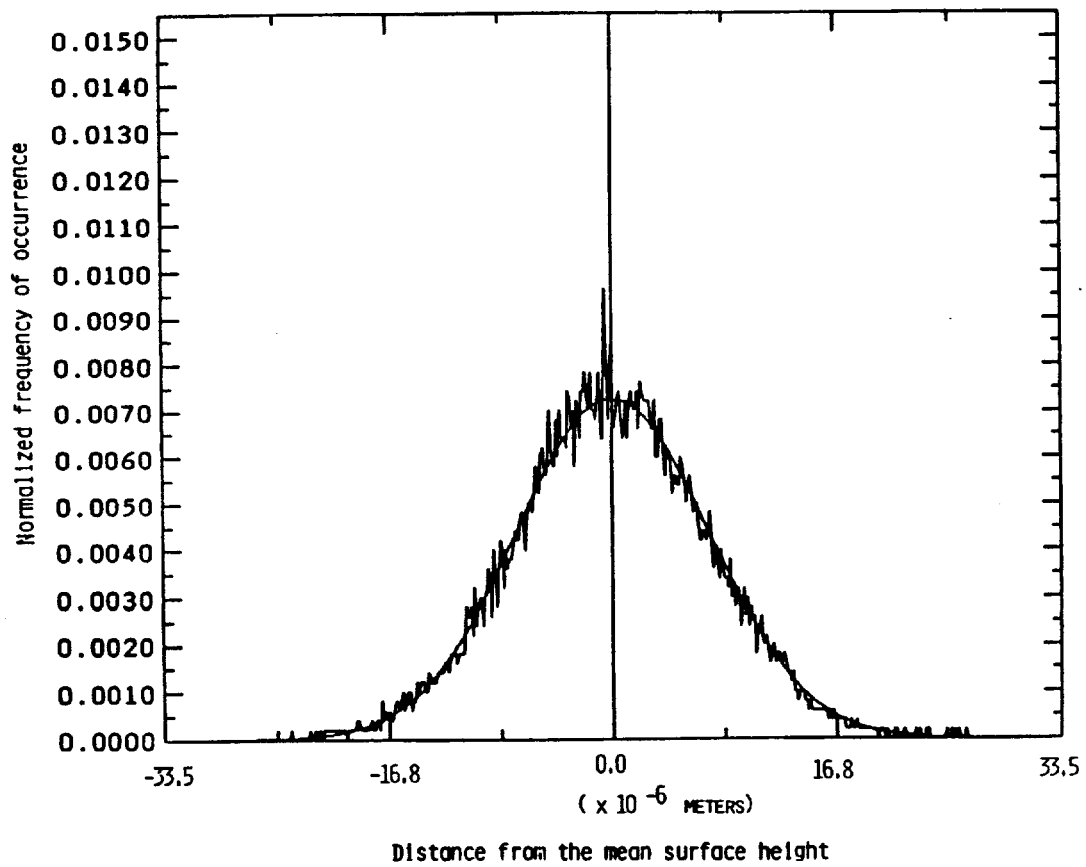


Figure 3.6 Normalized histogram for 24 grit sandblasted aluminum and a Gaussian curve of equal variance.



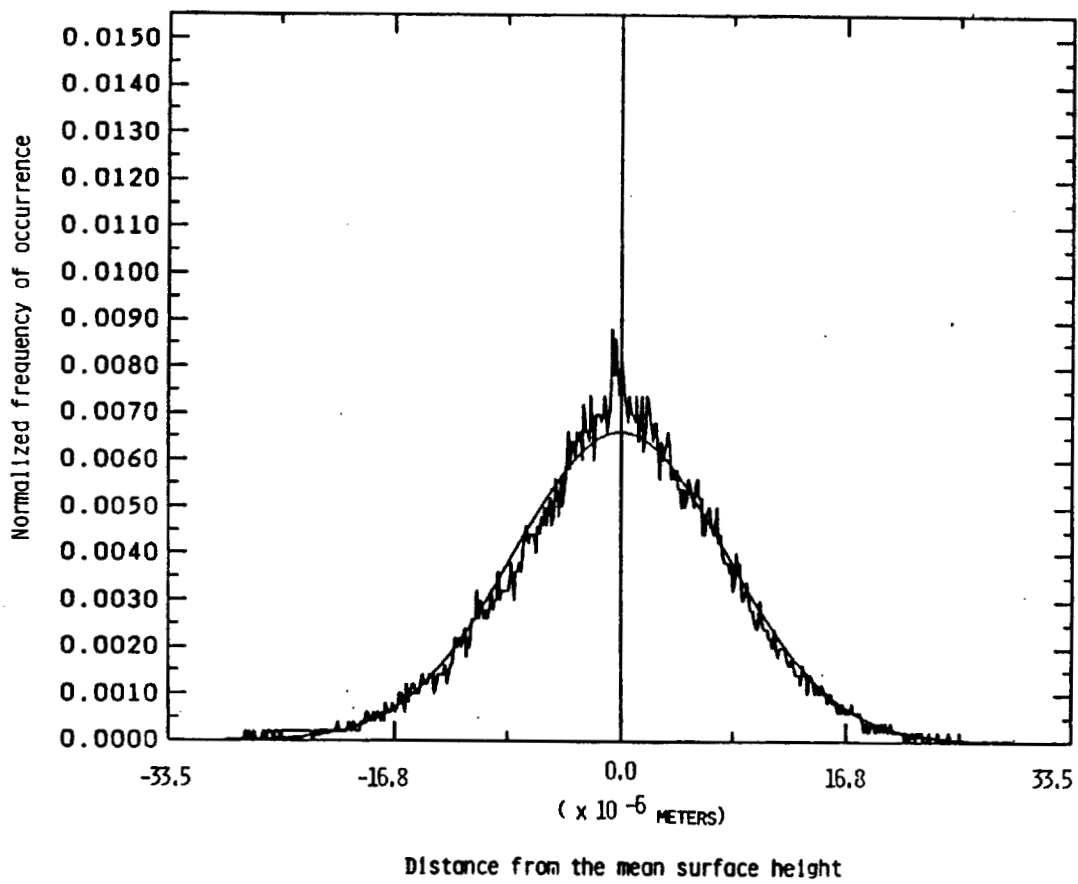


Figure 3.7 Normalized histogram for 16 grit sandblasted aluminum and a Gaussian curve of equal variance.

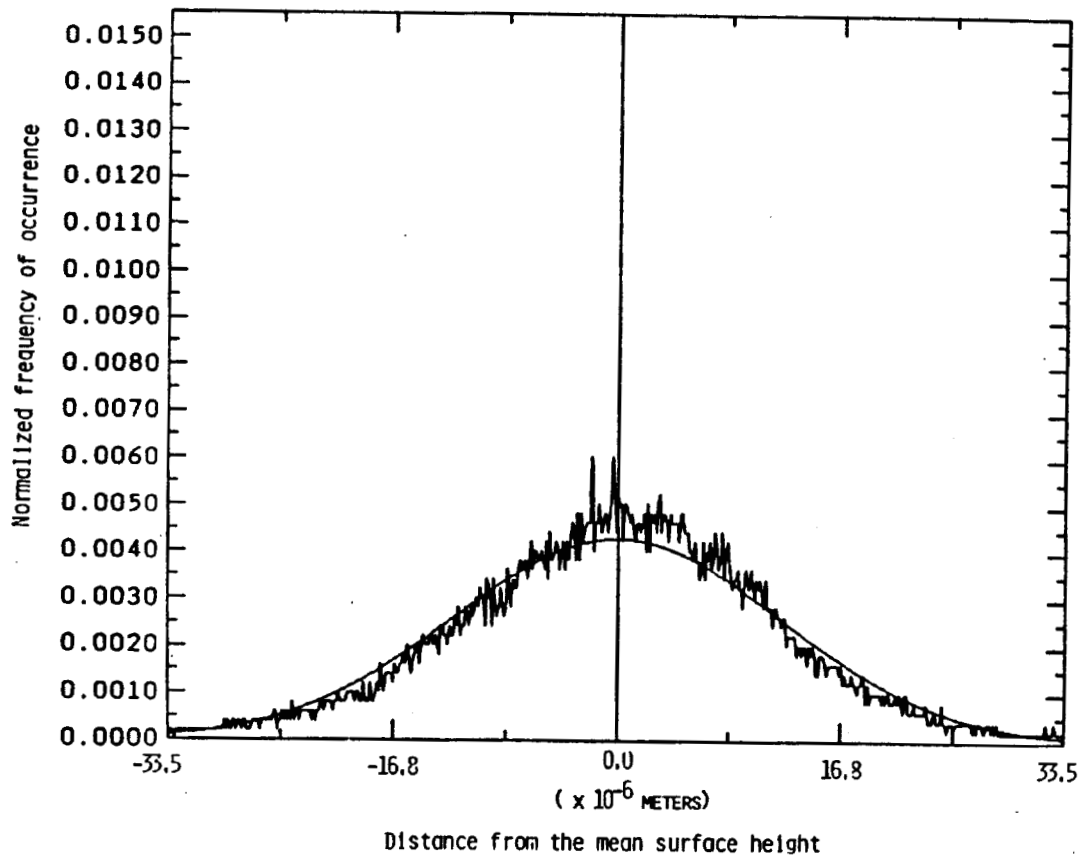


Figure 3.8 Normalized histogram for 8 grit sandblasted aluminum and a Gaussian curve of equal variance.

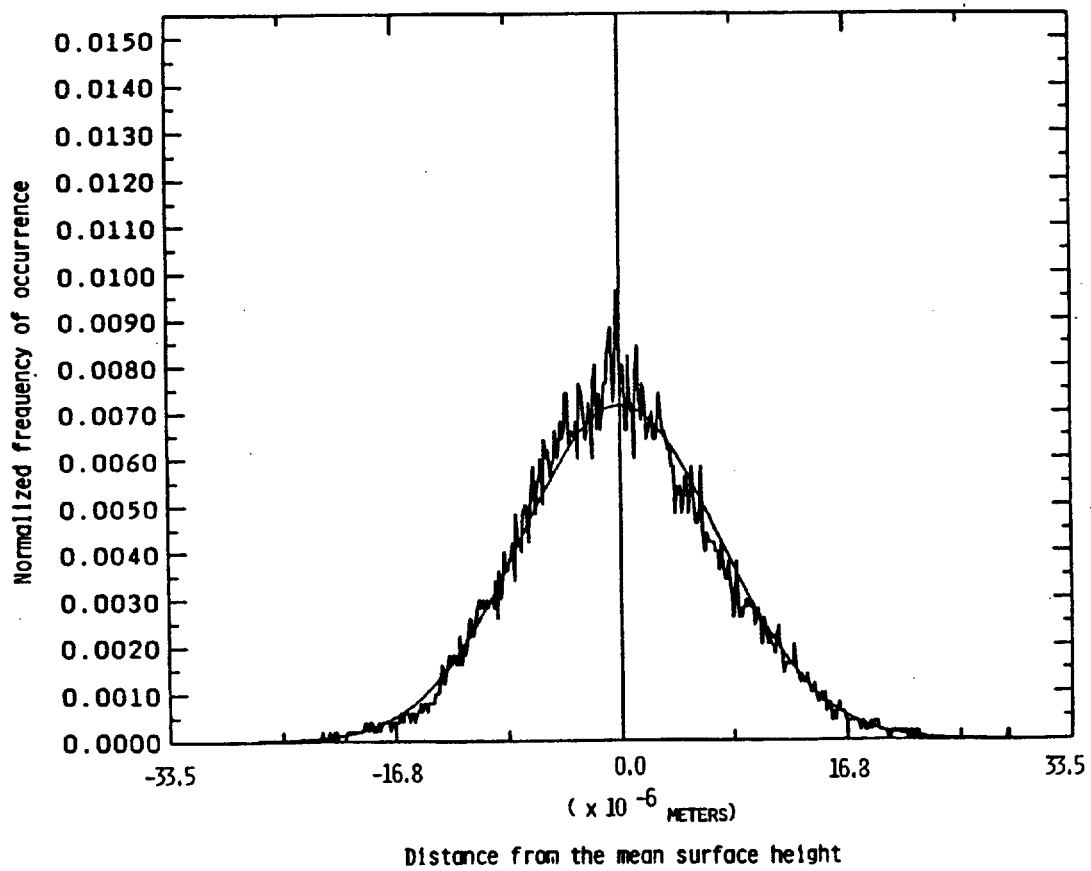


Figure 3.9 Normalized histogram for 600 grit silicon carbide sandpaper and a Gaussian curve of equal variance.

### 3.5 Autocorrelation Function and Correlation Length for Surface Profiles

Using the digitized surface profile data (as shown in Figure 3.3) the autocorrelation function and correlation length for each diffuse target type was calculated (with the exception of the flame sprayed aluminum target). The autocorrelation function was calculated using the NAG library of computer software [13]. The function used to calculate the autocorrelation is given in Eq.(3.2), where  $x_i$  represents the surface height of one of the ( $n=$ ) 5000 points in the digitized surface profile data.

$$r_k = \frac{\sum_{i=1}^{n-k} (x_i - \bar{x})(x_{i+k} - \bar{x})}{\sum_{i=1}^n (x_i - \bar{x})^2}, \quad (3.2)$$

where

$$\bar{x} = \sum_{i=1}^n x_i / n.$$

Since 12 probings were taken on each diffuse target type there were 12 autocorrelation functions for each type of diffuse target. The 12 functions were averaged together to produce the average autocorrelation function for each target type. The average autocorrelation function for each target type is shown in Figures 3.10-3.13. The corresponding average correlation length for each diffuse target type is shown in Table 3.3. The correlation length is

equal to the value of  $i$  in Eq.(3.2) at which the autocorrelation values is equal to  $1/e$  of its peak value.

**Table 3.3**

**The Average Auto Correlation Length**

Diffuse Target Type	Digital Value of the Correlation length (digital increments)	Metric Value of the Correlation length (meters)	Variance in 12 Samples of Correlation Length (meters)
30 Grit Sandblasted Aluminum	24	$4.29 \times 10^{-5}$	$0.52 \times 10^{-5}$
24 Grit Sandblasted Aluminum	24	$4.29 \times 10^{-5}$	$0.46 \times 10^{-5}$
16 Grit Sandblasted Aluminum	28	$5.0 \times 10^{-5}$	$0.87 \times 10^{-5}$
8 Grit Sandblasted Aluminum	54	$9.64 \times 10^{-5}$	$1.7 \times 10^{-5}$
600 Grit Sandpaper	31	$5.54 \times 10^{-5}$	$8.0 \times 10^{-5}$

The profilometer traveled an average length of 8.93 millimeters in each sampling of the target. When the analog signal was digitized it con-

tained 5000 points. Thus the distance between each sample point on the horizontal axis, in the digitized surface profile data, was approximately 1.79 microns. This information was used to translate the horizontal digital values on the correlation function and correlation length into metric values.

One other attribute reflected in Table 3.3 was the variance in the correlation lengths of the 12 traces taken on each target. In the case of sandblasted aluminum the 12 correlation lengths did not deviate significantly from the average correlation length measured for each target ( $< 20\%$ ). The case is quite different however, for the sandpaper target. Its correlation lengths varied greatly, sometimes reaching values twice its mean correlation length.

As can be seen from Figures 3.10-3.13 even after the averaging of the 12 autocorrelation functions the sandpaper displays a strong amount of periodicity which is probably associated with its manufacturing process. No such periodicity is noted in any of the sandblasted aluminum targets.

The correlation lengths measured and shown in Table 3.3 fall under the 100 micron range suggested by Goodman [14]. Fulfilling this criteria, allows the assumption (see assumption 3 of section 2.1) to be made that for a sandblasted aluminum target and an experimental set up as described in this thesis, (Chapter 4) the surface correlation length of the diffuse target has no effect on the correlation length (speckle size) of the speckle

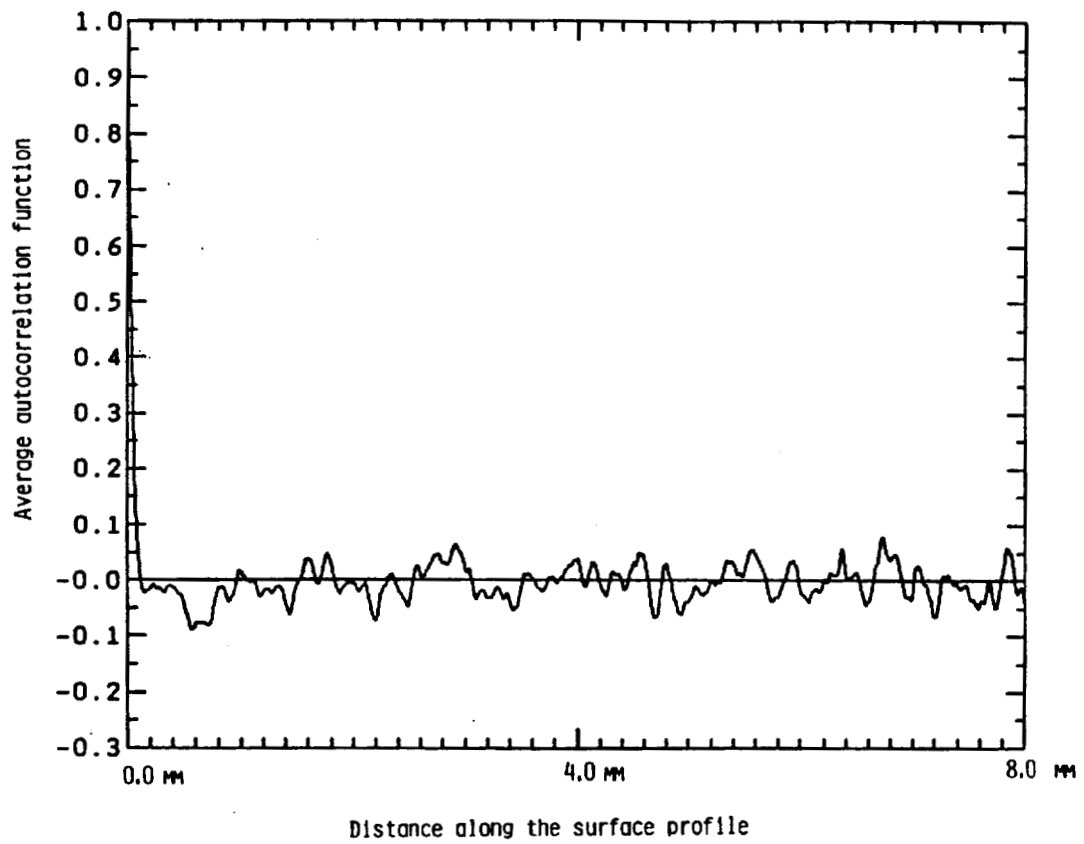


Figure 3.10 The average of the 12 autocorrelation function for the 30 grit sandblasted aluminum target.

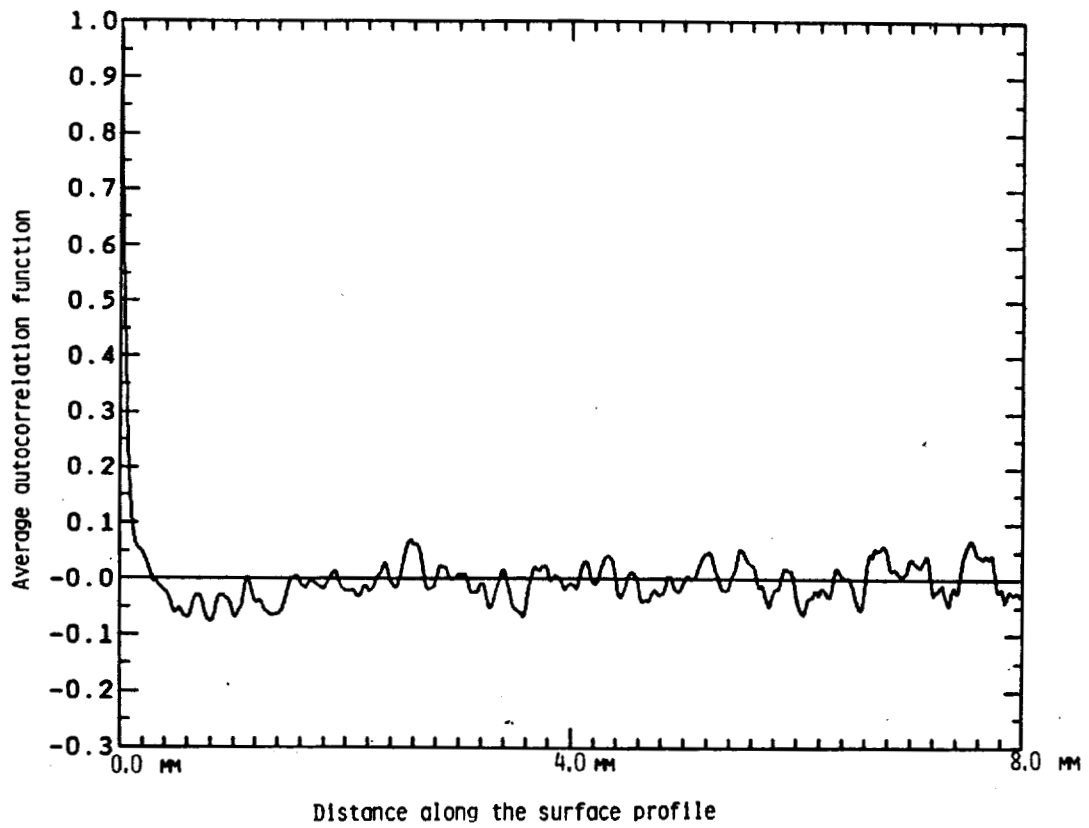


Figure 3.11 The average of the 12 autocorrelation function for the 16 grit sandblasted aluminum target.



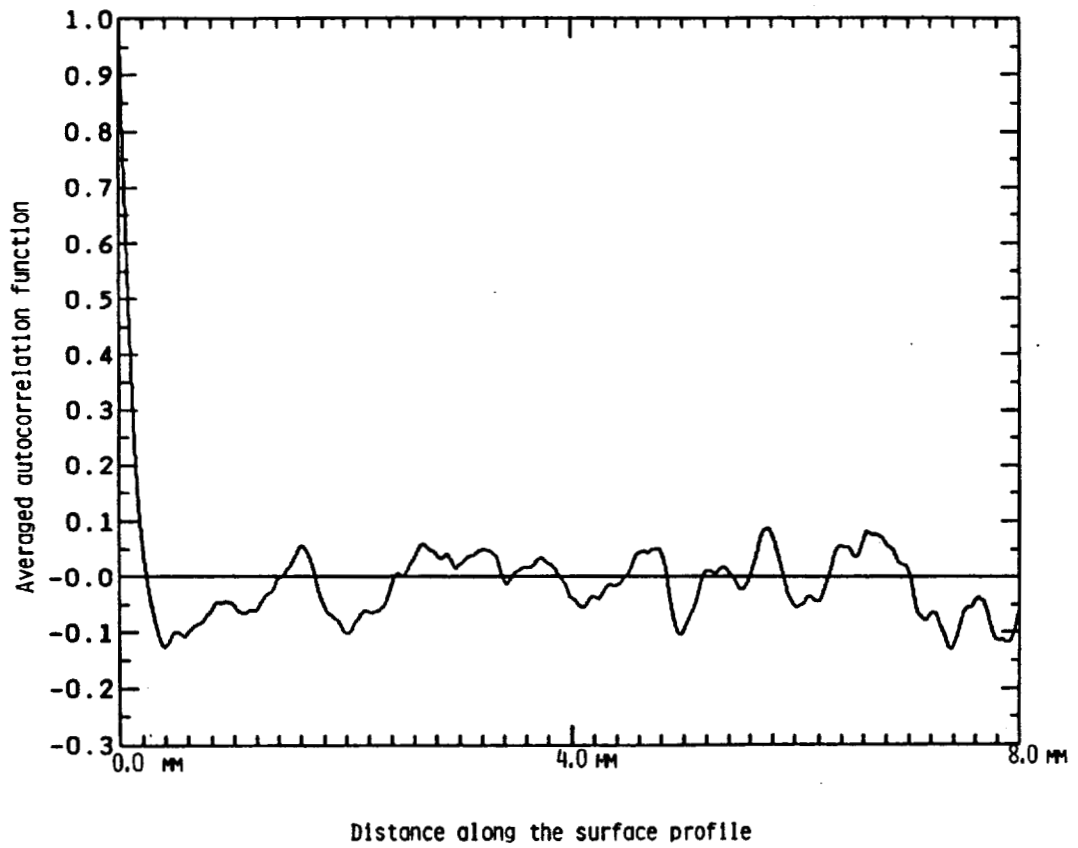


Figure 3.12 The average of the 12 autocorrelation function for the 8 grit sandblasted aluminum target.

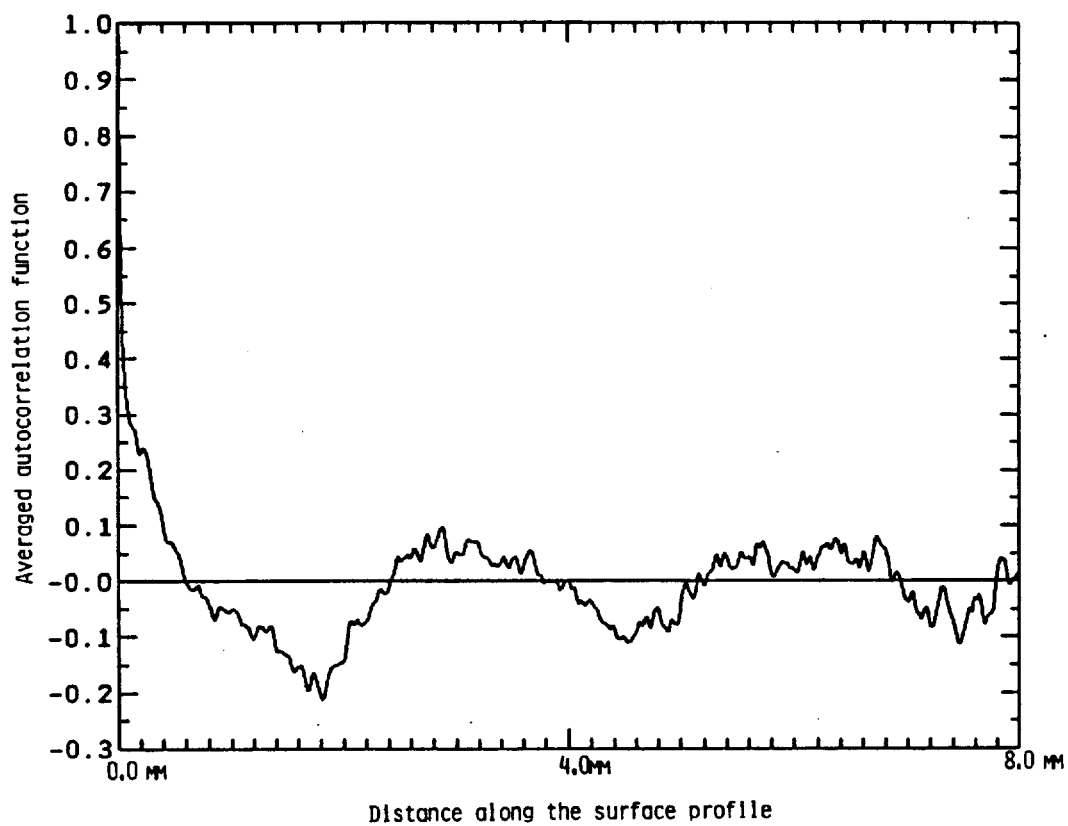


Figure 3.13 The average of the 12 autocorrelation function for the 600 grit sandpaper. The autocorrelation function for the sandpaper shows periodicity.

pattern produced. This assumption does not invalidate the premise of this thesis, that there is a relationship between the statistical attributes of the speckle pattern and the diffuse targets surface characteristics. It just states that such a relationship cannot be found by using the correlation length of the speckle pattern.

### **3.6 Power Spectrum of the Surface Profile**

On each of the digitized surface profiles a fast Fourier transform (FFT) was performed. The FFT was used to produce a power spectrum of the spatial frequencies present in each trace of the diffuse target. Since each diffuse target was traced 12 times there were correspondingly 12 power spectrums. The 12 power spectrums for each diffuse target type were averaged together to produce an average power spectrum for each target type. The average power spectrum of each target type is shown in Figure 3.14.

The convention used to size the grit is that the smaller the grit size number (i.e. 8) the larger in physical size is the grit. Thus, as expected, the larger grits (i.e. 8), used in producing the sandblasted aluminum targets, produced lower spatial frequencies. This is why the larger grits (smaller grit numbers) have more power in the lower frequency end of the

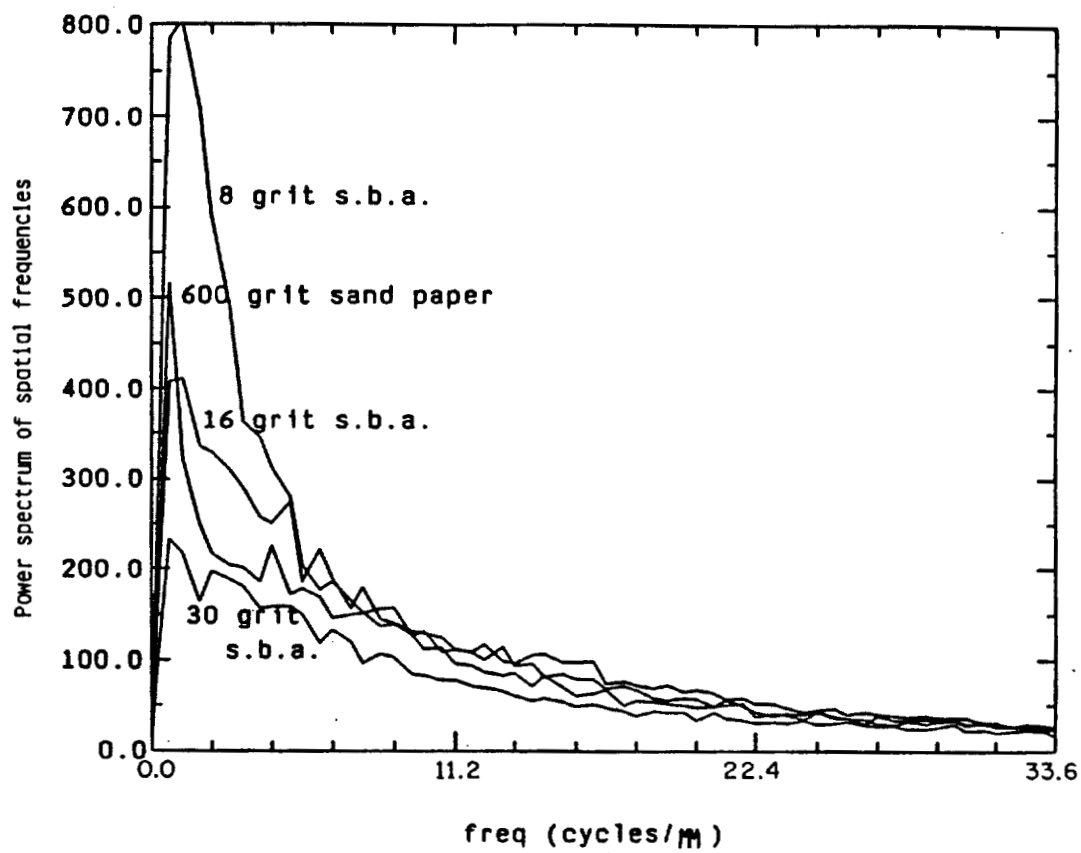


Figure 3.14 The average power spectrum for each diffuse target type.

power spectrum curves shown in Figure 3.14.

### 3.7 Summary of Results

It is concluded that the sandblasted aluminum target can be accurately characterized as a random surface, having a Gaussian distribution in its surface height fluctuations. However one question is still raised as to the validity of calling sandblasted aluminum a good diffuse surface for generating a fully developed speckle pattern in the infrared region ( $\sim 10$  microns). Its average surface heights are only on the order of the wavelength of the light and thus its fulfillment of the rough surface (Rayleigh) criteria might be questionable, however the speckle pattern generated was fully developed and had a normalized variance of unity. As pointed out in Rossi and Maystre [12] paper this region is known as the resonance zone. Further, the specular component of the reflected beam begins to play a much more dominate role in the developed speckle statistics. Thus, for sandblasted aluminum targets in the infrared zone, it may be considered appropriate at times to use the statistics developed by Goodman for speckle with a coherent back background.

The sandpaper failed to show any promise for use as a diffuse target. Although its surface height distribution is Gaussian, its large fluctuations

in correlation length and periodic nature in its correlation function discredit it as an effective randomly diffuse target.

## CHAPTER 4

### SPECKLE PHASE ANALYSIS

The experimental system used to measure the phase of the fields present in the speckle pattern is described in the two sections of this chapter. The first part of the chapter describes the optical heterodyne system (transmitter/receiver). Included in this section is a general overview of the optical system and the electronic instrumentation used to measure the return signal (speckle pattern). The second section contains a description of the type of data obtained from the system and the signal processing routines used to extract the phase statistics of the speckle pattern from this data.

#### 4.1 The Experimental Set Up For Measuring The Phase Of The Fields Present In The Speckle Pattern

##### 4.1.1 Transmitter/Receiver System

A diagram of the transmitter/receiver optical system (optical heterodyne system) is shown in Figure 4.1. The optical source for the system is a CO<sub>2</sub> waveguide laser operating at a wavelength of 10.6 microns. The CO<sub>2</sub>

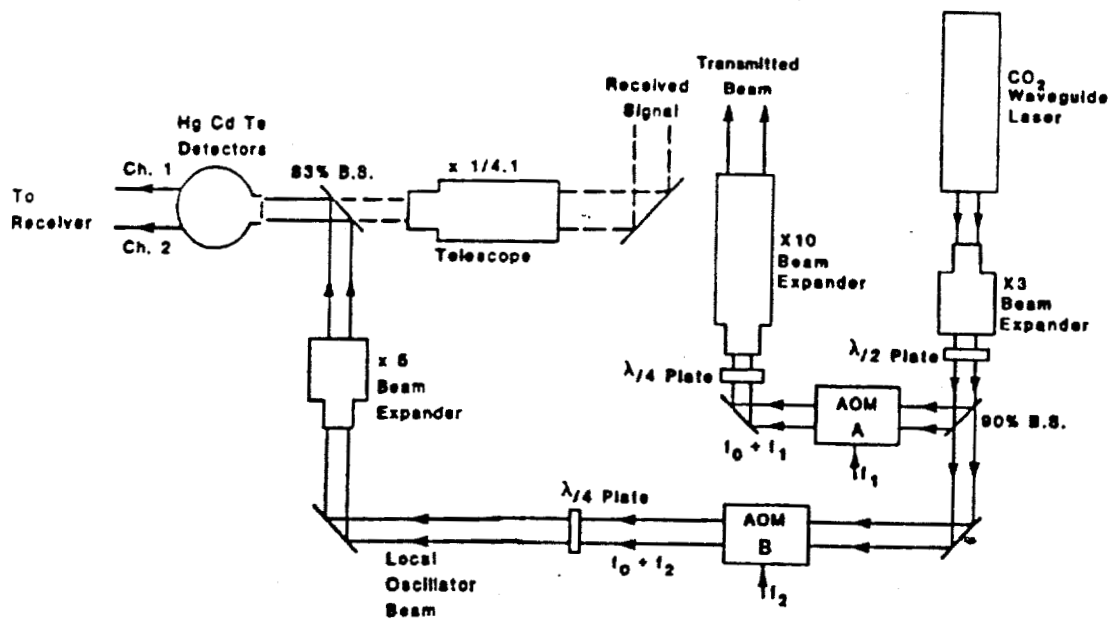


Figure 4.1 The transmitter/receiver optical system used to measure the phase of the fields present in the speckle pattern. The pattern is generated in the far field.



laser beam is first sent through a 3X beam expander and then into a half wave plate where its polarization is changed from horizontal to vertical to match the requirements for the acousto-optic modulator (AOM).

Before entering the AOM, the laser beam is split using a 90% beam splitter. 90% of the beam's energy, a little over one watt, is directed into the first AOM which frequency shifts the laser light by 37.5 MHz. The beam then passes through a quarter-wave plate that circularly polarizes the beam to eliminate fluctuations in the return signal due to polarization changes induced by the target. The circularly polarized beam then passes into a 10X beam expander that is used to focus the transmitted beam on the target.

The remaining 10% of the beam, that passed through the beam splitter, is used as an optical local oscillator (LO). The LO beam first passes into a second AOM where it is frequency shifted by 37.6 MHz. The purpose of using two AOMs is to provide isolation between the transmitted beam and the local oscillator. The LO is then directed into a quarter-wave plate for circular polarization and on into a 5X beam expander. The 5X beam expander provides a collimated beam that is several times larger than the detector, thus providing a plane wave source at the surface of the detector. In the middle (common focus) of the beam expander is a pinhole. The pinhole limits the field of view of the detectors and at the same time

cancel any spherical aberration induced by the lenses. Finally, 83% of the beam (LO) is reflected off a beam splitter and combined with the return signal before illuminating the detectors.

The transmitted beam is scattered by a 4 foot by 4 foot sandblasted aluminum target. The position of the beam illuminating the target changes in time due to the turbulence and the cross winds between the transmitter and the target. The light scattered from the diffuse target creates a speckle field (pattern) back at the receiver. The speckle field is directed by a two inch mirror through an afocal telescope onto a pair of detectors. The telescope is made up of two lenses with focal lengths 25.4 cm and 6.2 cm, yielding a magnification of 4.1. The return signal (speckle field) then passes through the 83% beam splitter to be combined with the local oscillator beam. The detectors are HgCdTe photoconductors and are placed at the focal plane of the first lens in the telescope. The HgCdTe detectors are 2mm x 2mm in dimension and are placed side by side 0.1 mm apart. The use of the telescope in the received signal path gives an effective spacing between the detectors of 8.6 mm.

The heterodyning of the LO signal, frequency shifted 37.6 MHz, and the received signal, frequency shifted 37.5 MHz, produces a signal at the surface of the detector equal to 100 KHz. The constant motion of the beam about the target due to turbulence and the cross wind keeps the

speckle field constantly moving about the plane of the detector. Thus the intensity measured by the detector is constantly changing. A more in-depth explanation of the optical system can be obtained by referring to the work done by Amzajerjian [15].

#### 4.1.2 Amplifiers and Phase Detectors

A block diagram of the electronic instrumentation used to measure the difference between the phase of the fields at two points (two detectors) in the speckle pattern, is shown in Figure 4.2. To understand conceptually the functionality of each piece of electronic instrumentation and the role it plays in measuring the phase of the fields present in the speckle pattern, the equations involved in the heterodyne process will be briefly reviewed.

Let  $E_1$  (Eq. 4.1) represent the amplitude and phase of the field present at both of the HgCdTe detectors due to the local oscillator.

$$E_1 = A_1 \cos[W_1 t] \quad (4.1)$$

The local oscillator is mixed at the face of the detectors with the speckle field created by the radiation scattered from the diffuse target in the direction of the receiver. The speckle field differs in amplitude and phase from point to point in the plane of the receiver (i.e. the speckle pattern).

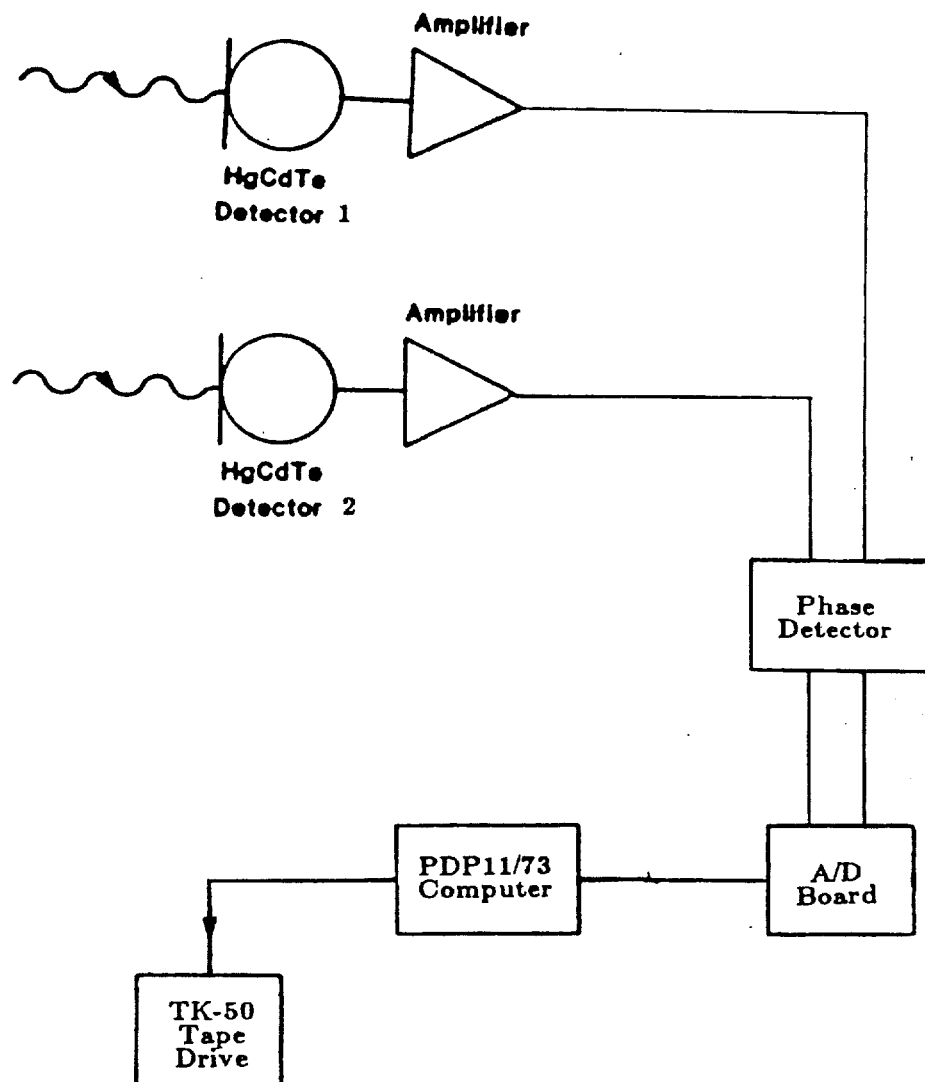


Figure 4.2 Electronic instrumentation used to measure the phase difference data.

Let the fields falling on the two detectors due to the return radiation (speckle pattern) be represented by  $E_2$  (Eq. 4.2) and  $E_3$  (Eq. 4.3).  $W_1$  is the optical frequency of the laser beam up-shifted by 37.6 MHz due to the second AOM (or the optical frequency of the LO) and  $W_2$  is the optical frequency of the laser beam up-shifted by 37.5 MHz due to the first AOM (or the optical frequency of the transmitted beam).

$$E_2 = A_2(t) \cos[W_2 t + \phi_2(t)] \quad (4.2)$$

$$E_3 = A_3(t) \cos[W_2 t + \phi_3(t)] \quad (4.3)$$

The amplitude and phase of the return signal changes in time due to the movement of the speckle pattern about the receiver plane (caused by turbulence in the beam propagation path). The phase of the speckle pattern (returned radiation) at each of the detectors is represented by  $\phi_1(t)$  and  $\phi_2(t)$ . The difference between the phase measured at each of the detectors, in time, is the information extracted by the electronic instrumentation.

The heterodyned signal created and detected by the HgCdTe detectors is found by adding the local oscillator (field) and returned signal (field) at each detector and taking the square of the sum to produce the intensity (yielding Eqs. 4.4 and 4.5).

$$I_1(t) = [E_1]^2 + [E_2]^2 + 2E_1 E_2 \quad (4.4)$$

$$I_2(t)=[E_1]^2+[E_3]^2+2E_1E_3 \quad (4.5)$$

Since the frequency response of the HgCdTe detector is relatively low it does not sense optical frequencies and the first two terms in Eq. 4.4 and Eq. 4.5 have no effect on the intensity measured by the detectors. Therefore these terms are dropped from the equations. The third term in each of the above equations can be expanded by using a cosine product rule, yielding Eqs. 4.6 and 4.7.

$$I_1(t)'=[A_1A_2(t)]\text{Cos}([W_1-W_2]t+\phi_2(t))+\text{Cos}([W_1+W_2]t+\phi_2(t)) \quad (4.6)$$

$$I_2(t)'=[A_1A_3(t)]\text{Cos}([W_1-W_2]t+\phi_3(t))+\text{Cos}([W_1+W_2]t+\phi_3(t)) \quad (4.7)$$

Again the detectors are not sensitive to signals in the optical regime. Thus the  $W_1+W_2$  term in the above equations does not effect the HgCdTe detectors. Eliminating these terms in Eqs. 4.6 and 4.7 yields Eqs. 4.8 and 4.9, respectively.

$$I_1(t)''=[A_1A_2(t)]\text{Cos}([W_1-W_2]t+\phi_2(t)) \quad (4.8)$$

$$I_2(t)''=[A_1A_3(t)]\text{Cos}([W_1-W_2]t+\phi_3(t)) \quad (4.9)$$

Equations (4.8) and (4.9) represent the heterodyned signals actually detected by the two HgCdTe detectors. The signals out of the detectors are amplified before being sent to the phase detector for processing. The

amplified signal is equal to the original signal times an amplification constant (K).

$$S_1(t) = K[A_1 A_2(t)] \cos([W_1 - W_2]t + \phi_2(t)) = KI_1(t)'' \quad (4.10)$$

$$S_2(t) = K[A_1 A_3(t)] \cos([W_1 - W_2]t + \phi_3(t)) = KI_2(t)'' \quad (4.11)$$

The amplified heterodyned signals, Eqs. 4.10 and 4.11, are processed by the phase detector (see Appendix 1 for schematic of phase detector) to extract the difference in the phase of the fields measured at the two detectors ( $\propto \phi_1(t) - \phi_2(t)$ ). The phase detector produces a voltage signal (between 0 - 2.5 volts) proportional to the phase difference ( $\phi_1(t) - \phi_2(t)$ ) in time. The phase detector is limited to detecting phase difference (dynamic range) in the 0 to  $\pi$  region. In this detection scheme, 0 volts is equal to 0 radians phase difference and 2.5 volts is equal to  $\pi$  radians phase difference. Phase difference values greater than  $\pi$  are mapped into the 0 to 2.5 volt region in a symmetric manner (see Figure 4.3). An extensive discussion of resolving phase difference values greater than  $\pi$  or less than 0 radians is investigated in section 4.2 of this chapter. A typical example of the phase difference data produced by the phase detector is shown in Figure 4.4.

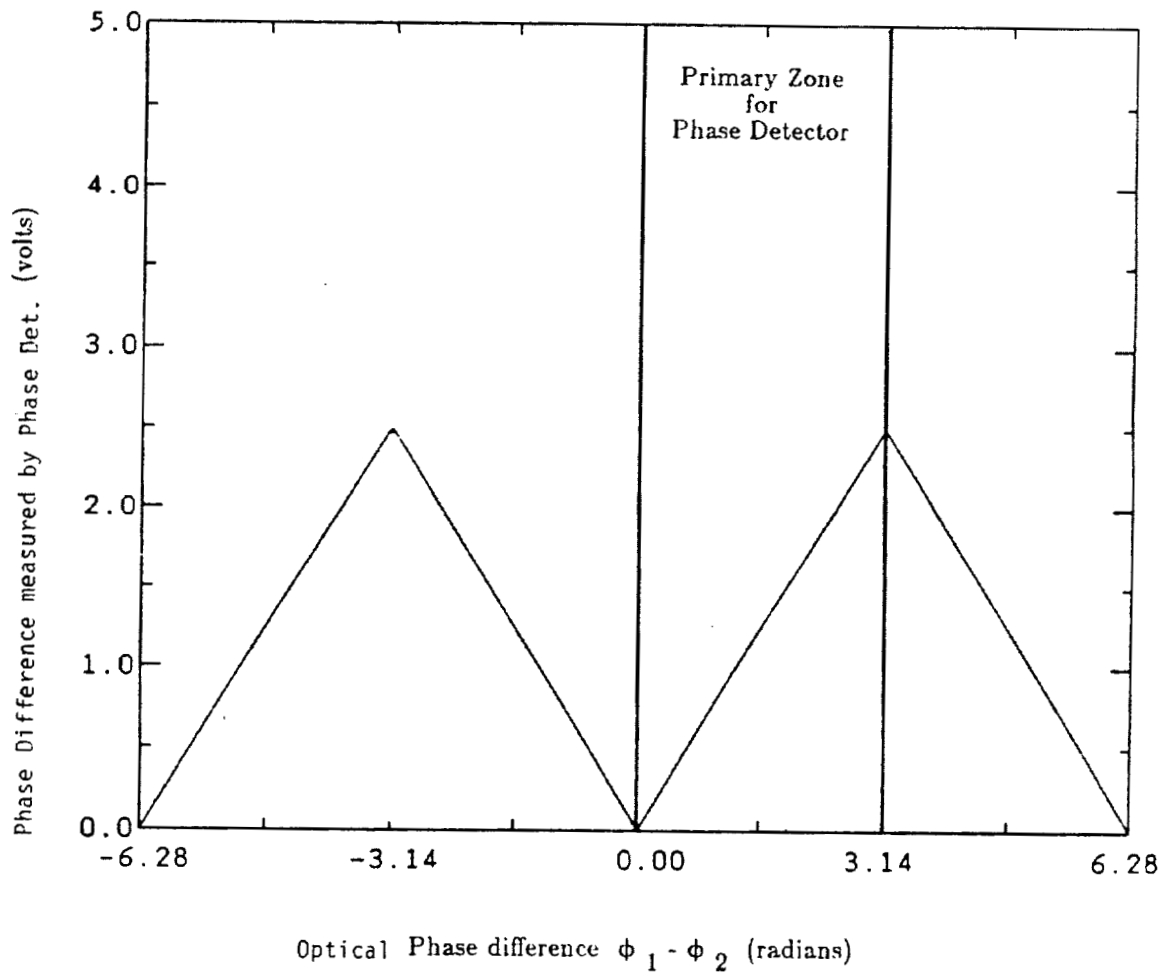


Figure 4.3 Example of the functionality of the phase detector. Phase difference values greater than  $\pi$  or less than 0 (radians) are mapped into the primary zone in the phase detector output.



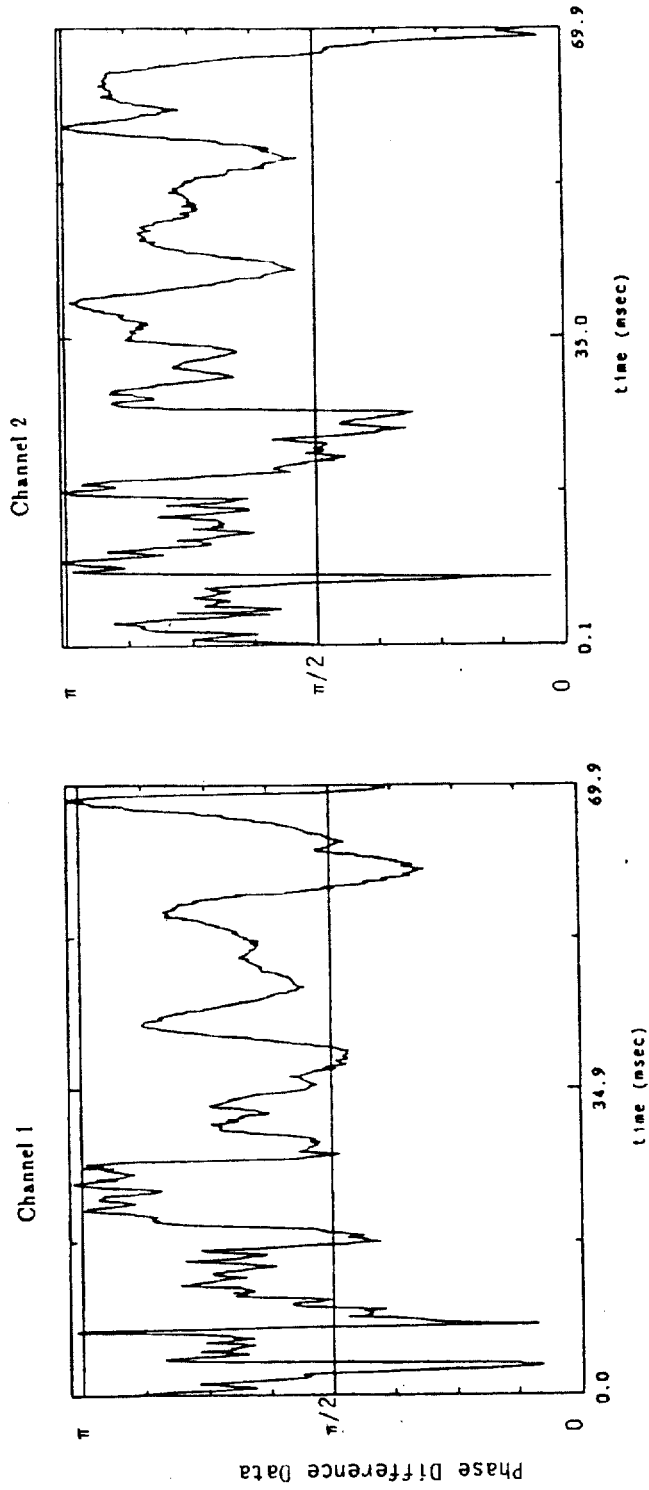


Figure 4.4 Typical example of the two channels of phase difference data, outputted by the phase detector.

The phase detector actually produces two channels of phase difference data. The first channel is as previously mentioned proportional to the difference between the phase of the fields ( $\phi_1(t) - \phi_2(t)$ ) measured at the two HgCdTe detectors. The second channel of data produced by the phase detector, is proportional to the phase difference plus  $\pi/2$  ( $90^\circ$  or  $\phi_1(t) - \phi_2(t) + \pi/2$ ). The second channel of information is used to unfold the phase difference data into the region that extends beyond the  $\pi$  dynamic range of the phase detector.

#### 4.1.3 A/D and Computer

The two channels of phase difference data produced by the phase detector are fed into a ADV11-A analog to digital (a/d) converter. The a/d is installed in a PDP11/73 computer that controls the sampling rate of the a/d board (see Figure 4.2). The analog phase difference data was sampled at a 70 microseconds ( $\mu\text{sec}$ ) rate. Since there were two channels of phase difference data connected to the a/d, the computer sampled each channel every 140  $\mu$  secs. The a/d was set up to digitize analog signals between  $\pm 5$  volts. The corresponding digital values ranging from 0 to 4096 (digital increments). Since the phase difference data (produced by the phase detector) ranged only between 0 to 2.5 volts, the corresponding digi-

tized data recorded ranged only from 2048 (0) to 3072 ( $\pi$ ) digital increments (radians).

The two channels of digitized phase difference data were stored in a buffer to ensure a continuous sampling of the analog data. The digitized data was then transferred to a TK-50 tape for processing at a later date. The computer memory was set up to record a maximum of 4.1 seconds of continuous data in each set. However only 3.5 seconds of each set of data was needed to generate the statistics of the phase difference data.

#### 4.2 Phase Data Analysis Tools

The phase difference data was analyzed statistically to try and find a relationship between the phase of the fields present in the speckle pattern and the roughness of the diffuse target used to generate the speckle pattern. The analysis of the phase difference data, recorded on a tk-50 (magnetic) tape cartridge, was performed in three major steps. First the raw phase difference data (see Figure 4.4) ,varying between 0 to  $\pi$ , was unfolded into phase difference changes varying from 0 to  $2\pi$  and then unfolded into phase difference changes greater than  $2\pi$  or less than 0 radians. This data was then high pass filtered to eliminate phase fluctuations caused by macrovariation in the surface roughness. From this high

pass filtered phase difference data a phase difference density function was created. Finally, a Gaussian curve was fitted to the phase difference density function and the standard deviation of the Gaussian curve measured. The standard deviation of the phase density function was the unique characteristic that linked the phase of the fields present in the speckle pattern to the r.m.s. roughness of the diffuse target.

#### 4.1.2 Unraveling The Phase Difference Data

The phase difference (PD) data was restricted to values between 0 and  $\pi$  by the dynamic range of the phase detector. However the phase of the received optical signal ( $\phi_1(t) - \phi_2(t)$ ) can change by many times  $2\pi$ . Therefore the output of the phase detector needs to be unfolded. This can be accomplished in principal by keeping track of the points in time where the PD data crosses the 0 or  $\pi$  boundary (see Appendix 2 for phase unfolding routine). In this way the PD data can be unfolded in time into phase changes much greater than the 0 to  $\pi$  range of the phase detector. Although unfolding is simple in concept, in practice it can be quite difficult.

Before proceeding further it is appropriate to consider, in some depth, the feasibility of unfolding data beyond the primary zone (dynamic range

of the phase detector) in which it was measured. For instance, whether the optical phase difference equals  $\pi$  or  $-\pi$  the phase difference measured at an isolated point in time by the phase detector is the same (see Figure 4.3). Suggesting that phase unfolding is an unrealistic process. However if the phase difference changes continuously in time, it is possible to resolve phase changes greater than the dynamic range of the phase detector by tracking the phase boundary transitions in time. In other words, as the phase is measured in time it may transition beyond the primary zone (i.e. past the  $\pi$  boundary) of the phase detector. However an observer would understand that the phase has just evolved past the primary zone (boundary) of the detector and the actual phase difference value is the current reading of the phase detector plus the dynamic range ( $\pi$ ) of the phase detector.

An illustration will help considerably at this point. Imagine a (12 hour) clock with only an hour hand. The clock is placed in a room with no windows or other sources for distinguishing whether it is night or day outside. An observer (graduate student) is somehow disoriented (too much homework) such that he loses his present perception of time. At 9:00 o'clock (on the clock in the room) the graduate student is placed in the room with the clock where he keeps an accurate measurement of the time. However, without a knowledge of whether it was night or day outside the

room, the observer could not distinguish between 9:00 am and 9:00 pm or the day of the week. If, however, the graduate student had been placed in the room at 9:00 am on a Monday morning and continuously monitored the clock he could distinguish between 9 am and 9 pm on the same clock. He accomplishes this by keeping track of the number of times the clock makes a transition past 12:00. Thus by periodically checking the clock an observer could resolve the clock that only had a dynamic range of 12 hours (primary zone) into a clock that read 0 to 24 hours or even 0 to infinitely many hours. This same concept can be applied to unfolding the phase difference measurements past the 0 to  $\pi$  dynamic range of the phase detector. By keeping track of the number of times the PD data transitions the boundary of the phase detector, the original optical phase difference ( $\phi_1(t) - \phi_2(t)$ ) data can be recovered.

The necessity of the second channel of phase difference data is not obvious from the above illustration. The second channel of phase difference data is needed because the phase detector is not restricted to move only in the clockwise direction, as was the clock in the above illustration. An example should help clarify this point. Figure 4.5 is an example of the optical phase difference and the corresponding PD data measured by channel 1 of the phase detector. In time the optical phase difference and the phase difference measured by channel 1 of the phase detector increase until

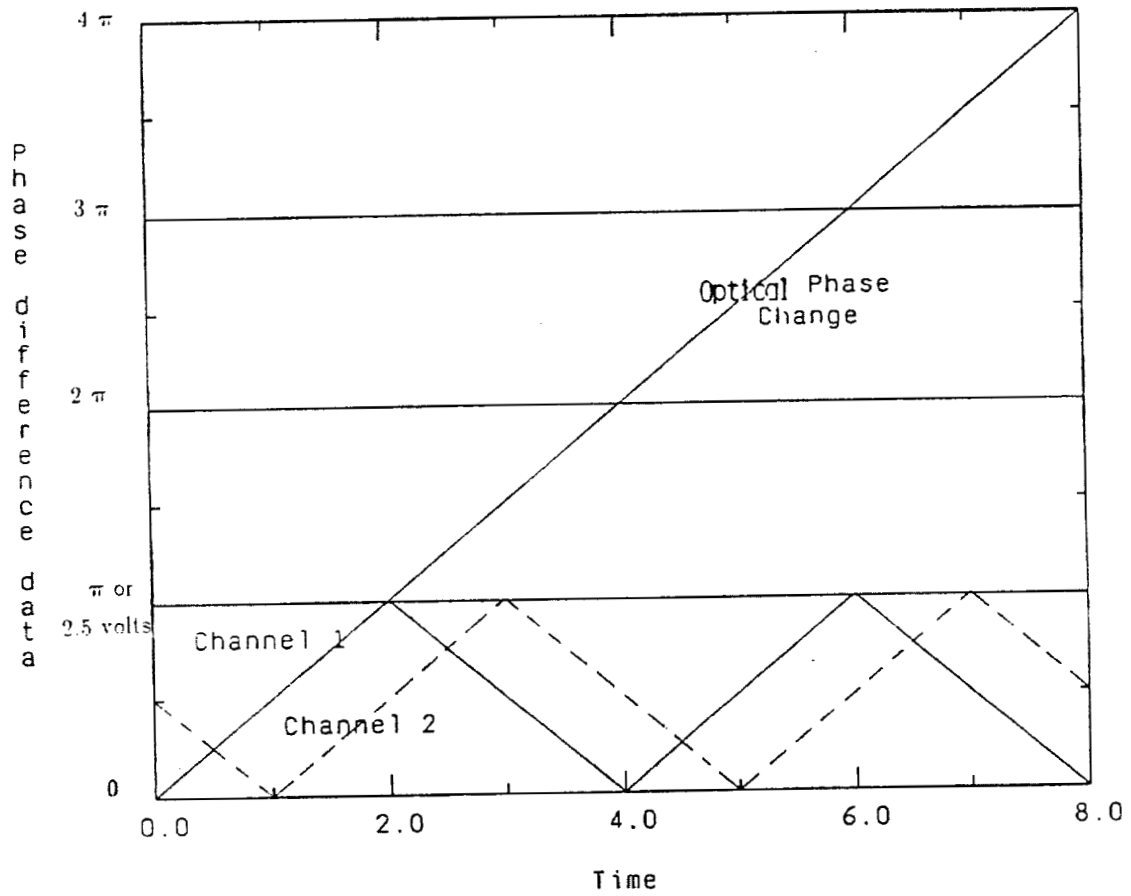


Figure 4.5 A simulation of a constantly increasing optical phase difference and the corresponding two channels of phase detector output (or PD data).

at time 2.0 the phase difference reaches a value of  $\pi$  (or 2.5 volts). The optical phase difference continues to increase past time 2.0 but the  $\pi$  dynamic range of the phase detector causes the PD data (out of channel 1) to decrease. At the time 4.0 the optical phase difference has increased to  $2\pi$  but the PD data measured by the phase detector has decreased to 0 radians (channel 1). Thus, as the optical phase difference increases at a linear rate in time, the corresponding PD data follows a triangular wave pattern.

Suppose however, that the optical phase difference begins to decrease at time 4.0 (see Figure 4.6) at the same rate it was increasing previously. Under such circumstances channel one of the phase detector output (PD data) would not show any change (compare Figures 4.5 and 4.6). The only noticeable difference in the phase detector output comes from inspecting channel 2 of the phase detector. Comparing channel 2 of Figures 4.5 and 4.6 shows that at time 4.0 the phase detector output of the second channel begins to increase when the optical phase difference begins to decrease. This illustrates the necessity of having two channels of output in order to accurately unfold the PD data.

By keeping track of the number of phase boundary transitions in the (channel 1) PD data and using the second channel of PD data to resolve ambiguities in the direction of change of the PD data, a signal processing



routine (see Appendix 1) can be developed to unfold the PD data into phase difference changes ranging from 0 to  $2\pi$  (see Figure 4.7). The 0 to  $2\pi$  phase difference data can then be unfolded into phase changes greater than  $2\pi$  or less than 0 radians. To do this a second channel of phase difference data is created 180 degrees out of phase with the first set of 0 to  $2\pi$  phase difference data. These two sets of phase difference data (ranging from 0 to  $2\pi$ ) are then processed to yield the actual optical phase differences (which is much greater than  $2\pi$ ). The same process of keeping track of phase boundary transitions and resolving ambiguities with the second channel of PD data (ranging from 0 to  $2\pi$ ) was applied to yield the optical phase difference data. An example of the two channels of 0 to  $2\pi$  phase difference data 180 degrees out of phase and the corresponding unfolded data is shown in Figure 4.8. Note that Figure 4.8 represents simulated phase difference data that was constantly increasing over the measuring period and does not represent real physical data. A typical example of phase difference (PD) data and the corresponding optical phase difference data is shown in Figure 4.9. In this example the optical phase difference (not shown) is increasing at a constant linear rate.

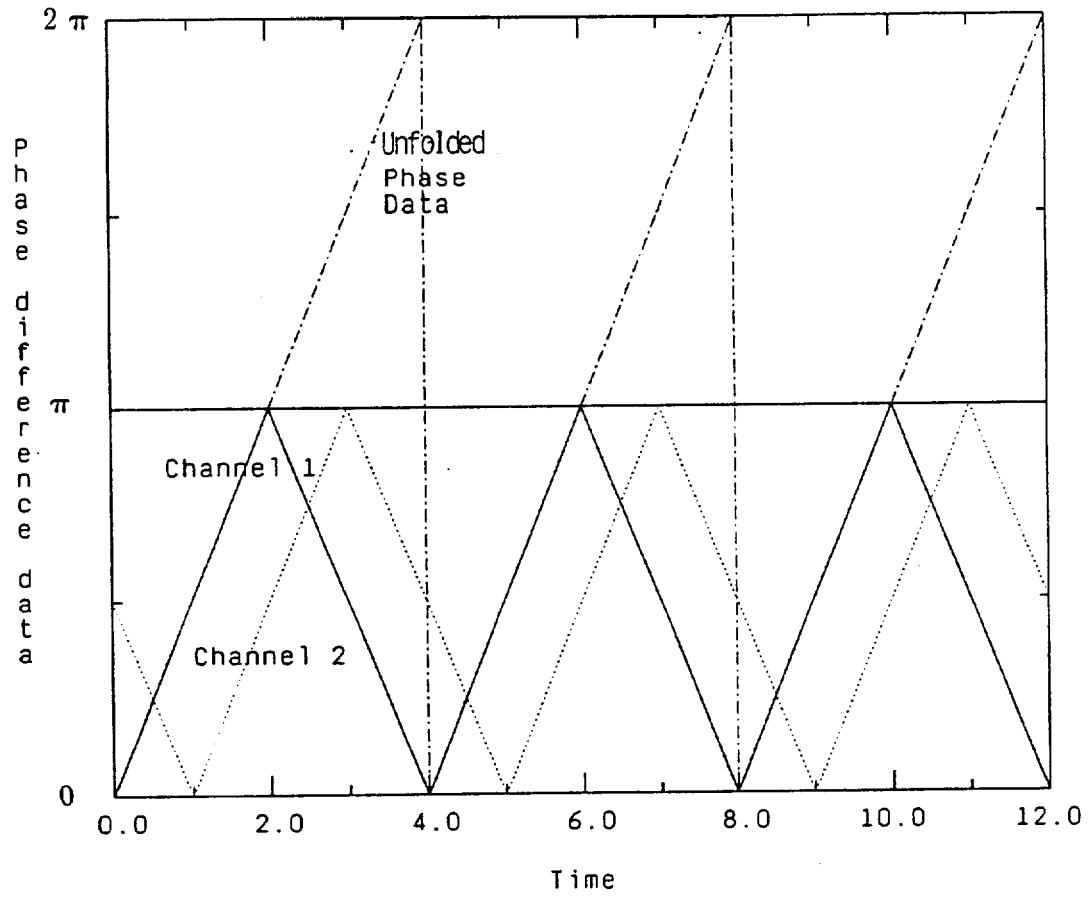


Figure 4.7 Phase difference (PD) data unfolded into the 0 to  $2\pi$  interval.

The optical phase difference is linearly increasing in time in this example.

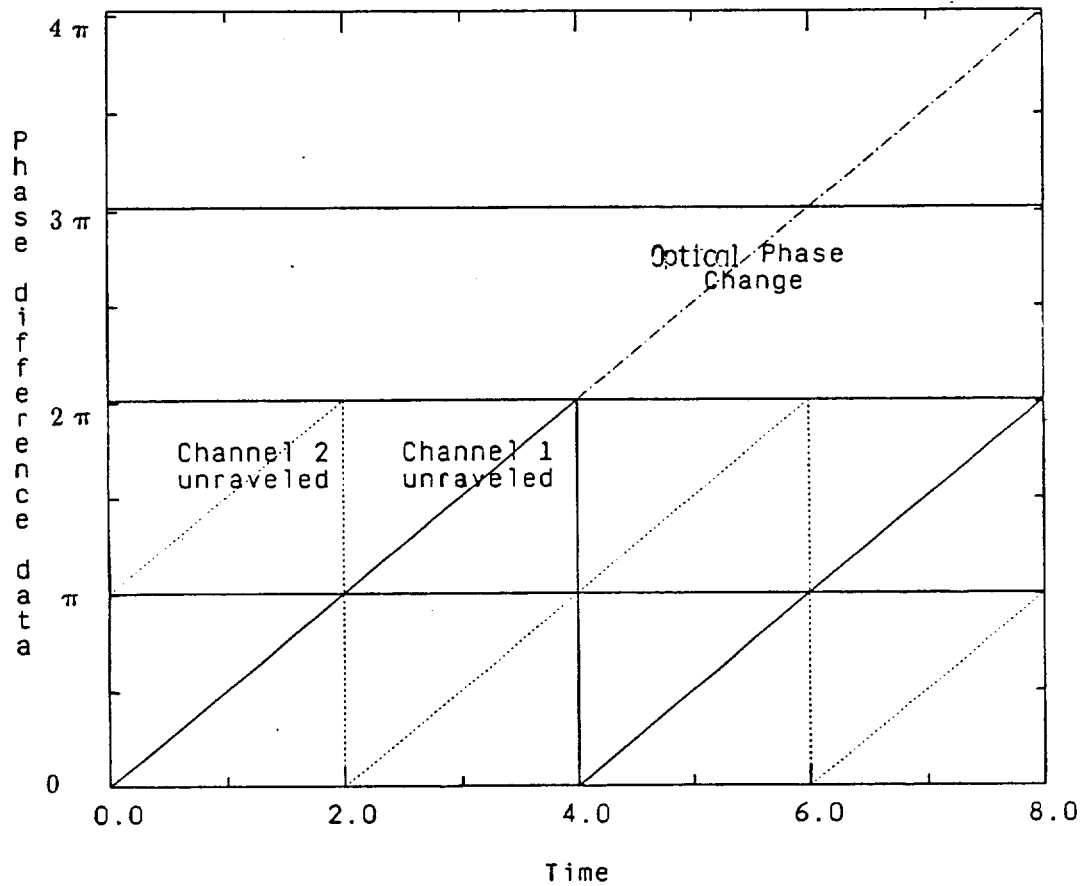


Figure 4.8 An example of the two channels of 0 to  $2\pi$  phase difference data being unfolded into the actual optical phase changes (which are greater than  $2\pi$ ). In this example the optical phase difference (not shown) is increasing at a constant linear rate.

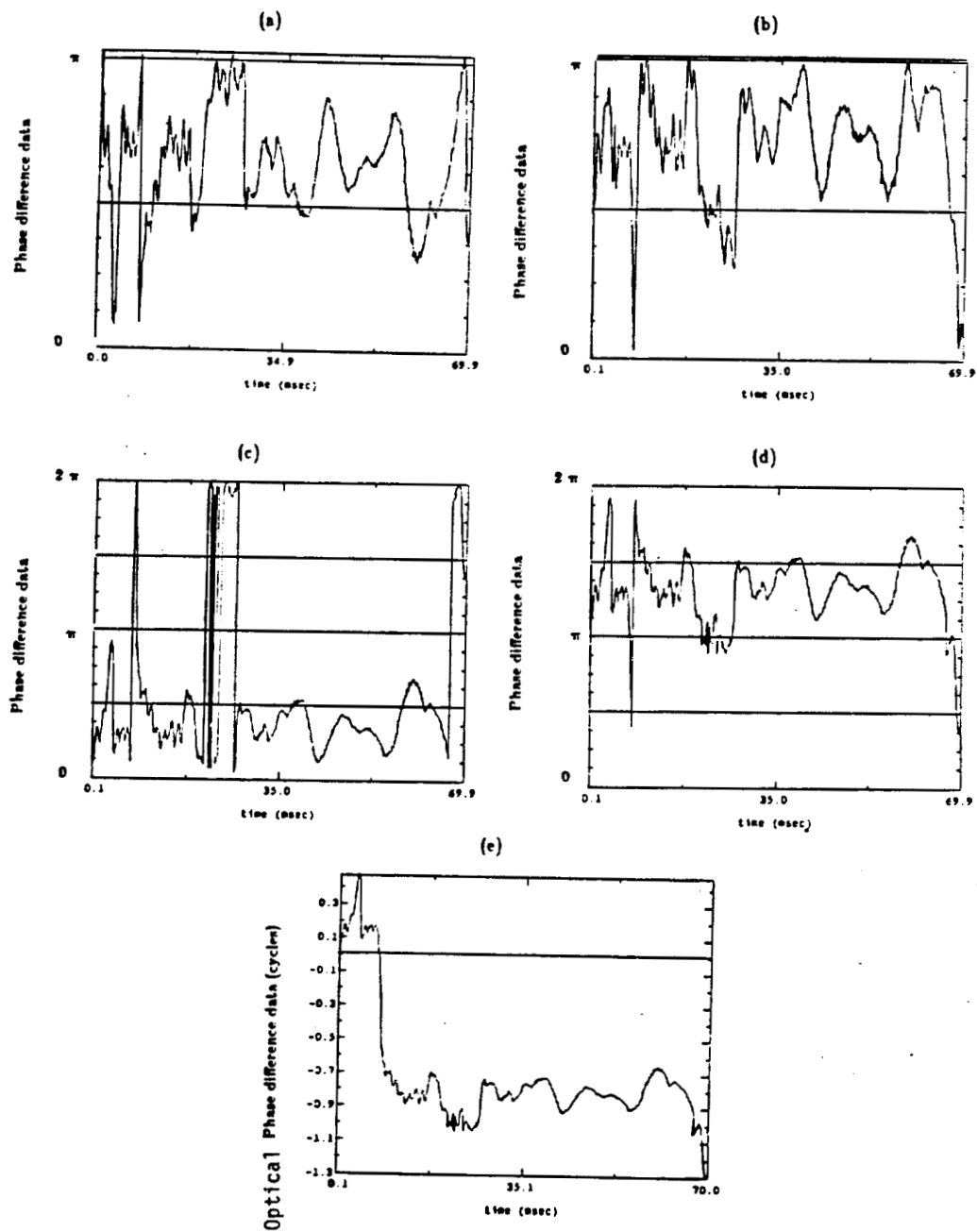


Figure 4.9 A typical example of the two channels of phase difference (PD) data and the corresponding unfolded data (optical phase difference data). (a) and (b) are the two channels of PD data varying between 0 and  $\pi$  and  $\pi/2$  out of phase. (c) and (d) are the PD data unfolded into the 0 to  $2\pi$  interval. Both these channels are  $\pi$  out of phase. (e) represents the totally unfolded PD data (optical phase difference data).

#### 4.2.2 Filtering and Creating the Phase Difference Density Function

At first it was believed that target types could be distinguished by measuring the total phase change (optical phase difference) for each target in a fixed amount of time (i.e. Figure 4.9(e)). After processing (unfolding) several sets of phase difference (PD) data (yielding optical phase difference data) it was determined that this method was not a successful means of distinguishing between targets. Further research into the relevant literature indicated that the diffuse targets that create the laser speckle pattern, were made up of two different attributes that effect the phase statistics of the speckle pattern. The first attribute is the microvariations in the surface. This attribute is generally uniform throughout the target and is responsible for such target characteristics as r.m.s. surface roughness, correlation length, and spatial power spectral density [7,12]. Macrovariations constitute the second attribute and represent large changes in surface characteristics, such as a warped target, or nonuniformity in target thickness. In Kadono's paper [7] it was pointed out that slow phase changes were most likely due to macro-surface characteristics instead of micro-surface characteristics. Consequently the unfolded phase difference data needs to be high pass filtered to eliminate slow phase changes caused by

macrovariations in the target's surface characteristics.

The optical phase difference (OPD) data was filtered using a 10 point running average technique (see Appendix 2), creating an average of the OPD data (known as ATPD data). An example of OPD data and the corresponding AOPD data is shown in Figures 4.10 and 4.11. The AOPD file contains 10 points less than the OPD data file, due to the averaging processing routine. However, since the OPD files contain approximately 25,000 points this is of little significance. The 10 point running average technique basically low pass filters the OPD data (see Figure 4.11).

After the AOPD file was created it was subtracted from the original file (OPD data). Thus producing a data file containing the high pass filtered OPD data (see Figure 4.12). In theory [7] the high pass filtered optical phase difference data (HPFOPD) contains only phase difference effects induced by the microsurface characteristics of the target (i.e. r.m.s surface height).

Using the HPFOPD data a probability density function (PDF) is created (see Figure 4.13). The PDF is found by forming a histogram of the HPFOPD data and normalizing the area to a sum of one (see Appendix 2 for software routine). After collecting several sets of experimental data, it was determined that the PDF's of the HPFOPD data sets were uniquely tied to the r.m.s. roughness of the diffuse targets creating the speckle

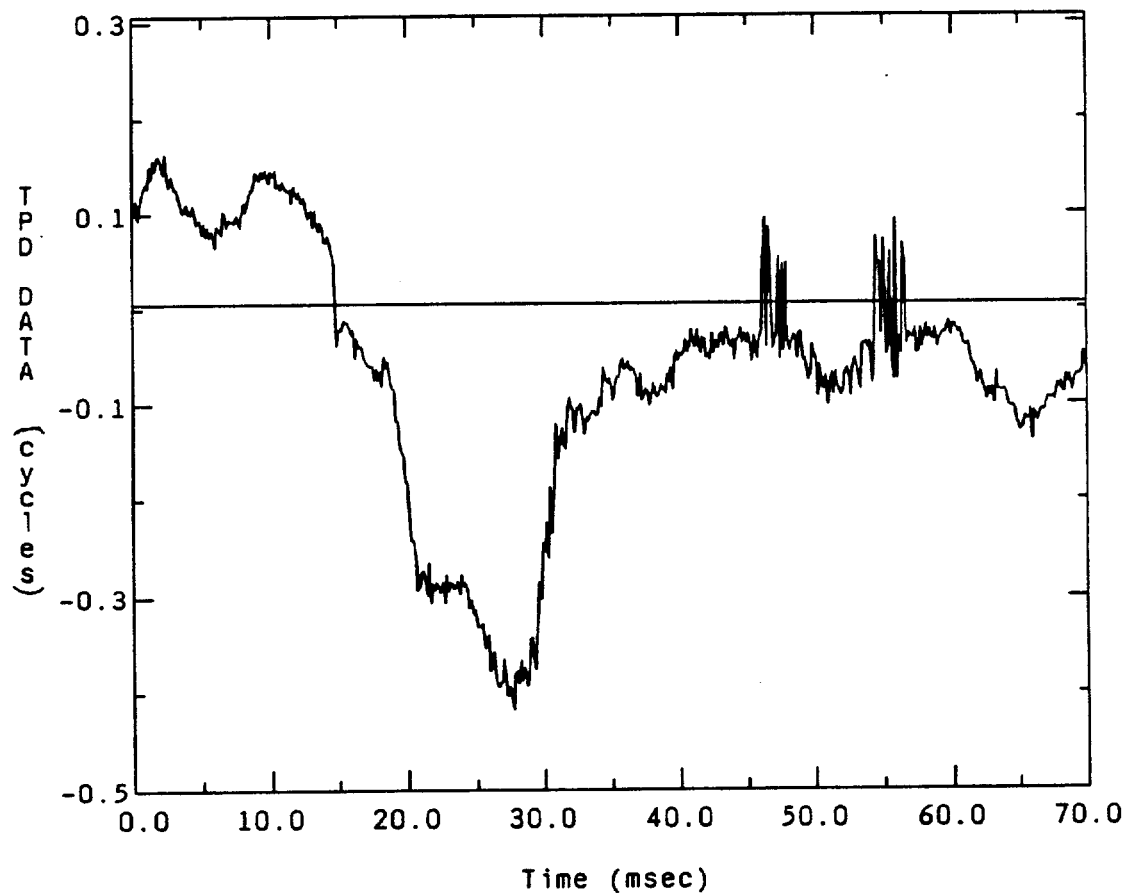


Figure 4.10 A typical example of optical phase difference data (OPD) for a 70 millisecond sampling period.

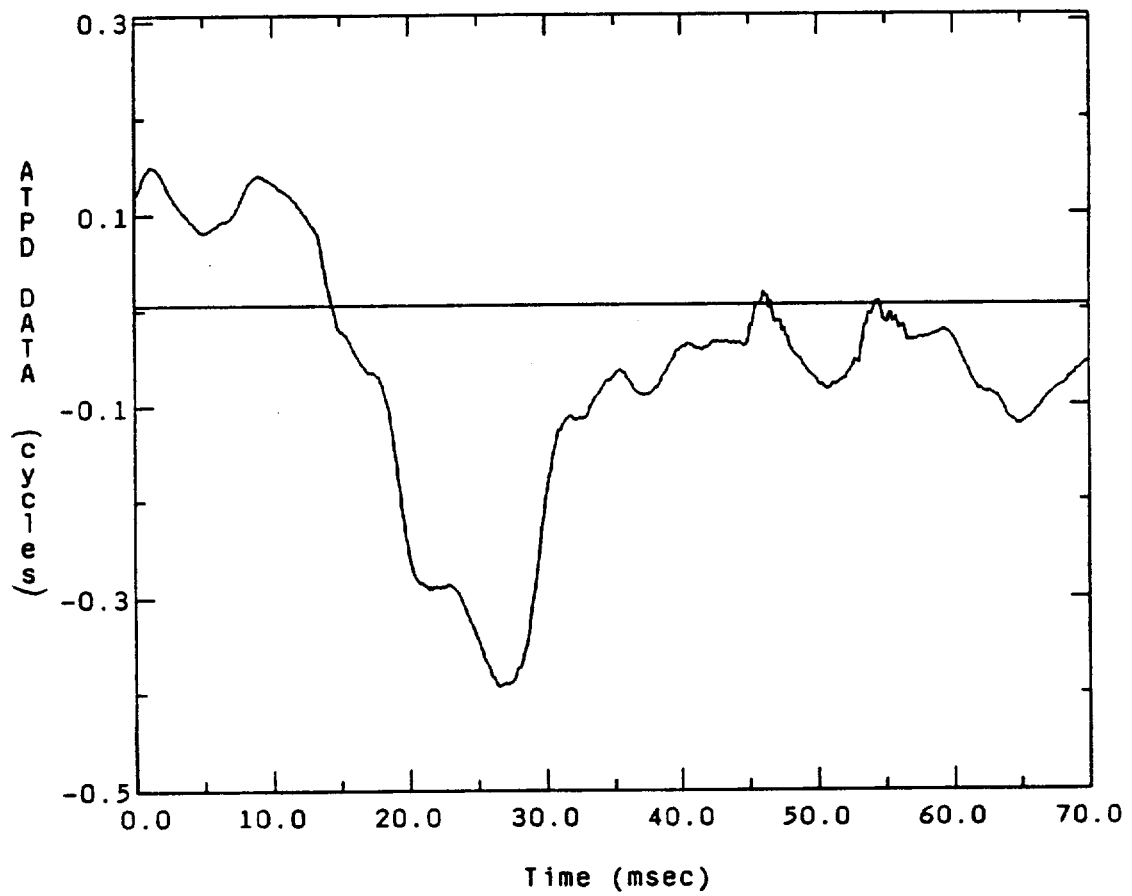


Figure 4.11 A 10 point running average (low pass filtering) of the OPD data (=AOPD).



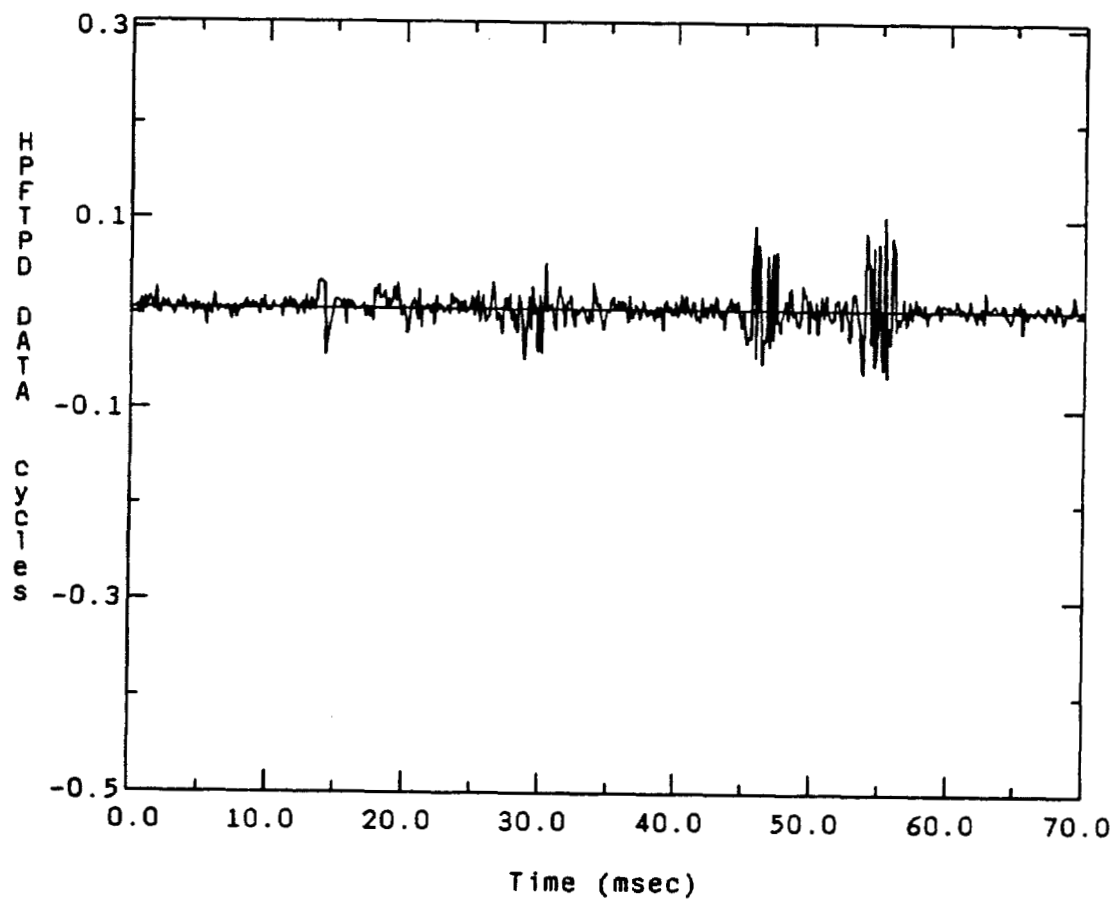


Figure 4.12 An example of the method by which the optical phase difference (OPD) data is high pass filtered (HPFOPD) to remove the fluctuations caused by macrovariations in the surface characteristics of the diffuse target.

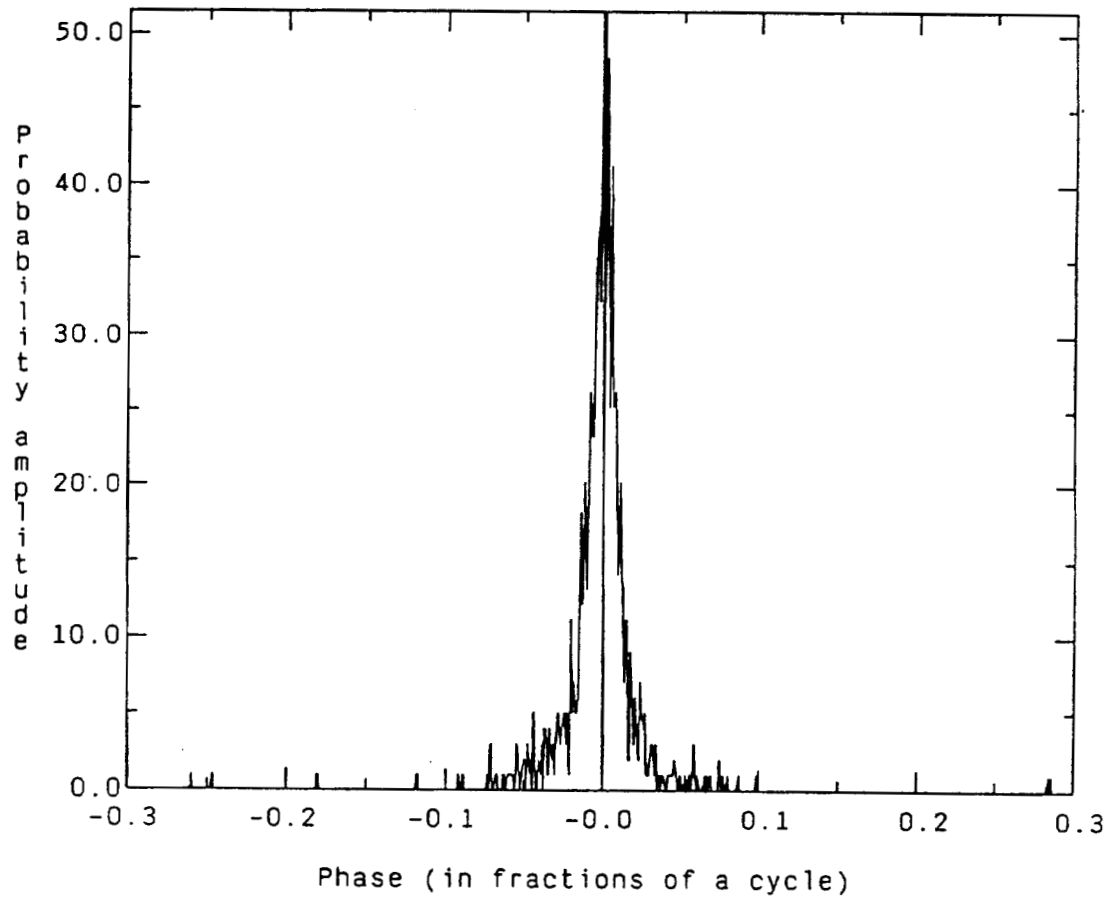


Figure 4.13 A probability density function for the HPFOPD data of Figure 4.12.

pattern. The width of the HPFOPD density function was the distinguishing characteristic that allowed for unique target recognition. The means of measuring the width (or standard deviation) of the HPFOPD density function is discussed in the next section.

#### 4.2.3 Fitting a Gaussian Curve to the Phase Density Functions

Since the experimental evidence seemed to indicate a direct correlation between the target roughness and width of the probability density function of the HPFOPD data, a method of measuring this width was needed. The most obvious indicator of the PDF's width seemed to be its variance (or standard deviation). This, however, was not a successful means of measuring the PDF's width, since the extremely long tails on the PDF might yield misleading results (see Figure 4.14). Since physically the tails of the PDF represent large rapid changes in the HPFOPD data, typical of system errors (i.e. loss of lock in the phase detector), the tails of the PDF curves were truncated. The PDFs were truncated beyond  $\pm 0.06$  cycles, at which point the amplitude of the curves had fallen to approximately one one hundredth of its peak value. By eliminating the tails of the PDF curves a more accurate representation of the correlation between the width of the HPFOPD density function and the r.m.s. roughness of the target could be

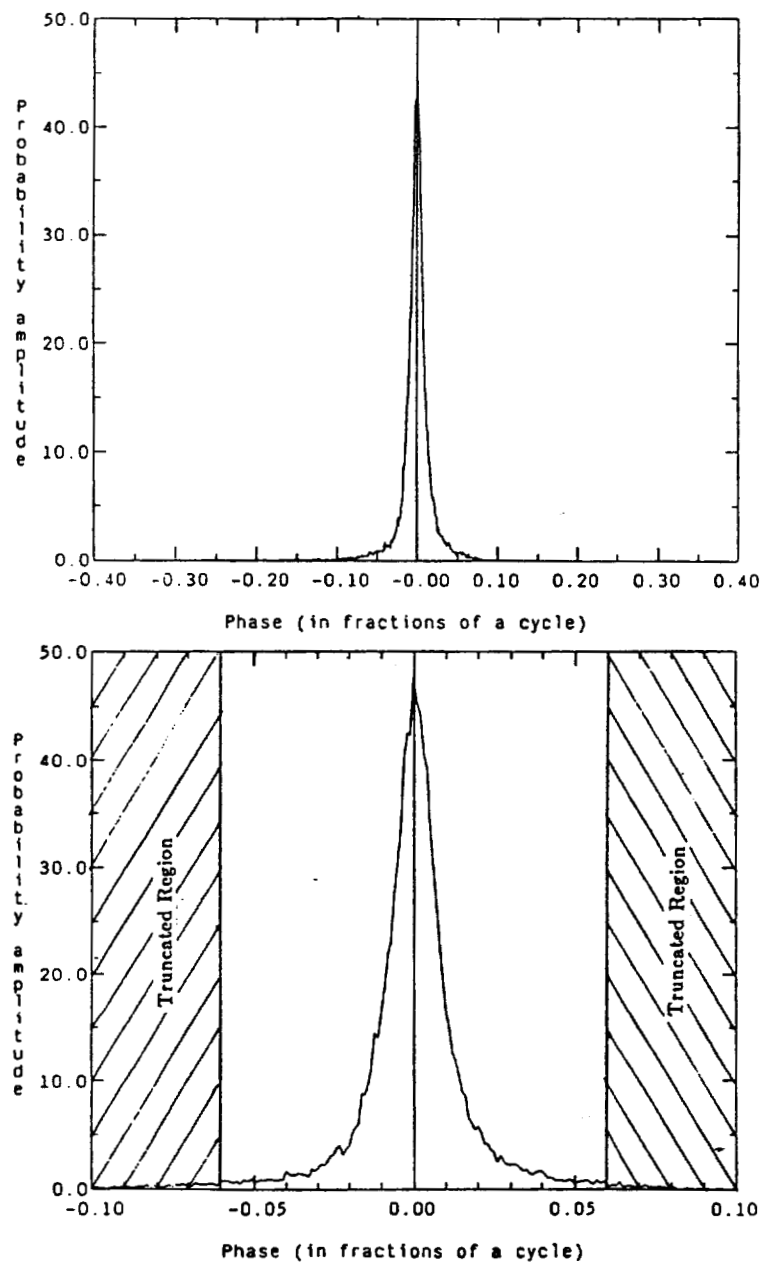


Figure 4.14 A typical example of the probability density function corresponding to the HPFOPD data (3.5 seconds worth of data). (a) The original density function before the truncation of the tails of the curve. (b) A blow up of the same curve with the truncated region indicated.

obtained.

The truncated PDFs were then fitted with the best possible Gaussian curve. This was done by generating an initial Gaussian curve and subtracting this curve from the truncated HPFOPD density function (see Appendix 2). The sum of the differences between the two curves is called the reference error. This process was repeated in an interactive manner until the lowest reference error was found. The lowest reference error was assumed to be the best fit curve (see Figure 4.15) to the HPFOPD truncated density function. Thus the standard deviation of the best fit Gaussian curve was the means used to measure the width of the HPFOPD density function.

The characteristics of the speckle pattern generated by each diffuse target were measured. The width (standard deviation of the best fit Gaussian curve) of the HPFOPD density functions turned out to be the statistical attribute of the speckle pattern that was uniquely tied to the r.m.s. roughness of the diffuse target (that generates the speckle pattern). Consequently, the standard deviation of the surface height variations (r.m.s. surface roughness) can be determined from the standard deviation of the PDF of the HPFOPD data. A list of the widths (standard deviation) of the truncated HPFOPD density functions corresponding to several types of diffuse targets is given in the next chapter.

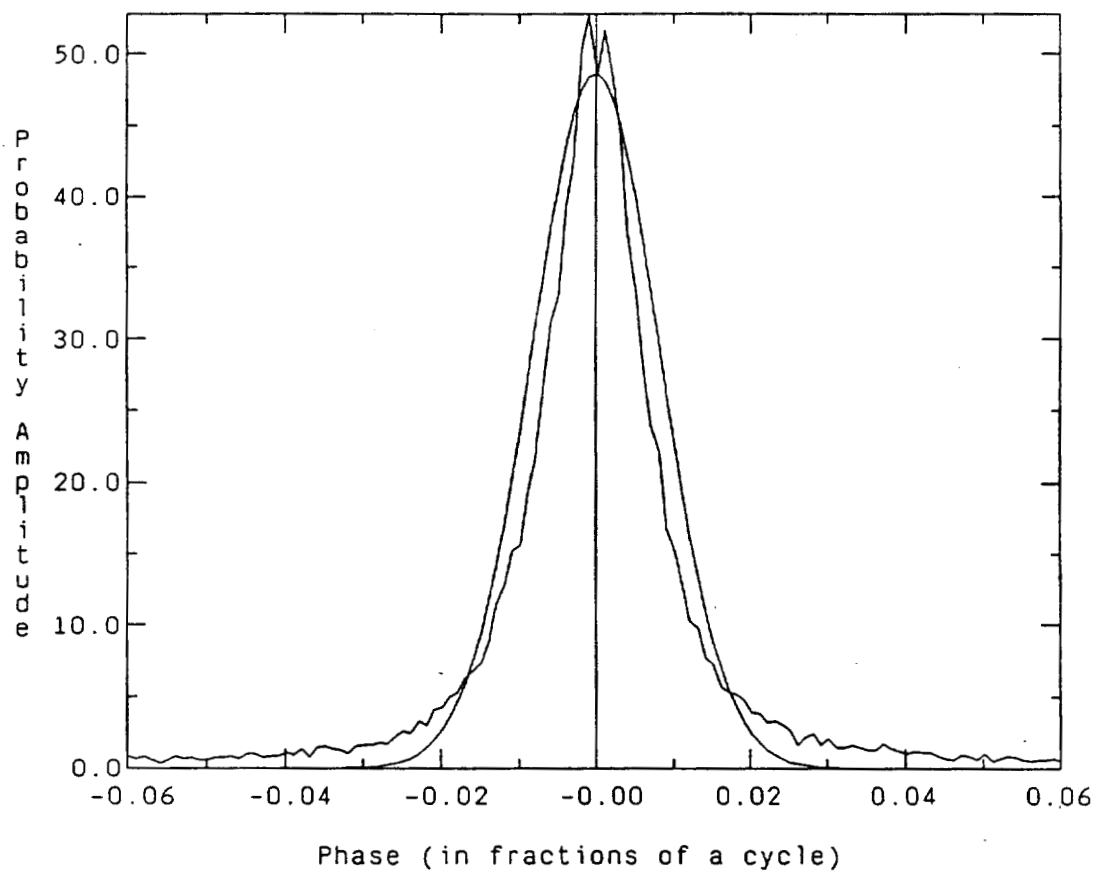


Figure 4.15 A typical HPFOPD probability density function along with the corresponding best fit Gaussian curve.

## CHAPTER 5

### CONCLUSIONS

It can be concluded, from the experimental results shown in this chapter, that the diffuse target types are distinguishable by statistically analyzing the phase of the fields present in the speckle pattern. The distinguishing characteristic being the standard deviation (width) of the high pass filtered optical phase difference data (HPFOPD). The Gaussian curves for several sets of HPFOPD data are shown in the first section of this chapter. A discussion of the experimental results, and its implications and applications to other areas, concludes the chapter.

#### 5.1 Summary of the Experimental Results

On two different days, under slightly different atmospheric conditions data was collected and analyzed. On each day several sets of data were taken on each of the diffuse target types. On the first occasion that successful data was recorded, the speckle patterns analyzed were generated by a 8 grit, 16 grit and 30 grit sandblasted aluminum (SBA) target. Three sets of phase difference (PD) data were recorded for each target type. The PD data was unfolded (processed) to yield the actual optical phase

difference data and then high pass filtered to eliminate gradual phase changes caused by macro-surface characteristics (i.e. nonuniformity in target thickness). The high passed filtered optical phase difference (HPFOPD) data was then used to form a probability density function of the phase difference values. A best fit Gaussian curve was then fit to each of the HPFOPD data sets, as shown in Figures 5.1-5.3. From this data it is apparent, that the larger the r.m.s. roughness of the diffuse target the broader the distribution of the HPFOPD data. Thus, the rougher 8 grit SBA target, has the broadest HPFOPD density function.

The standard deviation of the best fit Gaussian curves ( $\sigma_\phi$ ) shown in Figures 5.1-5.3 are plotted in Figure 5.4, against the standard deviation of the phase of the fields ( $\sigma_\theta$ ) measured at the target. The standard deviation of the phase of the fields measured at the target is given by the simple relationship shown in Eq. (5.1).

$$\sigma_\theta^2 = [4\pi/\lambda]^2 \sigma_h^2 \quad (5.1)$$

Eq. 5.1 shows a linear relationship between the variance of the target surface height variations ( $\sigma_h^2$ ) and the variance of the phase of the fields measured at the target ( $\sigma_\theta^2$ ) [1]. The standard deviation,  $\sigma_h$ , (r.m.s. roughness) of each diffuse target was measured using a profilometer (see table



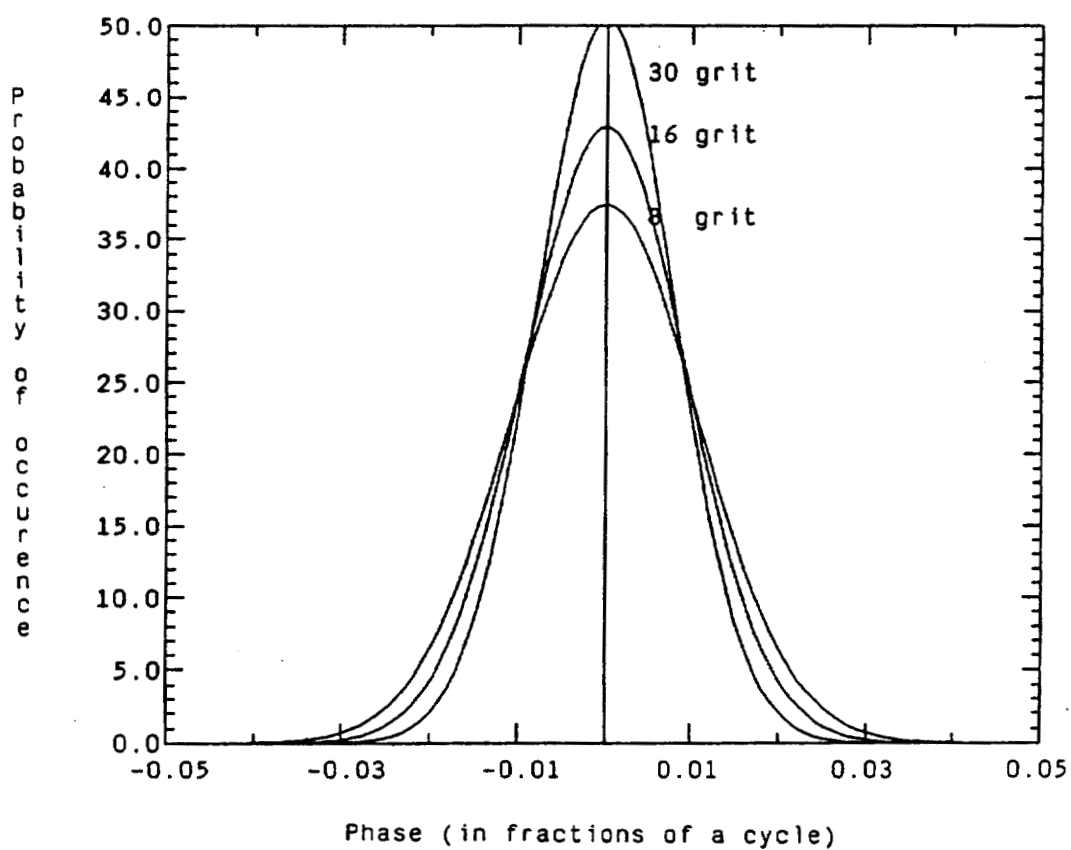


Figure 5.1 The best fit Gaussian curves corresponding to the first set of HPFOPD data taken on each target type is shown above. From this data it is apparent that as the target roughness ( $\sigma_h$ ) increases so does the width of the HPFOPD density function.

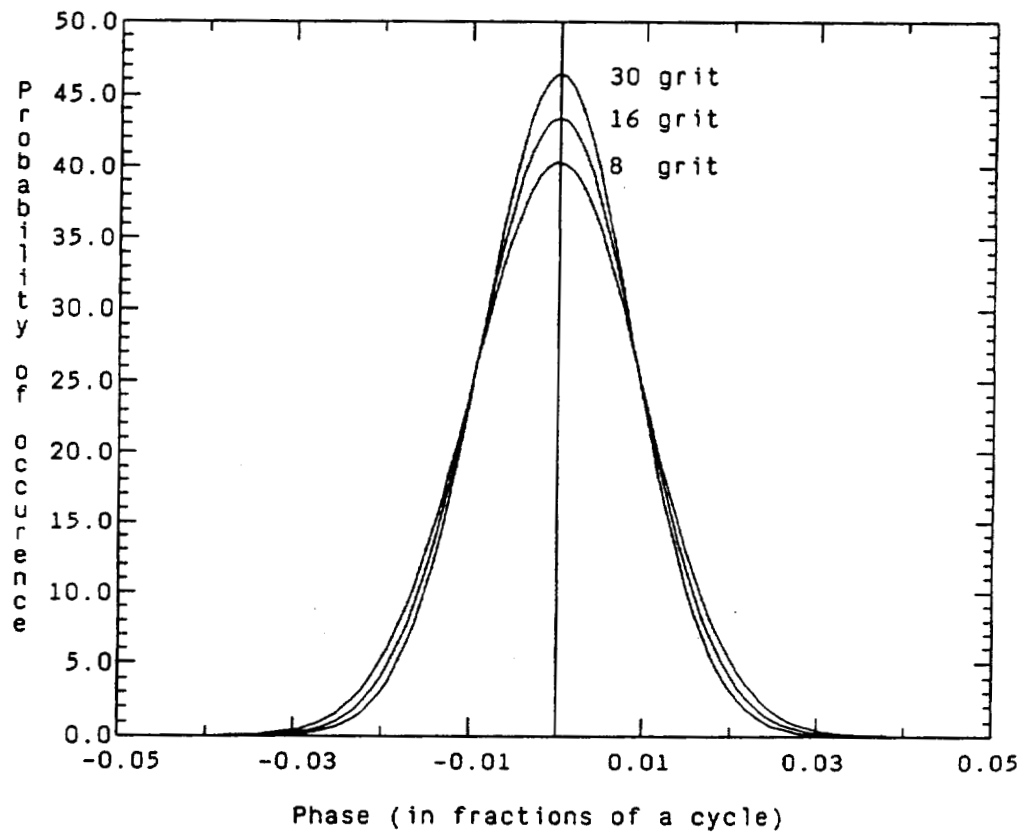


Figure 5.2 The best fit Gaussian curves corresponding to the second set of HPFOPD data taken on each target type is shown above. From this data it can be seen that as the target roughness ( $\sigma_h$ ) increases so does the width of the HPFOPD density function.

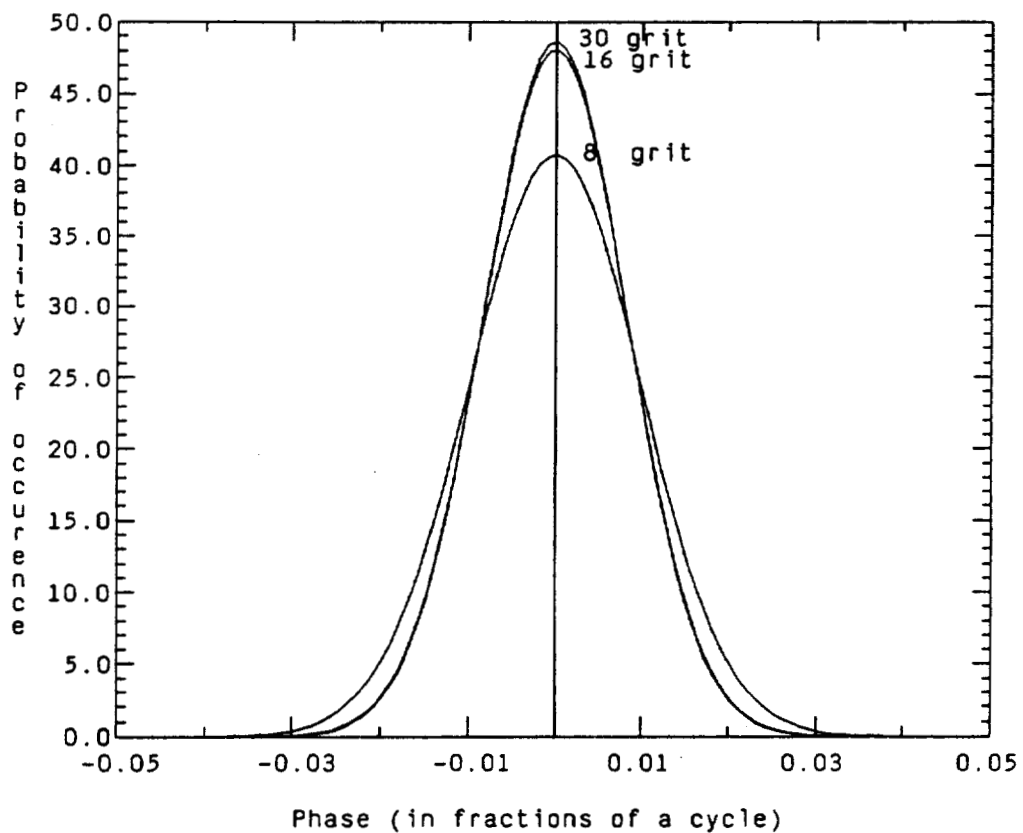


Figure 5.3 The best fit Gaussian curves corresponding to the third set of HPFOPD data taken on each target type is shown above. From this data it can be seen that as the target roughness ( $\sigma_h$ ) increases so does the width of the HPFOPD density function.

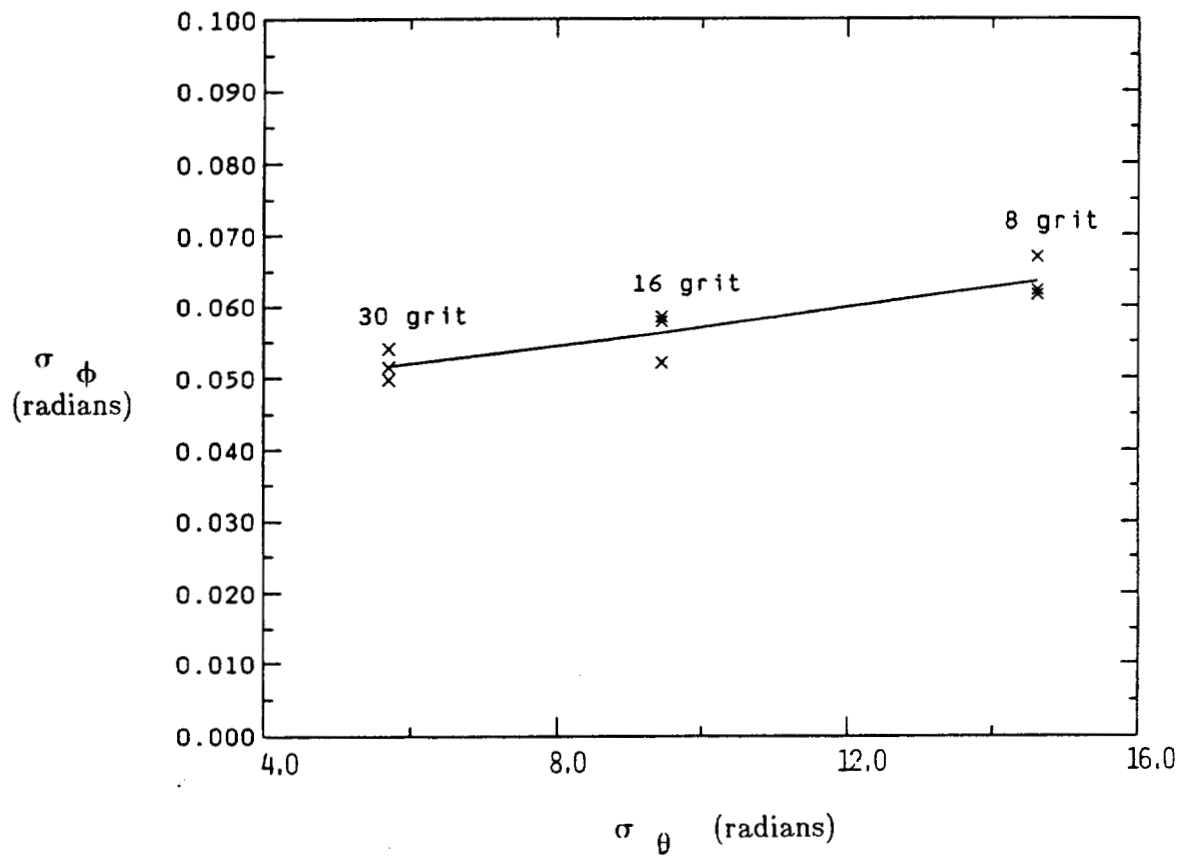


Figure 5.4 The standard deviations of the best fit Gaussian curves ( $\sigma_{\phi}$ ) for Figures 5.1-5.3 is plotted against the standard deviations of the phase of the fields measured at the target ( $\sigma_{\theta}$ ).

3.1). By using table 3.1 and Eq. 5.1, the standard deviation of the phase of the fields measured at the target ( $\sigma_\theta$ ) can be calculated. The standard deviation of the phase of the fields measured at the target ( $\sigma_\theta$ ) is then plotted versus the standard deviation of the Gaussian curves ( $\sigma_\phi$ ) in Figure 5.4. The data points in Figure 5.4 are fitted with a line using a linear mean square estimation technique.

In an attempt to extend the experimental results, the 30 grit target was used to create a flame sprayed aluminum target (FSA). The FSA target has a much rougher r.m.s. surface height. The rougher surface would provide further experimental verification of the principal, that an increase in the r.m.s. target roughness, produces an increase in the width of the HPFOPD density function.

Data was taken on the FSA target along with the other two targets (16 grit and 8 grit SBA). The results of the new data taken agree with the previously shown data (see Figures 5.5 and 5.6). Again it is found that as the r.m.s. roughness of the diffuse target increases, the standard deviation of the associated HPFOPD density function also increases.

The standard deviation of the Gaussian curves shown in Figures 5.5 and 5.6 were measured and combined with the previous data shown in Figures 5.1-5.3. The standard deviation of each Gaussian curve ( $\sigma_\phi$ ) was plotted (see Figure 5.7) against the standard deviation of the phase of the

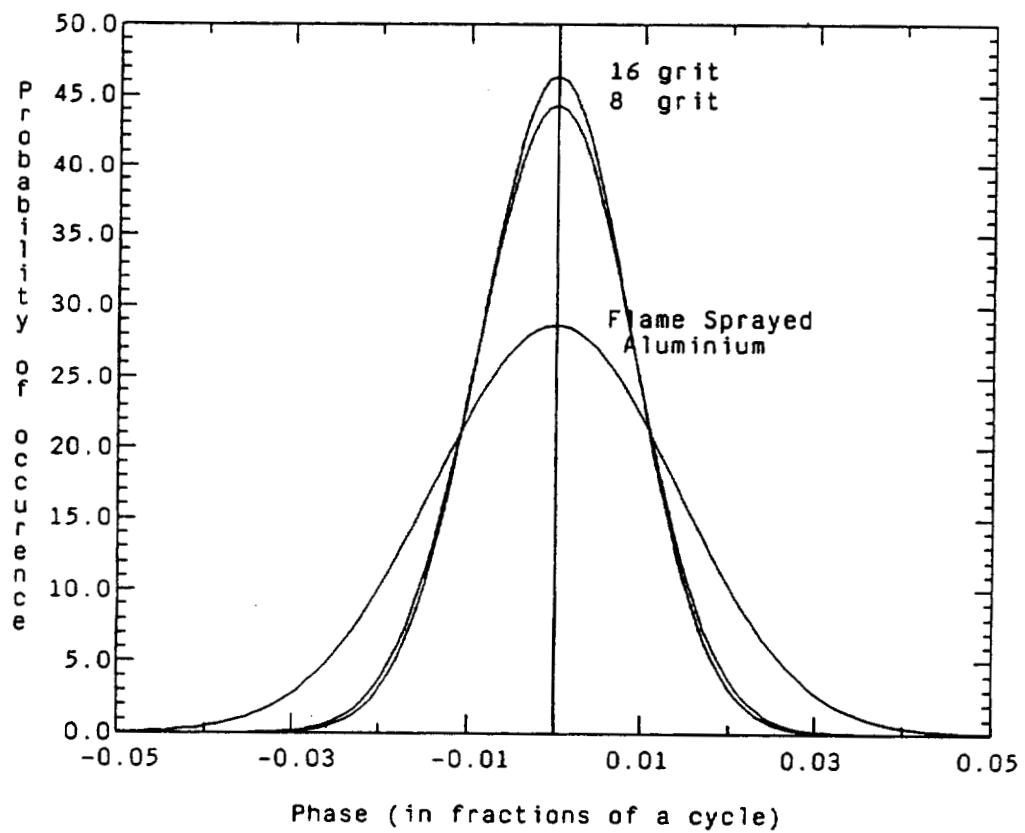


Figure 5.5 The best fit Gaussian curves corresponding to the first set of HPFOPD data is shown for several different target types. From this data it can be seen that as the target roughness ( $\sigma_h$ ) increases so does the width of the HPFOPD density function.

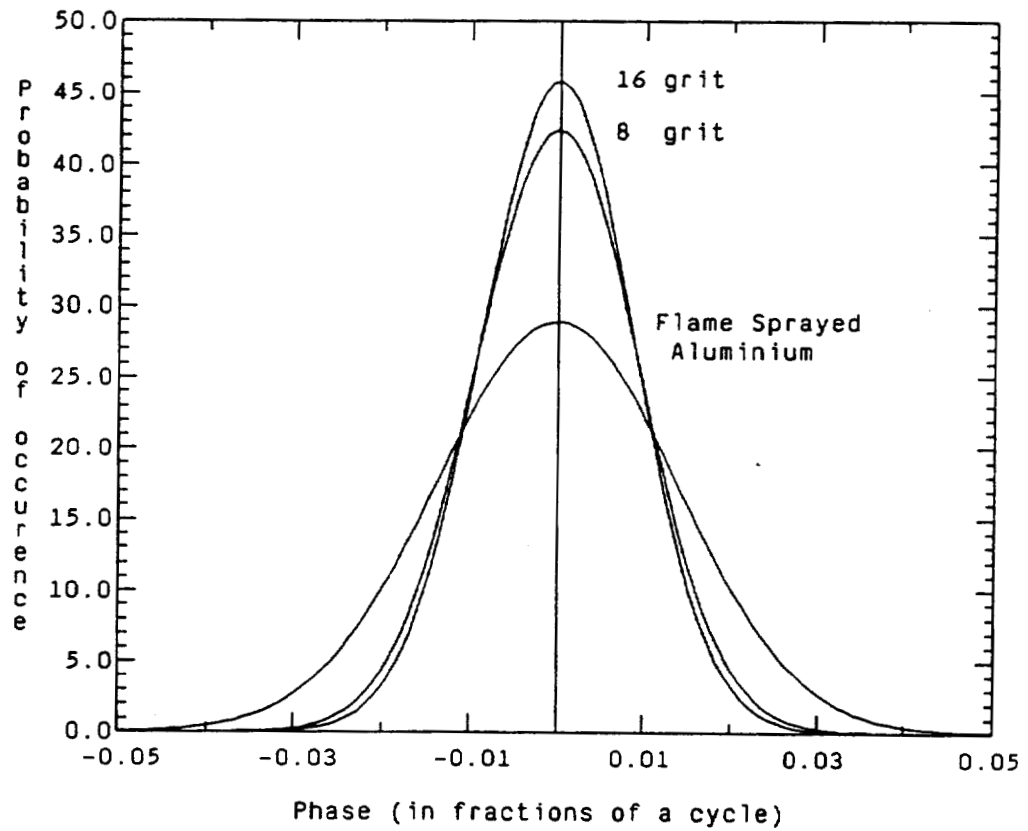


Figure 5.6 The best fit Gaussian curves corresponding to the second set of HPFOPD data is shown for several different target types.

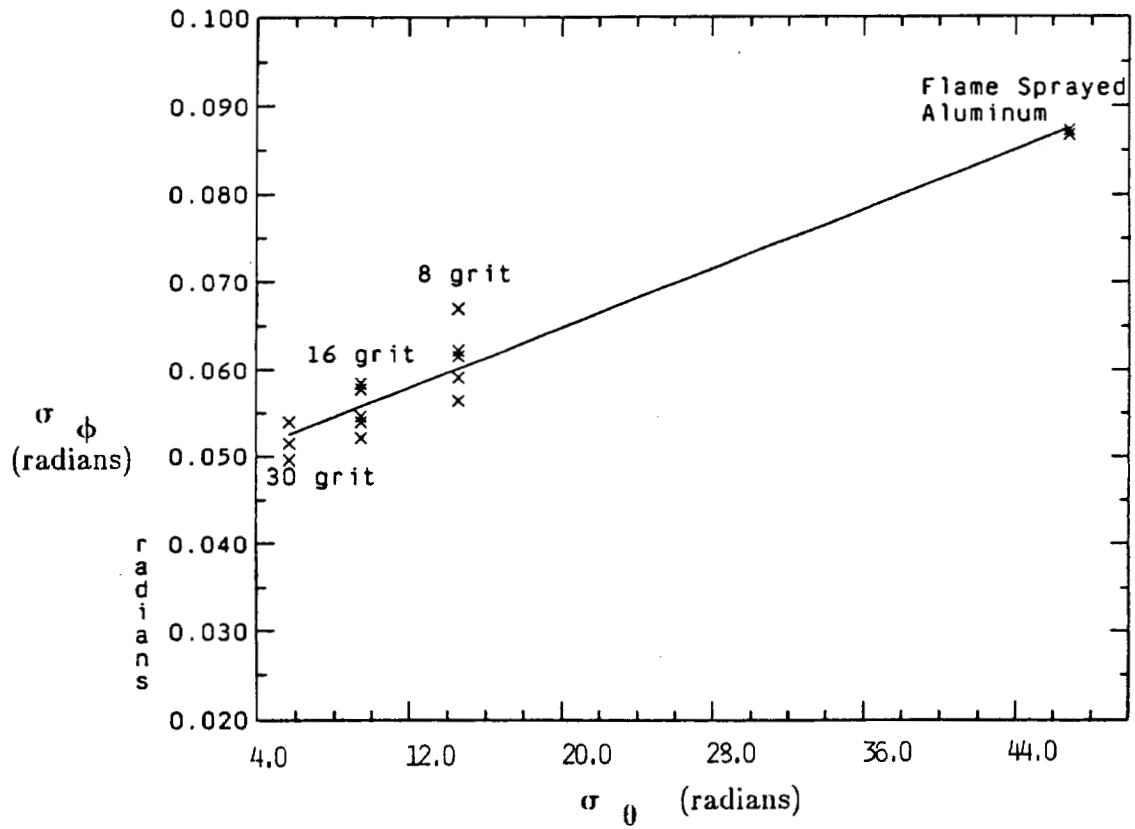


Figure 5.7 The standard deviations of the best fit Gaussian curves ( $\sigma_\phi$ ) for Figures 5.1-5.3 and Figures 5.4-5.5 are plotted against the standard deviations of the phase of the fields measured at the target ( $\sigma_\theta$ ).



fields measured at the target ( $\sigma_\theta$ ). Equation 5.1 was again utilized to determine  $\sigma_\theta$  given the r.m.s. roughness  $\sigma_h$  of the FSA target (see table 3.1). The data plotted in Figure 5.7 is again fitted with a line using a linear mean square estimation technique. The resulting graph continues to show that as the r.m.s. roughness ( $\sigma_h$ ) of a diffuse target increases, the width of the corresponding HPFOPD density function ( $\sigma_\phi$ ) also increases.

## 5.2 Discussion of Results

The results of the previously shown data have two predominate implications. First, a new technique has been developed, whereby remote diffuse targets can now be distinguished between based upon their r.m.s. roughness. Since objects are classified by their characteristics, the ability to determine an object's r.m.s. surface roughness could be extremely useful in the field of target recognition and sensor integration.

Secondly, comparing the present experimental results with those of Kadono, yields some interesting similarities. As stated in Chapter 1, the results of the two experiments cannot be directly compared because of the differences in the systems; Kadono's results were measured in a laboratory setting, ignored any atmospheric effects and used a transmitting diffuse target rather than a reflecting diffuse target. However, both results agree

qualitatively, that is an increase in the target roughness ( $\sigma_h$ ) will produce an increase in the width of the HPFOPD density function (for an r.m.s. roughness on the order of the wavelength).

One interesting side note, the use of flame sprayed aluminum as a standard for CO<sub>2</sub> lasers has become extremely common. However from the results measured in this paper (see Table 3.1), the r.m.s. roughness of the flame sprayed aluminum is not many times the wavelength of the light illuminating the target (only about 3 or 4 times the wavelength of a CO<sub>2</sub> laser). This assumption is essential to much of the basic work done in developing the statistics of laser speckle. Its implications are unknown.

## REFERENCES

1. H. E. Bennett, "Specular Reflectance of Aluminized Ground Glass and the Height Distribution of Surface Irregularities," *J. Opt. Soc. Am.*, Vol. 53, No. 12, Dec. 1963.
2. H. Fujii and T. Asakura, "Effect of Surface Roughness on the Statistical Distribution of Image Speckle Intensity," *Opt. Commun.* Vol. 11, No. 1, May 1974.
3. H. Fujii, T. Asakura, and Y. Shindo, "Measurement of Surface Roughness Properties by Using Image Speckle Contrast," *J. Opt. Soc. Am.*, Vol. 66, No. 11, Nov. 1976.
4. H. Fujii and J. W. Y. Lit, "Surface Roughness Measurement Using Dichromatic Speckle Pattern: an Experimental Study," *Appl. Opt.*, Vol. 17, No. 17, Sept. 1978.
5. H. M. Pedersen, "On the Contrast of Polychromatic Speckle Patterns and its Dependence on Surface Roughness," *Optica Acta*, Vol. 22, No. 1, Jan. 1975.
6. G. E. Sommargren, "Optical Heterodyne Profilometry," *Appl. Opt.* Vol. 20, No. 4, 15 Feb. 1981.

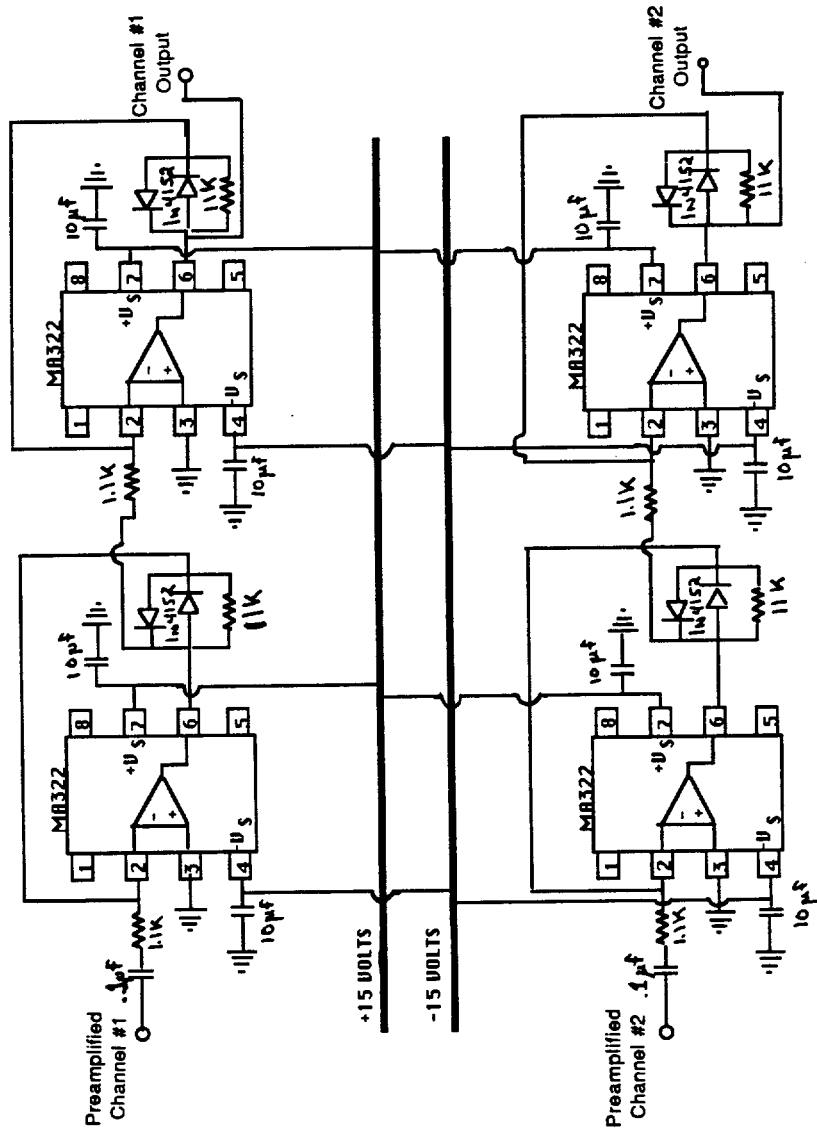
7. H. Kadono, N. Takai, and T. Asakura, "Experimental Study of the Laser Speckle Phase in the Image Field," *Optica Acta*, Vol. 32, No. 9/10, 1985.
8. J. Wang and P. Pruitt, "Laboratory reflectance measurements for coherent laser radar applications," *Appl. Opt.*, Vol. 23, No. 15, 1984.
9. M. Kavaya, R. Menzies, D. Haner, U. Oppenheim, and P. Flamant, "Target reflectance measurements for calibration of lidar atmospheric back scatter data," *Appl. Opt.*, Vol. 22, No. 17, 1983.
10. J. W. Goodman, "Statistical Properties of Laser Speckle Pattern, in *Laser Speckle and Related Phenomena*," J. C. Dainty, Ed. (Springer, Berlin, 1975).
11. J. Uozumi and T. Asakura, "First-order probability density function of the laser speckle phase," *Opt. Quant. Elect.*, Vol. 12, 477, 1980.
12. J. Rossi and D. Maystre, "Speckle: an electromagnetic theory for shallow rough surfaces," *Optica Acta*, Vol. 32, No. 11, 1985.
13. Published by Numerical Algorithms Group, Inc., 1101 31st Street, Suite 100, Downers Grove, Illinois 60515.
14. J. W. Goodman, "Some Effects of Target-Induced Scintillation on Optical Radar Performance," *Proc. IEEE*, Vol. 53, No. 11, Nov. 1965.

15. Farzin Amzajerdian, "Remote Sensing of Atmospheric Winds by Utilizing Speckle-Turbulence Interaction and Optical Heterodyne Detection," Ph.D. Thesis, Oregon Graduate Center, June 1988.

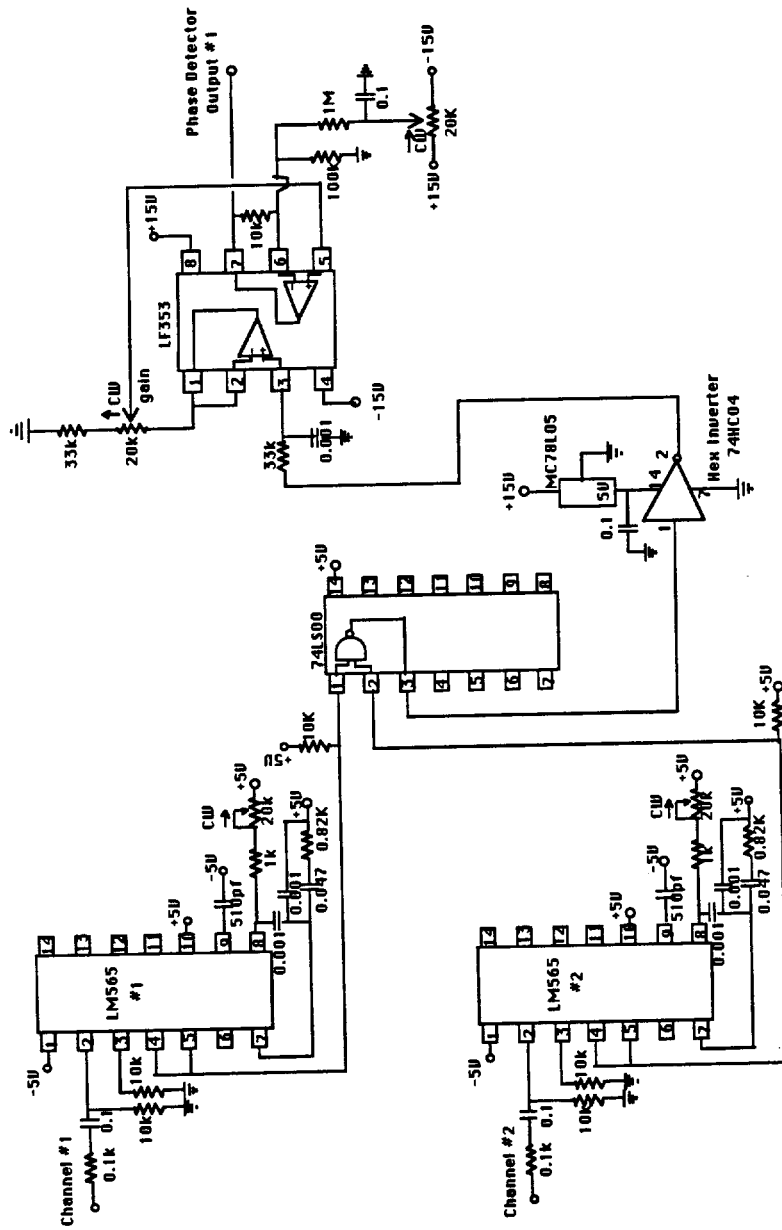
**APPENDIX 1**

**A Schematic of the Phase Detector**

### PREAMP TO PHASE DETECTOR

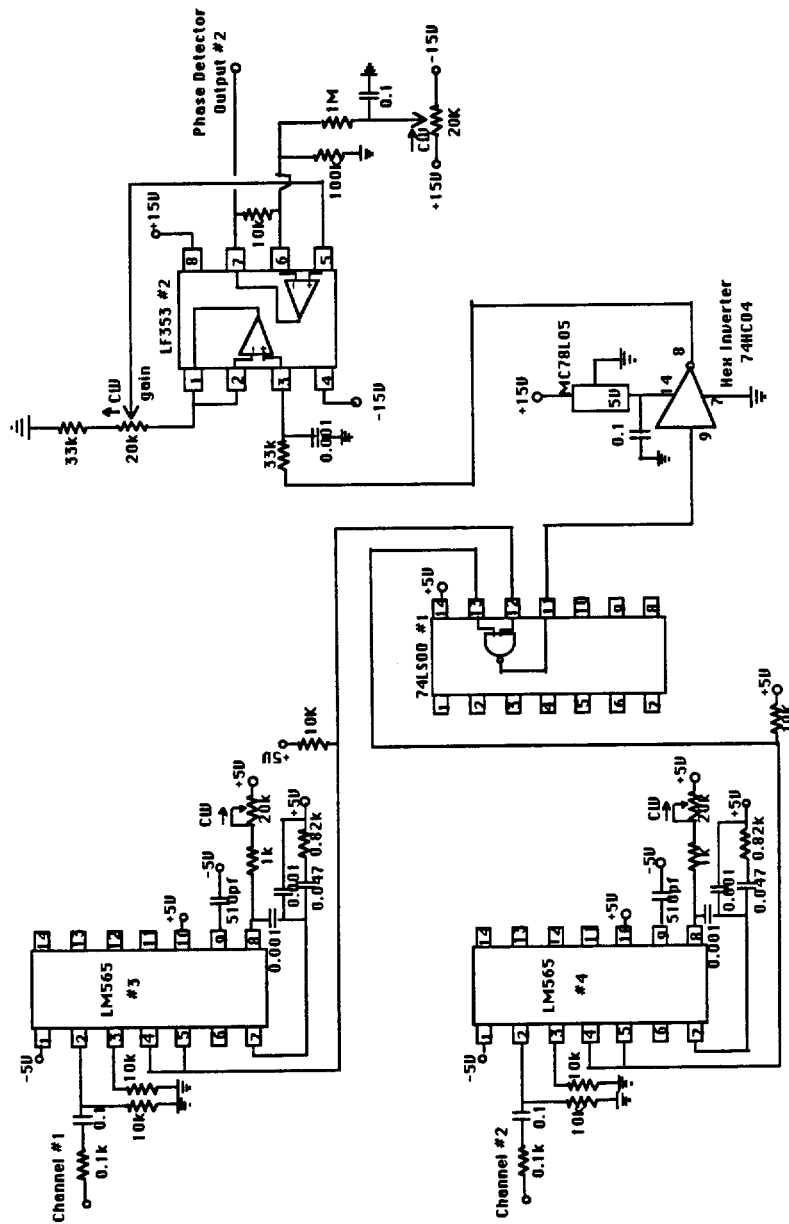


### Phase Detector (first 1/2)

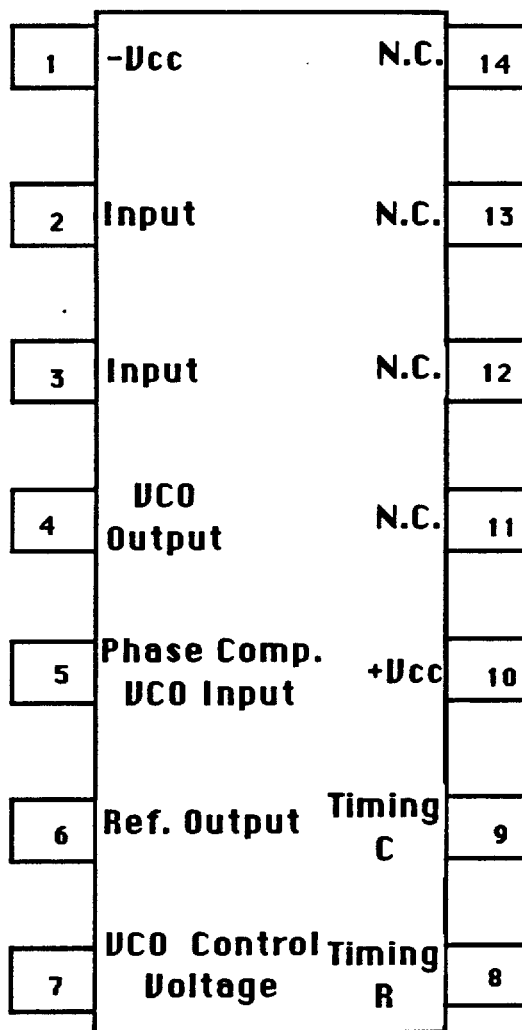




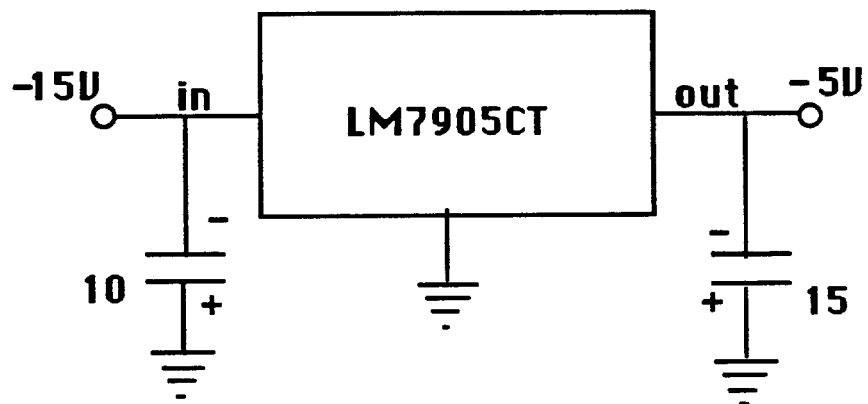
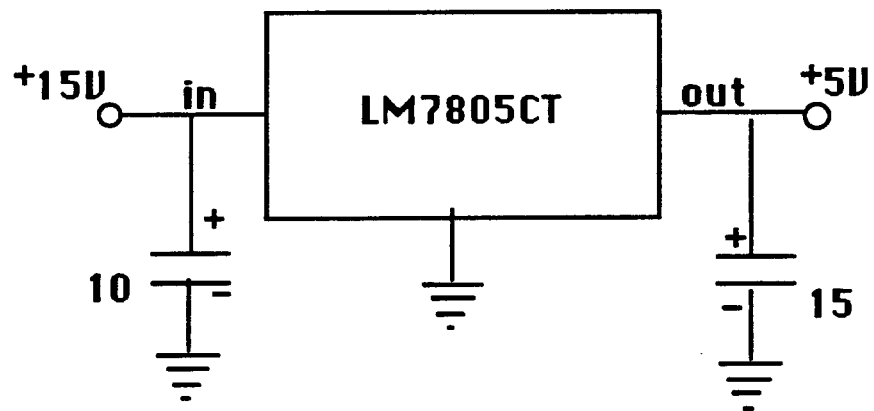
### Phase Detector (Second 1/2)



## Phase Locked Loop LM565



## Voltage Regulators for Phase Detector



## APPENDIX 2

The following appendix contains a copy of the signal processing routines used to process the phase difference data produced by the phase detector. The software routines were written to run on a Digital Microvax II computer.

```

c      program unravel
c
c      This program takes a phase vs time signal generated by the
c      phase detector (new 7/88) and unravels the 2 volt signal to
c      a 4v signal.
c
c      Written by John Peacock 8-2-88
c      Parts also written by D.Draper,Todd Cloninger
c      Modified:
c
c      dimension phil(50000),phi2(50000),h(50000)
c      integer nblks,ch1,ch2,phil,phi2,h
c      real t,x,samptime
c      character ofilnam*15,answ*1
c
c      print*, ' Input channel 1 filename for reading (< 16 char.)'
20    read (*,20) ofilnam
c      format (a15)
c
c      open (1,file=ofilnam,status='old')
c
c      print*, ' Input channel 2 filename for reading (< 16 char.)'
c      read (*,20) ofilnam
c
c      open (2,file=ofilnam,status='old')
c
c      print*, 'Total unraveled output filename (< 16 char.)'
c      read (*,20) ofilnam
c
c      open (9,file=ofilnam,status='unknown')
c
c      print*
c      print*, 'Input the number of blocks in the file (int =<100)'
c      read (*,*) nblks
c      print*, 'nblks=',nblks
c      print*
c
c      print*, 'Input the sample rate/channel (in msec) '
c      read (*,*) samptime
c      print*, 'samptime=',samptime
c
c      npts=number of data pts in the file of data per channel.
c      There are 500 pts per block.
c      npts=nblks*500
c
c*****
c
c      This part of the program uses the two channels of phase data
c      that vary between 0 to 2.5 volts (or 0 to pi) and are 90
c      degrees out of phase (new detector). The data is then unraveled
c      to produce two channels of phase data that range from 0 to 2pi
c      (or 0 to 5 volts) and are 180 degrees (pi) out of phase.
c
c      do 30 i=1,npts
c          read(1,*) t,ch1
c          read(2,*) t,ch2
c
c      convention is each channel goes between 0 to 2.5 volts or
c      digitally 2048 to 3072. However the detector may not be
c      completely accurate so the values may go over or under by
c      a little bit.
c          if (ch2 .le. 2560) then
c              phil(i)= ch1+1024
c              if (phil(i) .gt. 4096) phil(i)=4096

```

```

        else
            phi1(i)= -ch1+1024+4096
            if (phi1(i) .lt. 2048) phi1(i)=2048
        end if

        if (ch2 .gt. 2560) then
            phi2(i)= -ch1+4096+2048
            if (phi2(i) .gt. 4096) phi2(i)=4096
        else
            phi2(i)= ch1
            if (phi2(i) .lt. 2048) phi2(i)=2048
        end if
30    continue

C*****
c
c    This part of the program outputs the two channels of data
c    that range from 0 to 2 volts and are pi out of phase. This
c    data is analogous to that produced by the old phase detector.

    print*,'Do you wish to output the two channels of '
    print*,'unraveled 0 to 2 volt data.'
    print*
60    read(5,60) answ
    format(a1)

    if ((answ.eq.'y').or.(answ.eq.'Y')) then

        print*,' Input the first filename for writing (< 16 char.)'
        read (*,20) ofilnam

        open (3,file=ofilnam,status='unknown')

        print*,' Input the second filename for writing (< 16 char.)'
        read (*,20) ofilnam

        open (8,file=ofilnam,status='unknown')

        do 50 i=1,npts

            write(3,*) i*samptime,phi1(i)
            write(8,*) i*samptime,phi2(i)

50    continue

        close(3)
        close(8)

    end if
C*****
c
c    This part of the program unravels the data into intervals
c    greater than two pi. Analysis taken directly from D.Drapers
c    program.

    c=0
    n=0

    do 200 i=1,npts
        if (phi1(i).gt.3584) go to 170
        if (phi1(i).lt.2560) go to 180
        if (phi2(i).gt.3584) go to 160
        if (phi2(i).lt.2560) go to 163
        if (c.eq.1) go to 165
        h(i)=phi1(i)
        go to 190

```

```
160     if (c.eq.1) go to 162
161     go to 168
162     n=n+1
163     go to 168
164     if (c.eq.1) go to 167
165     go to 168
166     h(i)=phi2(i)
167     go to 190
168     n=n-1
169     h(i)=phi1(i)
170     c=0
171     go to 190
172     if (c.eq.1) go to 175
173     n=n+1
174     h(i)=phi2(i)
175     c=1
176     go to 190
177     if (c.eq.1) go to 175
178     n=n-1
179     go to 175
180     h(i)=h(i)+n*1024
181
182     continue
183
184     *      convert phase data to floating point
185     x=float((h(i)-2048)/2048.0)
186     t=i*samptime
187
188     *      write corrected data in file
189     *      express phase in cycles
190     write(9,600) t,x
191
192     continue
193     format(1x,f8.2,2x,f15.4)
194
195     close(1)
196     close(2)
197     close(9)
198
199     end
```





```

        temp(j)=phi(i)
        k=k+1
        filtered(k)=sum/float(n)
        j=j+1
    end if
100  continue
    print*, 'completed reading and npt filtering data'
    npts2=npts-(n-1)
    print*, 'npts2=', npts2
    open (8, file='nptfilt.dat', status='unknown')
    do 150 i=1, npts2
        write(8, *) t1*i, filtered(i)
150  continue
c*****
c      This part of the program subtracts the filtered data from the
c      original data and calculates the maximum and minimum y values of
c      the new (low freq filtered) data set.
c
    offset=ifix(float(n)/2.0)
    rmax=-100.0
    rmin=100.0
    npts2=npts-(n-1)
    print*, 'offset=', offset

    do 200 i=1, npts2
        phi(i)=phi(i+offset-1)-filtered(i)
c      phi(i)=phi(i)-filtered(i)
        rmax=Amax1(phi(i), rmax)
        rmin=Amin1(phi(i), rmin)
200  continue
    print*, 'completed the subtraction'
    open (9, file='filtered.dat', status='unknown')
    do 250 i=1, npts2
        write(9, *) t1*i, phi(i)
250  continue
c*****
c      This part of the program performs a histogram on the newly
c      created (high freq) data file (ie. or low freq filtered).
c
    print*, 'the max and min phase (in cycles) of the filtered'
    print*, 'data set is:'
    print*, 'max=', rmax
    print*, 'min=', rmin

    print*, ' Select and initial bin size for the histogram'
    read (5, *) rbin

    nbins=ifix((rmax-rmin)/rbin)
    print*, ' The number of bins is ', nbins
    j=0

    do 300 i=1, npts2
        j=nint((phi(i)+abs(rmin))*float(nbins)/abs(rmax-rmin))
c      print*, 'j=', j
        hist(j)=hist(j)+1
300  continue
c*****
c      This part of the program normalizes the histogram to produce
c      a phase density function. Then the mean and standard deviation
c      of the density function are calculated.
c

    sum=0.0

```

```
do 400 i=0,nbins
    sum=sum+hist(i)*rbin
400 continue
    print*,'sum=',sum

    avrg=0.0
    avrgsq=0.0
    x=rmin
    stdev=0.0

c    sum=1.0

    do 500 i=0,nbins
        rhist(i)=float(hist(i))/sum
        avrg=avrg+x*rhist(i)*rbin
        avrgsq=avrgsq+(x**2)*rhist(i)*rbin
        write(2,*) x,rhist(i)
        x=x+rbin
500 continue

    stdev=(avrgsq-(avrg**2))**0.5

    print*,'The mean of the desity distribution is:',avrg
    print*
    print*,'The standard deviation is:',stdev
    print*

    close(1)
    close(2)

end
```

```

program phdist
c
c The purpose of this program is to take a set of processed
c phase data and find its associated distribution between
c 0 and 1 cycles. This gives us the phase difference distribution
c between 0 and 2pi.
c
real t,amp,dec(50000),den(0:99)
real avrg,stdev,var
integer i,temp,nblks,npts
character ofilnam*15
c
print*
print*,' Input file filename (<16 char.)'
read (*,20) ofilnam
20 format (a15)
open (8,file=ofilnam,status='unknown')

print*
print*,' Input the name of the output file (<16 char.)'
read (*,20) ofilnam
open (9,file=ofilnam,status='unknown')

print*
print*,' Input the number of blocks to be processed (= <100)'
read (*,*) nblks

npts=nblks*500
avrg=0.0
do 100 i=1,npts
    read(8,*) t,amp
    dec(i)=abs(amp-Aint(amp))
    avrg=avrg+dec(i)
    temp=Aint(dec(i)*100)
    den(temp)=den(temp)+1
100 continue
avrg=avrg/npts

var=0.0
stdev=0.0
do 150 i=1,npts
    var=(dec(i)-avrg)**2 + var
150 continue
var=var/npts
stdev=var**0.5
print*
print*,'The mean of the desity distribution is:',avrg
print*
print*,'The standard deviation is:',stdev
print*

do 200 i=0,99
    write(9,*) i,den(i)
200 continue

close(8)
close(9)

end

```

```

program gaussfit
c
c This program take a set of phase density data and comes up with
c the best fit gaussian curve with help from the user. The
c program then outputs the corresponding gaussian curve to a file
c

real phi,amp,phimeas(500),probmeas(500)
real sigma,error,x,sum
integer i,npts
character ofilnam*15,answ*1

c
print*
print*,' Input file filename (<16 char.)'
read(*,20) ofilnam
format(a15)
20  open(8,file=ofilnam,status='unknown')

print*
print*,' Input the name of the output file (<16 char.)'
read(*,20) ofilnam
open(9,file=ofilnam,status='unknown')

print*
print*,' Input the number of points in the file (integer)'
read(*,*) npts

print*
print*,' Input the first approx. for sigma of the density fn'
read(5,*) sigma

j=0
sum=0.0
do 100 i=1,npts
c      read(8,*) phi,amp
      print*,'phi=',phi,'amp=',amp
      if(phi.gt..06) goto 200
      if(phi.ge.-.06) then
          j=j+1
          phimeas(j)=phi
          probmeas(j)=amp
          sum=sum+amp
      end if
100  continue

200  continue
npts=j
print*,'number of pts of interest in file=',npts
print*,'the area between -.06 and .06 is =',sum

error=0.0
do 300 i=1,npts
c      x=gauss(phimeas(i),sigma)
      error=error+(probmeas(i)-x)**2
c      print*,'probmeas=',probmeas(i)
c      print*,'gauss=',x
300  continue

print*
print*,'The error =',error
print*,'sigma=',sigma
print*
print*,'Do you wish to try another sigma ?'
read(5,350) answ
format(a1)
350  if((answ.eq.'N').or.(answ.eq.'n')) goto 400

```

```
print*
print*,'input sigma'
read(5,*) sigma
goto 200
400 continue
do 500 i=1,npts
write(9,*) phimeas(i),gauss(phimeas(i),sigma)
500 continue
close(8)
close(9)
end
function gauss(phi,sigma)
real phi,sigma,gauss,x,y
x=(1/(2*3.14159)**0.5)
y=(phi**2)/(2*(sigma**2))
gauss=x*Exp(-y)/sigma
return
end
```

```

program fouriertransform
c
c Purpose: This routine reads data from a disk file and
c           then preforms a fft on the data. An output file
c           is produced, containing the power spectrum of
c           the input. (power spectrum = the energy at each
c           frequency).

integer Pnps, Pnpsd2
parameter(Pnps = 1000, Pnpsd2 = Pnps/2, ibeep = 7)
c Pnps is the Parameter for the Number of Points used to find
c the Spectrum (power spectral density)

real psd(Pnpsd2+1)
real dfreq,t
double precision x(Pnps), s(Pnps)
integer ix(Pnps)
integer i, j, k, ix, ifail
integer tlu,tcsr,fn,rn,ifc,offset
logical eoff,errf,eotf
character ofilnam*15,ofilnam2*15

c*****
c It has been found through trial and error that the nag library
c fft program is not effective with two many points and in fact is
c wrong. To correct this problem the input data file will be
c broken into nb files of equal length. The fft will be performed
c on each of these files and the nb fft of the output will be
c averaged together.
c*****
c
c The above has been corrected and the file sizes are limited
c only by the value you input for Pnps. You can still use nb
c to perform the fft in chunks with Pnps/nb pts in each chunk.
c*****
c
c Pnps=the number of data pts in each of the sets of data.
c nb*Pnps=the total number of data pts in the input file.

c nb=the number of files the data is broken into before the fft is
c performed.
c nb = 5
* We will have nb files of Pnps thousand data points.

do 70 i=1,Pnpsd2+1
* clears an array
psd(i) = 0
70 continue

print 210,' This option reads data from disk & ',
* 'calculates the fft and power spectrum.'
210 format(a,x,a)
print 210,'The sample mean is subtracted before using',
* 'the FFT routine in the NAG library.'
print 210,'The spectrum is generated for each block',
* '(1000 values) of data.'
print 210,'A file for graphing is produced by',
* 'averaging these spectrums.'
print *
print *

c
c This part of the program allows for the input file to be

```

```

c      from a data file.
c
211 write(*,*)
   print*,'Input data file name? (15 char. or less)'
   read(*,240) ofilnam
   print*,' File name is: ',ofilnam
   open (10,file=ofilnam,status='unknown')

240 format(a15)
   write(*,*)
   print*,'Output power spectrum filename ? (15 char. or less)'
   read(*,240) ofilnam2
   print*,' File will be named: ',ofilnam2

*      get sampling interval (usec)
   print*,'Enter the sampling interval (micro sec)'
   read(*,245) ifc
245 format(i5)
   dfreq = 1 / (ifc * 1.0e-6 * Pnps)
*      This is the smallest
   write(*,*) 'dfreq=',dfreq
*      resolvable frequency.
c      Note the freq range from 1/T to N/T, where T is the
c      total sampling time. T=ifc(sample rate in microsec)* #pts.

   print*,'Data Processing in Progress!'

   open (8,file=ofilnam2,status='unknown')

do 34 i=1,nb
   issn=issn+1
   k=1
   offset = 0
   do 11000 k=1,Pnps
c      ix(j)=are the digital phase values read in
c      t=the real values of time at which the phase is measured
       read(10,63) t,ix(k)
*      reads the data in from the
*      input file previously specified
63      format(x,f8.2,i8)
       offset = offset + ix(k)
*      sum of all measurements.
11000      continue

c      Calculate the average value of the set of data pt (pnps data pts
c      in the set).
       offset = -offset / Pnps
       write(*,*) 'offset=',offset
c      calculates the average value

c      remember the data varies from 0 to 4 volts so 0-2048
c      are negative values and 2048-4096 represent positive values.
c      To incorporate this in the data the average is subtracted
c      off. This also eliminates a high dc component.

       do 18 j=1,Pnps
c      x(j)=are real values of the phase minus the mean value
       x(j) = dfloat(ix(j) + offset)
18      continue

       j=Pnps
c      write(*,*) 'j= ',j
       ifail = 0
c      This calculates the fft. The data is in array x the
c      fft data will be returned in x. j represents the
c      number of data points in x. s is a working

```

```

c      directory not important for output. ifail is
c      status word indicating success or failuer. Anything
c      but zero is failure.
c
c      call c06faf(x,j,s,ifail)
c      write(*,*) 'ifail=',ifail
c
c      The fft data is complex. To come up with the signal
c      we treat it like the signal represent amplitude and we
c      want intensity. The real parts are stored in the first
c      N/2 values and the imiginary parts in the rest.
c
c      Calculate Power Spectral Density
c      The output signal looks like
c      z = a + ib
c      n   n   n
c
c      To find the amplitude of this complex signal,which represents
c      the fft amplitude we take the square of both signals and add
c      together.
c      psd(1) = psd(1) + abs(x(1))
c      do 1500 j=2, Pnpsd2
c      The averaging of the fft's.
c      psd(j) = psd(j) + sqrt(x(j)**2 + x(Pnps+2-j)**2)
1500    continue
c      psd(Pnpsd2+1) = psd(Pnpsd2+1) + abs(x(Pnpsd2+1))
c
c      34    continue
c
c      35    write(*,*)
c      do 1100 j=0,Pnpsd2
c      write(8,270)j*dfreq,psd(j+1)/nb
1100    continue
c      270    format(x,f6.1,x,f11.3)
c
c      print 280, ibeep
c      280    format(a1$)
c
c      ist=tstate (tlu,fn,rn,errf,eoff,eotf,tcsr)
c      print*, ' block address is ',rn,', errf=',errf,',eoff=',eoff
c
13000  close(8)
c      close(10)
c      end

```



```

c      program autocor
c      The purpose of this program is to calculation the
c      autocorrelation function.
c
      dimension a(5000),b(5000)
      integer x,n,flag,nk
      character ofilnam*15
      double precision a,b
      double precision t,var,avrg

      print*, ' Input the filename for reading (< 16 char.)'
10     read (*,10) ofilnam
      format (a15)

      open(1,file=ofilnam,status='unknown')

      print*, ' Input the filename for writing (< 16 char.)'
      read (*,10) ofilnam

      open(2,file=ofilnam,status='unknown')

      n=5000

c      Calculate the average square data value.
      do 20 i=1,n
30         read (1,30) t,x
            format(x,f8.2,i6)
20         a(i)=float(x)
      continue

      nk=2500
      flag=0

c      Calls a Nag library routine to calculate the mean
c      variance and autocorrelation.
c
      print*, 'nk=',nk
      print*, 'n=',n
      call G13ABF(a,n,nk,avrg,var,b,t,flag)
      print*, 'nk=',nk

c
      print*, 'stat=',t
      print*, 'ifail=',flag
      print*, 'mean=',avrg
      print*, 'variance=',var

      do 60 i=1,2500
70         write(2,70) i,b(i)
60         format(x,i6,x,f10.5)
      continue

      close (1)
      close (2)
      end

```

```

c      program avrgcor
c
c      The purpose of this program is to calculation the
c      average of several autocorrelation functions.
c
      dimension a(5000)
      integer flag,n,t
      character ofilnam*15
      real a,sum,x

      open(1,file='sbamid1.cor',status='old')
      open(2,file='sbamid2.cor',status='old')
      open(3,file='sbaedgel.cor',status='old')
      open(4,file='sbaedge2.cor',status='old')

      print*, ' Input the filename for writing (< 16 char.)'
      read (*,10) ofilnam
10     format (a15)

      open(9,file=ofilnam,status='unknown')

      n=5000
      flag=0

c      Calculate the average square data value.
      do 20 i=1,n
          sum=0.0
          read (1,30) t,x
          format(x,i6,x,f10.5)
          sum=float(x)
          read (2,30) t,x
          sum=float(x)+sum
          read (3,30) t,x
          sum=float(x)+sum
          read (4,30) t,x
          sum=float(x)+sum
          a(i)=sum/4.0
          if ((a(i).lt. .3679).and.(flag.eq.0)) then
              print*, ' The correlation length =',i
              flag=1
          end if
20     continue

      do 60 i=1,5000
          write(9,70) i,a(i)
          format(x,i6,x,f10.5)
70     continue
60     continue

      close (1)
      close (2)
      close (3)
      close (4)
      close (9)
      end

```

```

c      program avrgfreq
c
c      The purpose of this program is to calculation the
c      average of several forier transform data sets.
c
      dimension a(1002)
      integer n
      real a,sum,x,t

      open(1,file='30sba1.fft',status='old')
      open(2,file='30sba2.fft',status='old')
      open(3,file='30sba3.fft',status='old')
      open(4,file='30sba4.fft',status='old')
      open(8,file='30sba5.fft',status='old')
      open(9,file='30sba6.fft',status='old')
      open(10,file='30sba7.fft',status='old')
      open(11,file='30sba8.fft',status='old')
      open(12,file='30sba9.fft',status='old')
      open(13,file='30sba10.fft',status='old')
      open(14,file='30sba11.fft',status='old')
      open(15,file='30sba12.fft',status='old')

      open(19,file='30sbaavrg.fft',status='unknown')

      n=501

c      Calculate the average data values.
      do 20 i=1,n
          sum=0.0
          read (1,30) t,x
          format(x,f6.1,x,f11.3)
30         sum=float(x)
          read (2,30) t,x
          sum=float(x)+sum
          read (3,30) t,x
          sum=float(x)+sum
          read (4,30) t,x
          sum=float(x)+sum
          read (8,30) t,x
          sum=float(x)+sum
          read (9,30) t,x
          sum=float(x)+sum
          read (10,30) t,x
          sum=float(x)+sum
          read (11,30) t,x
          sum=float(x)+sum
          read (12,30) t,x
          sum=float(x)+sum
          read (13,30) t,x
          sum=float(x)+sum
          read (14,30) t,x
          sum=float(x)+sum
          read (15,30) t,x
          sum=float(x)+sum
          a(i)=sum/12.0
          a(i+501)=t
20      continue

      do 60 i=1,501
          write(19,70) a(i+501),a(i)
70         format(x,f6.1,x,f11.3)
60      continue

```

```
close (1)
close (2)
close (3)
close (4)
close (8)
close (9)
close (10)
close (11)
close (12)
close (13)
close (14)
close (15)
close (19)
end
```

```

c      program corlength
c
c      The purpose of this program is to calculation the
c      correlation lengths for the sand paper data sets.
c
      dimension a(5000),b(5000)
      integer x,n,flag,m,counter
      character ofilnam*15
      real a,b
      real t,sum,avsqr,avrg

      print*, ' Input the filename for reading (< 16 char.)'
      read (*,10) ofilnam
10     format (a15)

      open(1,file=ofilnam,status='unknown')

      print*, ' Input the filename for writing (< 16 char.)'
      read (*,10) ofilnam

      open(2,file=ofilnam,status='unknown')

      n=5000
      sum=0.0

c      Calculate the average square data value.
      do 20 i=1,n
30         read (1,30) t,x
            format(x,f8.2,i6)
            a(i)=float(x)
            avrg=avrg+a(i)
20     continue

c      print*, ' sum=',sum
      sum=0.0
      avrg=avrg/n

      do 25 i=1,n
25         a(i)=a(i)-avrg
            sum=sum+a(i)**2
            continue

      avsqr=sum/(float(n))
      sum=0.0
      b(0)=1.0
      flag=0
      m=n-1
      counter=0

c      Calculating the correlation length.
      do 40 i=1,m
          sum=0.0
          do 50 j=1,(n-i)
              sum=sum+a(j)*a(j+i)
50         continue
          print*, ' sum=',sum
          b(i)=sum/((n-i)*avsqr)
c      The correlation length is defined as the x value for
c      which the correlation is less than 1/e.
          if ((b(i) .lt. .3679).and.(flag .eq. 0)) then
              print*, ' The correlation length is =',i
              flag=1
c      This limits the correlations calculated
c      to 2 times the correlation length.

```

```
print*, ' m=', m
print*, ' i=', i
print*, ' counter=', counter
c      if (m .gt. (5*i)) then
        counter=5*i
        counter=n-1
      end if
print*, ' counter=', counter
      end if
40    if ((counter.ne.0).and.(i.ge.counter)) goto 45
      continue
print*, ' i=', i

45    print*, ' average square value=', avsq
      print*

      if (counter .eq. 0) counter=n-1

      do 60 i=0, counter
        write(2,70) i,b(i)
70      format(x,i6,x,f10.5)
60    continue

      close (1)
      close (2)
      end
```

```

c      program surfden
c      This program calculates the variance, mean, and probability
c      density distribution of a set of data.
c
integer n,x,avrag2
integer a(5000),b(2049)
character ofilnam*15
real avrag,var,sum1,sum2
real t

n=5000

print*, ' Input the filename for reading (< 16 char.)'
read (*,20) ofilnam
20 format (a15)

open (1,file=ofilnam,status='unknown')

print*, ' Input the filename for writing (< 16 char.)'
read (*,20) ofilnam

open (2,file=ofilnam,status='new')

sum1=0
sum2=0
do 30 i=1,n
      read(1,40) t,x
c      format for data file also x must be integer
40 format(x,f8.2,i6)
      a(i)=x
      sum1=sum1+float(x)
c      print*, 'sum1=',sum1
30 continue
avrag=(sum1/n)
c      print*, 'sum1=',sum1

c      print*, ' The average = ',avrag
50 format ( ' The variance = ',f12.4)

avrag2=nint(avrag)
print*, ' The average = ',avrag2

out=0
sum1=0
do 100 i=1,n
      x=a(i)-avrag2+1024
      sum1=(a(i)-avrag2)**2+sum1
c      print*, ' x = ',x
      if ((x .lt. 2048).and.(x.gt.0)) then
          b(x)=b(x)+1
      else
          out=out+1
      end if
100 continue

var=sum1/n
write (*,50) var

print*, ' The number of pts. out of region = ',out

do 110 i=-1024,1024
      write(2,120) i,b(i+1025)
120 format(x,i6,x,i6)
110 continue

close(1)
close(2)
end

```

## VITA

The author was born on the 14th of April 1962, in Chicago, Illinois. In 1980 he began his undergraduate work in physics and mathematics at Elmhurst College in Elmhurst, Illinois. In 1984 he completed his Bachelor of Science degree at Elmhurst College.

In June of 1984 the author accepted a part-time fellowship and part-time staff position with the Hughes Aircraft Corporation in Southern California. While at Hughes the author worked for the Ground Systems and Missile Systems Divisions while attending some classes at the University of California, Riverside and University of Southern California.

In September of 1986 the author returned to graduate school on a full-time basis at Oregon Graduate Center in Beaverton, Oregon. While at the Oregon Graduate Center the author pursued a Master of Science in Applied Physics with emphasis in the area of laser speckle.

In march of 1989 the author accepted a position with the General Dynamics Corporation in Rancho Cucamonga, California. The author is currently pursuing a career in the field of image processing.